AD-A147 176

AFWAL-TR-84-2032

SUPERCONDUCTING ROTOR DYNAMICS

R. D. Blaugher
Westinghouse Electric Corporation
Research & Development Center
Pittsburgh, Pennsylvania 15235

September 1983

Final Report for the Period September 1979 to September 1983

Aero Propulsion Laboratory
Air Force Wright Aeronautical Laboratories
Air Force Systems Command
Wright-Patterson Air Force Base, Ohio

NOTICE

When Government drawings, specifications, or other data are used for any purpose other than in connection with a definitely related Government procurement operation, the United States Government thereby incurs no responsibility nor any obligation whatsoever; and the fact that the government may have formulated, furnished, or in any way supplied the said drawings, specifications, or other data, is not to be regarded by implication or otherwise as in any manner licensing the holder or any other person or corporation, or conveying any rights or permission to manufacture use, or sell any patented invention that may in any way be related thereto.

This report has been reviewed by the Office of Public Affairs (ASD/PA) and is releasable to the National Technical Information Service (NTIS). At NTIS, it will be available to the general public, including foreign nations.

This technical report has been reviewed and is approved for publication.

REX L. SCHLICHER, CAPT, USAF
Power Systems Branch
Aerospace Power Division
Aero Propulsion Laboratory

B. L. MCFADDEN, ACTING CHIEF
Power Systems Branch
Aerospace Power Division
Aero Propulsion Laboratory

FOR THE COMMANDER

JAMES D. REAMS
Chief, Aerospace Power Division
Aero Propulsion Laboratory

"If your address has changed, if you wish to be removed from our mailing list, or if the addressee is no longer employed by your organization please notify AFWAL/POOS, *W-PAFB, OH 45433 to help us maintain a current mailing list".*

Copies of this report should not be returned unless return is required by security considerations, contractual obligations, or notice on a specific document.

UNCLASSIFIED

SECURITY CLASSIFICATION OF THIS PAGE

REPORT DOCUMENTATION PAGE

1a. REPORT SECURITY CLASSIFICATION: UNCLASSIFIED	1b. RESTRICTIVE MARKINGS: NONE
2a. SECURITY CLASSIFICATION AUTHORITY: N/A	3. DISTRIBUTION/AVAILABILITY OF REPORT: Approved for public release: distribution unlimited
2b. DECLASSIFICATION/DOWNGRADING SCHEDULE: N/A	
4. PERFORMING ORGANIZATION REPORT NUMBER(S): N/A	5. MONITORING ORGANIZATION REPORT NUMBER(S): AFWAL-TR-84-2032
6a. NAME OF PERFORMING ORGANIZATION: Westinghouse R&D Center; 6b. OFFICE SYMBOL (If applicable): AFWAL/POOS	7a. NAME OF MONITORING ORGANIZATION: Aero Propulsion Laboratory (AFWAL/POOS)
6c. ADDRESS (City, State and ZIP Code): 1310 Beulah Road, Pittsburgh PA 15235	7b. ADDRESS (City, State and ZIP Code): Air Force Wright Aeronautical Laboratories, Wright-Patterson Air Force Base, Ohio 45433
8a. NAME OF FUNDING/SPONSORING ORGANIZATION; 8b. OFFICE SYMBOL (If applicable)	9. PROCUREMENT INSTRUMENT IDENTIFICATION NUMBER: F33615-79-C-2026
8c. ADDRESS (City, State and ZIP Code)	10. SOURCE OF FUNDING NOS.

PROGRAM ELEMENT NO.	PROJECT NO.	TASK NO.	WORK UNIT NO.
62203F	3145	32	48

11. TITLE (Include Security Classification): Superconducting Rotor Dynamics

12. PERSONAL AUTHOR(S): R. D. Blaugher

13a. TYPE OF REPORT	13b. TIME COVERED	14. DATE OF REPORT (Yr., Mo., Day)	15. PAGE COUNT
FINAL	FROM Sep 79 TO Sep 83	1983/ Sep/ 30	155

16. SUPPLEMENTARY NOTATION

17 COSATI CODES			18. SUBJECT TERMS (Continue on reverse if necessary and identify by block number)
FIELD	GROUP	SUB. GR.	Analysis of the Coolant Dynamics of a Superconducting Generator Rotor Undergoing Rotation
1002	1313	2003	

19. ABSTRACT (Continue on reverse if necessary and identify by block number)

This report is a review of the work performed to develop an experimental test rotor (RTF) to evaluate acceleration effects on superconducting Nb_3Sn coils. The RTF was specifically modeled after the General Electric 20 MVA Advanced Rotor Design with respect to the centrifugal loading, cryogenic design, mechanical support and construction for the superconducting coils. This report reviews most of the important design considerations and details the superconducting test coil design and fabrication.

20. DISTRIBUTION/AVAILABILITY OF ABSTRACT	21. ABSTRACT SECURITY CLASSIFICATION
UNCLASSIFIED/UNLIMITED ☒ SAME AS RPT. ☐ DTIC USERS ☐	UNCLASSIFIED

22a. NAME OF RESPONSIBLE INDIVIDUAL	22b. TELEPHONE NUMBER (Include Area Code)	22c. OFFICE SYMBOL
CAPTAIN REX L. SCHLICHER	513-255-3835	AFWAL/POOS

DD FORM 1473, 83 APR EDITION OF 1 JAN 73 IS OBSOLETE.

SECURITY CLASSIFICATION OF THIS PAGE

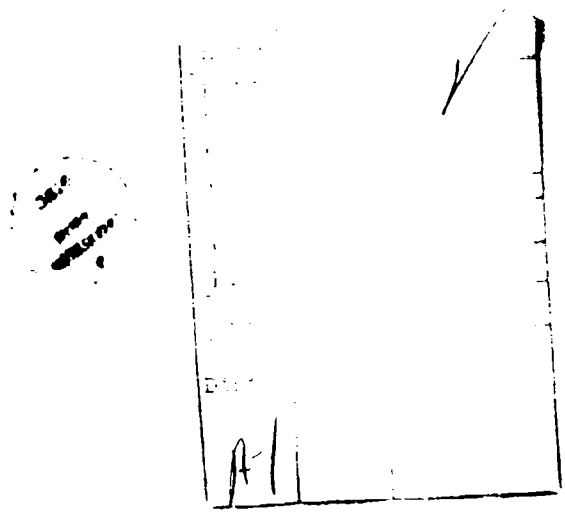

SUMMARY

Since 1971, the USAF Aero Propulsion Laboratory (APL WPAFB) has sponsored exploratory research and development programs aimed towards the application of superconducting generators to airborne and/or outer-space missions. The present program, entitled "Superconducting Rotor Dynamics," was conceived as a investigation of the performance of Nb_3Sn potted racetrack windings in environments simulating the conditions of a superconducting generator during an airborne mission. The originally perceived program was very ambitious and because of funding constraints many of the possible tasks which could have been performed were never pursued. However, this four-year program which spanned from September 1979 to September 1983 did achieve two major accomplishments.

The most significant accomplishment under this program was the development of winding and impregnation techniques to be used in the formation of potted racetrack coils using Nb_3Sn superconducting windings. The techniques developed were suitable for both S-glass insulated Nb_3Sn conductors and Cu2S insulated Nb_3Sn conductors. Experimental testing was used throughout this effort to qualify the techniques developed.

The second significant accomplishment under this program was the confirmation through analysis that a small scale model of a rotor could be used to simulate conditions on superconducting windings that closely approximate the conditions in a superconducting generator subjected to rapid mechanical acceleration and pulsed excitation. Included in this effort, was the modifications made to the "spin-test" rotor for future testing racetrack coils excited to no more than 1200A while cooled by a self-re[illegible]ated helium flow system. Many of the tasks in this latter effort were deferred due to funding constraints.

The accompanying report details the accomplishments under this contract. The information presented in this report has been made as complete as possible not only to document the effort performed under this program but to provide sufficient background to allow future programs to use a rotating test facility for qualifying untried winding designs.

FOREWORD

This final technical report is a review of the work performed under contract F33615-79-C-2026 to develop an experimental test rotor (RTF) to evaluate acceleration effects on superconducting Nb_3Sn coils. The RTF was specifically modeled after the General Electric 20 MVA Advanced Rotor Design with respect to the centrifugal loading, cryogenic design, mechanical support, and construction for the superconducting coils. This report reviews most of the important design considerations and details the superconducting test coil design and fabrication. Work on this program was initiated in September 1979 under Project 3145, Task 32 and Work Unit 48.

Captain Rex L. Schlicher/AFWAL/POOS directed the work covered in this report. The Westinghouse Program Manager was R. D. Blaugher, Manager of Cryogenic Technology and Electronics at the Research and Development Center.

The important contribution of A. S. Venturino is specifically acknowledged who participated through this and past programs with the Air Force. Acknowledgement is given to J. H. Murphy, G. R. Wagner, and P. W. Eckels who helped in preparing this report. Also acknowledged are the technical contributions from R. L. Kolek, C. L. Zeise, and G. R. Wagner and technical assistance from J. Buttyan and P. J. Steve. Mrs. Marilyn B. Cross is thanked for typing the manuscript.

TABLE OF CONTENTS

Section		Page
I.	INTRODUCTION	1
	1. "Spin-Test" Rotor	2
	2. "Spin-test" Cryogenic Description	4
II.	DESIGN OF THE RTF AND SUPERCONDUCTING TEST COILS	7
	1. RTF Design	8
	a. Magnetic field calculations and Base Winding Design	8
	b. Modified RTF Cryogenic Design	11
	(1) Helium Inlet/Outlet Considerations	13
	(2) Vapor Cooled Power Lead	13
	(3) Torque Tube Cooling Considerations	15
	c. Structural Materials Selection	15
	(1) Low Modulus Interface Material	15
	(2) Coil Support Material	19
	d. Mechanical Design	20
	(1) Disassembly of the "Spin Test"	23
	(2) Coil Support Structure	23
	(3) Centrifugal Containment Shell	27
	(4) Vacuum Shell	32
	(5) Exciter Modification	32
	2. Superconducting Test Coil Design	32
	a. Conductor Design	34
	(1) Conductor Verification	39
	b. Circular Coil and Termination Design and Development	43

c. Circular Coil and Dummy Race Track Coil

Fabrication and Test..... 47
(1) Circular Coil..... 47
(2) Dummy Racetrack Coil..... 49

III. FABRICATION AND TEST OF THE Nb3Sn TEST COILS..... 59

1. Coil Fixture and Mold Design..... 59

2. Impregnation System and Procedure..... 61

(a) Impregnatin Procedure..... 64

3. Superconducting Coil Fabrication..... 65

4. Instrumentation..... 68

5. Data Acquisition and Reduction..... 70

IV. CONCLUSIONS AND RECOMMENDATIONS.....

Appendix

A Chronological Record of Events..... 74

B Acceleration Tests on a Model Superconducting Rotor..... 83

C Examination of Stick-Slip Motion in Superconducting Dipoles..... 109

D Data Acquisitional Telemetry..... 119

E Recent Developments on Methods for Superconductor Joining..... 127

REFERENCES 143

LIST OF ILLUSTRATIONS

Figure		Page
1	Spin Test Rotor	3
2	Variation of Peak Magnetic Field with Coil Geometry	9
3	Modified Rotating Test Facility (RTF)	12
4	Heat Leak versus Helium Flow Rate for the RTF Power Leads	16
5	Exciter Cooling Coils and Radiation Shield	17
6	RTF Detailed Schematic	22
7	Coil Support G11CR Block	24
8	Superconducting Coil Support Detail	25
9	Superconducting Coil Support Structure	26
10	Finite Element Analysis for Winding and Support System (from Reference 3)	28
11	Centrifugal Shell End Flange and Stub Shaft Assembly	29
12	Drive End Flange Detail	30
13	Exciter End Flange Detail	31
14	Vacuum Shell Detail	33
15	Superconducting Test Coil Detail	35
16	Conductor Cross Section at 100X	37
17	Cable Design from General Electric Phase I Report	38
18	Ic vs H from IGC Data for Optimized Heat Treatment	40
19	Ic vs H for Strands and Butt Resistance Welded Joints	41

20	Lead Transition Conceptual Design	44
21	Lead Transition Mock-up	46
22	Dipole Test Coil - Lead Transition Face	50
23	Dipole Test Coil - Sensor Face	51
24	Dipole Test Coil Field Profile - Longitudinal	53
25	Dipole Test Coil Field Profile - Vertical	54
26	Dipole Test Coil Field Profile - Bore	55
27	Metallographic Examination of Dummy Racetrack Section A.7X, B.25X	58
28	Test Coil during Winding	60
29	Test Coil in Potting Mold	62
30	Schematic of Impregnation System	63
31	Nb_3Sn Dipole Test Coil (Coil #1)	67
32	Nb_3Sn Dipole Test Coil (Coil #1 and #2)	69
33	Nb_3Sn Coil Support with Instrumentation	72
B-1	Generalized Airborne System	86
B-2	Schematic of Spin-Test Rotor	87
B-3	Spin-Test Rotor Installed on Test Stand	88
B-4	Superconducting Coils Mounted on Support Structure	89
B-5	Spin-Test Helium Flow System	91
B-6	Copper Heat Exchanger	92
B-7	Helium Supply System	95
B-8	Magnetic Field and Temperature Degradation of the Current Carrying Capacity of Nb-Ti Conductors	99
B-9	Acceleration Test with Subcooled Inlet Condition	104
B-10	Superconducting Coil Excitation at 8000 rpm	106

C-1 Mechanical Stability Model for a Self-Supported Conductor in a Dipole Winding..... 111

C-2 Mechanical Stability Model for an Externally-Supported Conductor in a Dipole Winding..... 113

D-1 Acquisition and Telemetry with Current Multiplexing..... 120

D-2 Data Acquisition and Telemetry -- No Current Multiplexing..... 125

D-3 Comparison between the Two Modules..... 126

E-1 Short Sample Critical Current for Welded and Unwelded NbaSn Wire..... 134

E-2 Cross Section of Butt-Welded NbaSn Wire (SEM)..... 136

E-3 Filament Joining at Butt-Welded Interface (SEM)..... 136

LIST OF TABLES

Table		Page
1	Pertinent Parameters of the Main Lead.....	14
2	Properties of Mylar and Polycarbonate.....	19
3	Dielectric and Tensile Properties of Mylar and Makrofol K6.....	20
4	Test Coil Electrical Measurements.....	56
B-1	Quench Current for Different Ramp Rates.....	98
C-1	Example Calculations for the Spin-Test Rotor Coil.....	116
C-2	Example Calculations for the 300 MVA Field Coil.....	116
E-1	Average Mechanical Strength for Welded and Unwelded NbaSn Wire.....	134
E-2	300 MVA Superconductor Specification.....	137

SECTION I

INTRODUCTION

The USAF Aero Propulsion Laboratory (APL WPAFB), since 1971, has sponsored exploratory research and development programs directed toward airborne superconducting generators.[1-3] These programs have addressed specific system operating requirements which impose high mechanical and thermal loads on the superconducting field winding.[4,5] The most severe problem that has been identified is a fast start up requirement. The generator system which includes a gas turbine prime mover and rectified [illegible]t be fully operational within a time as short as one second. As a [illegible] it may be necessary to accelerate the rotor to design speed, i.e. [illegible]bine speed, while simultaneously exciting the field winding. The superconducting winding must be able to withstand the one second magnetic field ramp and compressional load without normalizing. These additive factors create a transient heat load which severely affect the superconductor performance.[6]

Theoretical treatment using ac loss theory and thermohydraulic analysis can provide some estimates on the winding performance during a rapid start up mode. However, some assumptions on expected heat transfer and mechanical integrity, i.e., little or no conductor motion, are necessary. The surest method to evaluate the winding performance is to model the winding experimentally and subject it to conditions representative of the generator during rapid start-up.

A rotating test facility (RTF) was thus designed and constructed to evaluate these mechanical and electrical effects on superconducting rotor coils. This "spin-test" rotor was specifically designed to reproduce the geometry, mechanical, and thermal conditions which occur

in a high-speed superconducting generator. Complete details on the "spin-test" rotor design, construction, and previous testing are presented in AFAPL-TR-77-39. During the initial phase of the present program additional rotating tests on the spin-test rotor were carried out. These tests, reported in Appendix B, were an extension of the original testing as detailed in the "spin-test" final report. The following sections provide a brief review of the original "spin-test" design and a detailed description of the helium management system.

1. "Spin-Test" Rotor

The "spin-test" rotor shown in Figure 1 consists of a metallic inner, cryogenically cooled, rotating cylinder which contains the superconducting test coils and a fiberglass outer stationary vacuum enclosure.

The inner structure which houses two racetrack field windings is attached at both ends to stub shafts by means of thin wall "torque tubes" which also provide thermal isolation. Each torque tube is vapor cooled by a system of wound cooling tubes which were copper brazed to the outer wall. Both stub shafts extend beyond the ends of the stationary outer cylinder through oil lubricated (vacuum) face seals. The excitation slip rings and an inlet helium transfer coupling are incorporated into the non-driven stub shaft.

The end plates of the stationary outer dewar house the bearing and vacuum seals and support the rotor on the test bed. The central portion of the stationary fiberglass dewar is cooled with liquid N_2 which provides a low temperature ambient for the inner helium cooled rotor. This outer cylinder is constructed from two tubes of non-metallic fiber glass-epoxy composite which eliminates eddy current losses or field reflections which would occur from a metallic outer surface.

The rotor coils in the first "spin-test" were constructed with a step tructure which incorporated cooling passages to allow both radial

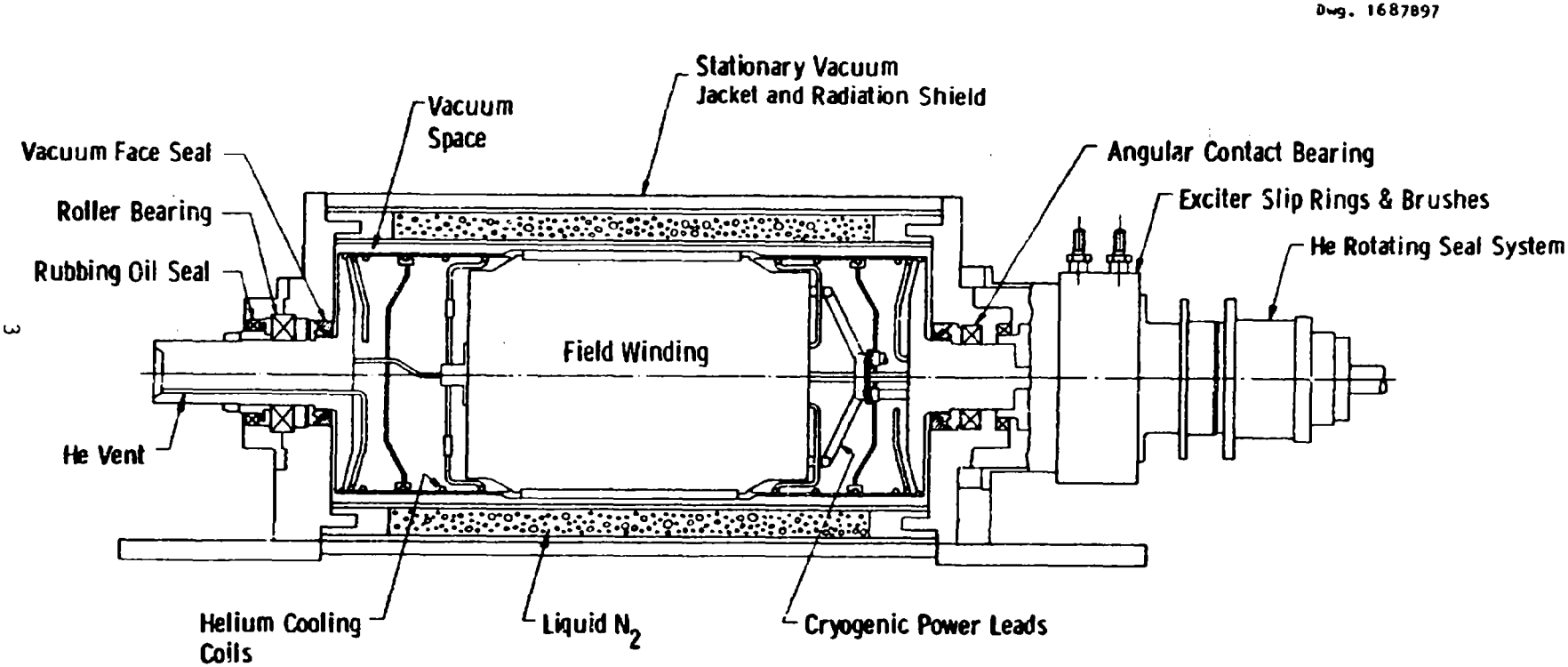

Figure 1. Spin Test Rotor

and axial flow capability. The current rating of these coils easily allowed field levels of 4T. The superconductor was a Nb-Ti copper matrix multifilamentary (rectangular) conductor with a PYRE-ML insulation system. Thermometers were integrated into the winding in order to evaluate the temperature distribution during the rotating tests.

The shafts, torque tubes and rotor body, were designed for operating (torque and rotational) stress levels corresponding to 12,000 rpm and acceleration levels of 1257 rad/sec^2 (0 to 12,000 rpm in one second). The gear box and drive motor system, however, are limited to a full speed acceleration of approximately 2 to 4 sec. The basic structural material was Inconel 718 for the outer shells and Inconel 600 for the stub shafts.

2. "Spin-Test" Cryogenic Description

The helium flow stream is supplied to the "spin-test" by a helium transfer coupling.[7] This transfer system incorporates the helium seals and the inlet bayonet which provides the stationary/rotating interface for the helium flow. The helium stream upon entering the rotor encounters a copper impeller which rapidly accelerates the fluid to body speed and provides nearly complete phase separation. The dense liquid is diverted outward through a hollow copper finned heat exchanger located in the center or pole of the winding. The copper fins, central copper core and impeller basically constitute the mean heat exchanger which is specifically designed to remove the heat produced by compressional processes. The heat absorbed in the fins flow radially inwards to the cold copper core producing gas due to liquid boil-off. This gas combines with the inlet gas and flows outward through radial tubes to cool the drive end thermal transition shell. This gas then returns on-axis and exits the rotor through orifices mounted on the stub shaft.

The helium liquid flowing off-axis exits the hollow copper fin at the winding OD and then moves radially inwards providing added cooling due to decompression. The liquid level within the winding is controlled by a dam which also feeds a helium pool to cool the electrical leads. The lead cooling is essentially self-regulating with added heat producing increased flow to the lead. The winding also incorporates an auxiliary heat exchanger which is thermally connected to the main or central heat exchanger at the core ID. This auxiliary heat exchanger provides additional capability for heat removal from the helium contained in the winding. During a rapid spin-up mode, the helium isolated in the winding will experience compressional heating. This heating will produce high convective flow velocities in the radial passages and around the auxiliary heat exchanger thus maintaining nearly isothermal conditions.

The heating or gas produced in the winding moves radially inwards to a gas plenum located near the axis of rotation. The gas in this plenum is expelled through tubes to cool the anti-drive thermal transition shell. The gas is then fed through the exciter drive shaft to orifices located on the slip ring flange.

This cryogenic scheme was designed to provide nearly isothermal cooling for the winding during the mechanical transients and the associated compressional heating for a rapid spin-up condition. The monolithic copper stabilized Nb-Ti conductor utilized in this rotor would show excessive heating during the required one-second excitation. This combined ac loss and even minor conductor movement under spin-up would most assuredly quench the winding.

Appendix C contains an extensive review of the heating due to conductor motion which may occur during acceleration of a superconducting dipole.

A detailed consideration of the heating and cooling aspects of the "spin-test" indicate that the cryogenic scheme in the first

"spin-test" rotor was not necessarily the limiting factor in the winding performance.[6]

This design approach (as developed by GE in their Advanced Rotor Program)[3,8] considered a higher current, higher T_c cabled Nb_3Sn conductor which offered improved thermal margin and lower ac loss performance over both cabled and monolithic Nb-Ti. In addition advanced non-metallic composites were substituted for the internal metallic coil supports which eliminated eddy current heating in the support structure. This report details the design approach, modeling studies and construction details to develop a "spin-test" rotor based on the GE advanced rotor design. This new "spin-test" design will be subsequently referred to as the Rotating Test Facility (RTF) to distinguish it from the earlier "spin-test" rotor.

SECTION II

DESIGN OF THE RTF AND SUPERCONDUCTING TEST COILS

The following sections review the mechanical, cryogenic and structural details of the RTF. As mentioned earlier the GE advanced rotor design served as a basis for the present redesign and proposed modeling of the RTF. Aspects of the GE design approach and cryogenic description are thus reviewed with emphasis on those details which have a direct impact on the RTF design.

Complete details on the GE design are presented in the Phase I report, AFAPL-TR-77-68, titled "Superconducting Rotor Research" and References 8 and 9. The observed acceleration sensitivity and lack of thermal margin for the previous Nb-Ti based rotors suggested that a more advanced conductor and cooling system should be evaluated for the Air Force application. A new design approach was thus selected which was specifically oriented at the combined mechanical and electrical transients produced by a one-second spin-up and excitation.

The basic goal in the GE design approach was to utilize an advanced Nb_3Sn multifilament conductor which offered an increased thermal margin and higher current capability. The added temperature margin for the Nb_3Sn conductor should easily withstand the projected thermal load during the one-second magnetic ramping and spin-up.

As a result of the Nb_3Sn conductor selection, certain design constraints were established for the winding and overall rotor design. A multi-stranded cabled Nb_3Sn conductor was selected which offered a reasonable bend diameter for winding after reaction. This conductor approach thus suggested the use of a fully impregnated or potted winding which offered the optimum design for limiting the conductor motion. A

wind after reaction approach was dictated by the desire of the Air Force to utilize conductor available from a separately funded Air Force development effort. This conductor was fully reacted Nb_3Sn cable which could be satisfactorily wound without degradation providing the bending strain was limited to 1.0 percent.

1. RTF Design

a. Magnetic Field Calculations and Base Winding Design

Field calculations schematically illustrated in Figure 2 were run to evaluate the influence of coil cross-section and length on the overall field strength. In addition, the interaction of two identical coils was determined with respect to their separation with the coils connected in series linking so that the peak field was enhanced.

The assumed current density in the magnetic field calculations was 1.5×10^4 A/cm^2 which corresponds to the General Electric base design analysis for a peak field of 6.8 tesla.[3]

An initial evaluation varied the coil cross-section from 4.5 to 9.0 in^2 holding the overall coil length to 10 in. (with a constant inner radius of 1.5 in.).

The peak field for the two-coil configuration at a 1.0 in. separation varied from 4.5 tesla (for a 2" x 2.25" cross section) to 7.5 tesla (for a 3" x 3" cross section). A 2.85" x 2.85" cross section came very close to the desired field with a value of only 6.7 tesla. The racetrack length, however, was only 1.3 inches compared to a racetrack length of 3.0 inches in the General Electric advanced rotor design. The 2.85" x 2.85" cross section, however, was nearly identical to the General Electric design (8.12 in^2 compared to 8.38 in^2).

A field calculation was then run for a 3.0 in. long racetrack with the same 2.85" x 2.85" cross section. The longer coil (11.7 in.) showed a reduced peak field of 6.2 tesla at a one-inch separation for

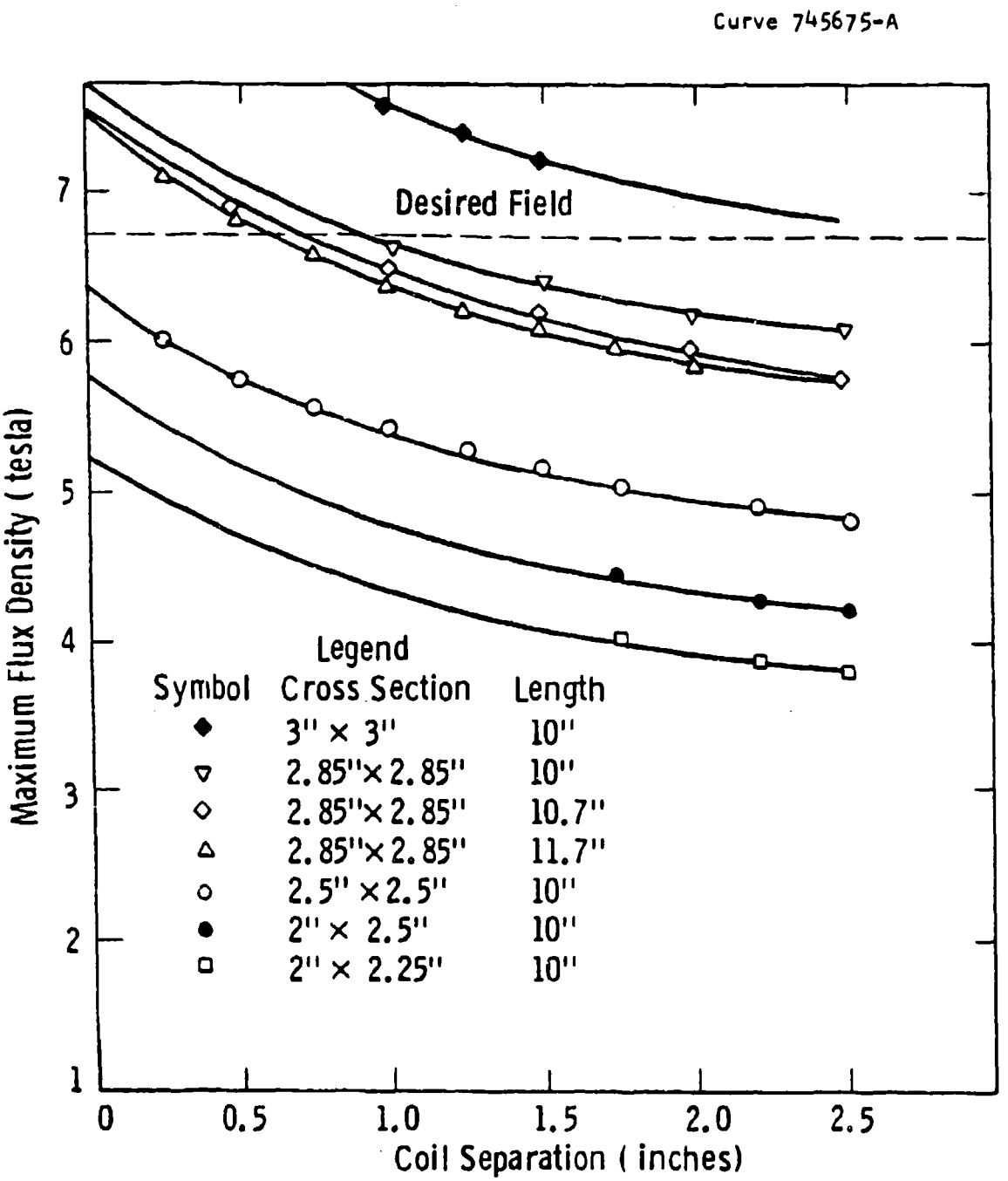

Figure 2. Variation of Peak Magnetic Field with Coil Geometry

the two-coil case which is reduced somewhat from the desired 6.8 tesla value.

The spin-test Nb_3Sn model coils was to be designed to satisfy the following goals:

- The peak field and peak Lorentz force were to be close to the General Electric advanced rotor design under similar current and temperature conditions.
- The coil racetrack was to experience similar bending loads or deflections as would have occurred in the General Electric design at the design current.

The overall coil structure compressive load and other mechanical constraints were to be designed to be similar to the General Electric advanced rotor configuration.

The deflection for the straight section of a racetrack coil at a fixed field and current scales as the square of the racetrack length, assuming that the straight section is self supported. (Appendix C) It was thus clear that the potential for mechanical instability scales as the square of the racetrack length. The deflection for the 3" racetrack would thus be nine times greater than for the 1" length. The 3" two-coil configuration, however, was reduced in field by approximately 10% at a separation of 1.0 in. compared to a 1" racetrack two-coil configuration.

For these reasons, the design approach for the Nb_3Sn spin-test coils was basically to accept a compromise with respect to obtaining the desired 6.8 tesla peak field level and representing equivalent mechanical stability. Thus, a coil cross-section nearly identical to the General Electric design, i.e., 2.85" x 2.85" was selected, the racetrack length was reduced to 2" which represented a reasonable length for illustration of the mechanical loading, and slightly reduced peak field level of approximately 6.5 tesla was determined to be the result of this compromise.

It is important to note that the peak fields occur near the inner surface of the coil bore on the straight length of the racetrack. Actual field mapping tests were performed on the Dummy racetrack coil which is reported in Section 2.2.

b. Modified Cryogenic RTF Design

In the modified RTF design (Figure 3), the helium flow entering the rotor is diverted off-axis by radial tubes. These tubes provide liquid-gas separation with theliquid accumulating in a pool which surrounds the coil modules. Flow passages or channels are machined in the composite supports, which allow convective helium flow over the entire surface of the coil module. Losses or heating in the winding will produce a density change with the lighter warmer fluid moving radially inwards. A vapor-liquid interface will be formed which supplies gas to cool the torque tube extensions. The current leads are directly fed with liquid from the pool which surrounds the coil module.

An additional helium reservoir is located within the pole piece for each of the dipole coils. This helium reservoir thus provides maximum cooling to the high field region.

An outstanding feature of the GE advanced rotor cryogenic design is its basic self-regulating action. Heating in the current leads and winding modules will attempt to decrease the liquid pool depth; the resultant change in pressure will automatically readjust the pool level by adding liquid from the central supply.

The GE cryogenic scheme, however, is subject to an overall temperature rise during a rapid spin-up since the compressional heating must be absorbed within the winding. In addition, a rapid spin-up may produce liquid slugging through the torque tube heat exchanger with a resultant evacuation of the helium pool in the winding.

The basic question with the GE cooling scheme with its fully potted winding is its ability to withstand the thermal load of a simultaneous excitation and spin-up. The fully potted structure has a

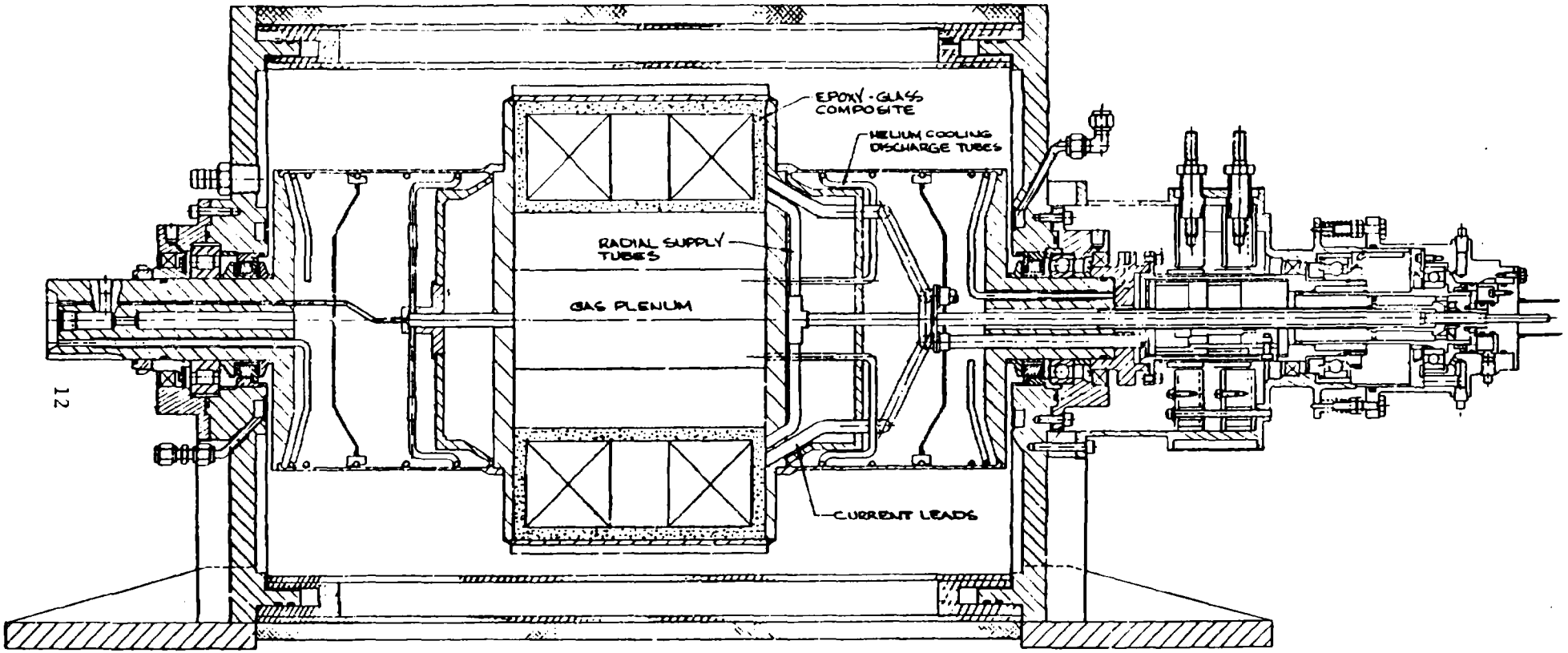

Figure 3. Modified Rotating Test Facility (RTF)

high internal thermal impedance (poor heat transfer) which essentially means the entire thermal load must be stored within the conductor and potting. The success of this design is thus completely dependent on the high thermal margin offered by the Nb_3Sn conductor. The winding temperature for a simultaneous one second excitation and spin-up will be close to 7°K which leaves only a 1.5°K temperature margin.* It is thus clear that this design approach must be experimentally tested to evaluate the actual performance under cooling and mechanical conditions which duplicate the GE design approach. The modified RTF design and test would in fact have evaluated these questions.

(1) Helium Inlet/Outlet Considerations

The helium pool radius was established at a 1.0-inch radius. It was concluded that the inlet "T" tube must be well insulated and a vapor trap containing spin-up vanes positioned in the inlet tube. The radial leg of the "T" flow regulator will extend to a 2.0" radius. This allows regulation with an inlet dewar at 1.2 atm.

The "T" tube inlet is located in the vacuum space external to the cold rotor winding space. This location provides the space necessary for thermal insulation relative constraction and assembly. Boiling occurs at the pool surface formed by the "T" tube and the vapor released leaves the rotor via tubes that form the torque tube pumps. The pumps raise the helium pressure to just over atmospheric for exhaust from the rotor.

(2) Vapor Cooled Power Lead

The main current lead will carry ~1000A at the normal operating conditions. The lead is designed for minimum heat load at the cold end which is due to heat conduction from the warm end at room temperature and from the joule heating in the lead. Heat conduction increases by

*The superconductor current density $J_c > 2 \times 10^4 A/cm^2$ is specified at 6.8 Tesla and 8.5°K.

increasing the lead cross-section while joule heating decreases. An optimum area can be found that will give the minimum heat leakage for a given lead length and current. A safety factor has to be applied by increasing the lead area since the optimum design is very close to the burnout condition in which the lead temperature increases indefinitely with time. We have a safety factor of 2.1 which is probably on the high side but will slow the transient temperature response of the lead in case of coolant stoppage.

The current lead, shown in the RTF schematic (Figure 3) is self-sufficient since the helium it evaporates at the cold end is driven back to the warm end by the static pressure generated by the rotation.

The heat leakage to the cold end will evaporate helium that will intercept the heat conducted to the cold end. The pressure at the warm end of the lead is atmospheric (~ 1.2 atm) and the friction drop in the lead (< 0.1 atm) sets the coolant level at the cold end. Helium enters the lead at a radius of 1.5 in. at which the static pressure is ~2 atm. Liquid helium will fill the current lead jacket till the pressure balance is satisfied. The pertinent parameters of the lead are given in Table 1.

TABLE 1

PERTINENT PARAMETERS OF THE MAIN LEAD

Design Current	1000A
Strand Diameter	0.0254 cm
Total Copper Area	0.4 cm2
Number of Strands	790
Factor of Safety	2.1
Cold End Load Per Lead Pair at 1000A	3.8 ℓ/hr (3.0W)

A computer analysis was performed on the power leads using the previously tested (300A) 0.12 cm^2 cross-section. The results are shown in Figure 4. This cross section showed excessive heating at a 1000A current level. The present design layout allows up to 0.6 cm^2 cross section for the internal power lead connection. A lead this large would require minor modification to the stub shaft penetration. The previous spin-test power lead design utilized a 0.375" OD with 0.313" ID stainless tube which has a 0.077 in^2 (0.795 cm^2) cross section. The finely stranded conductor and insulation system, however, take up considerable space with the cable size basically determined by the ability to incorporate it within the power lead conduit.

If a current lead should lose its coolant, its temperature will go up with time. The higher the cross-sectional area of the lead the longer it takes to reach some temperature level. A model of the lead was tested to be certain that it would not burnout under loss of coolant since this is a fast spin-up test.

(3) Torque Tube Cooling Considerations

The vapor cooled torque tubes for the RTF are the same as those for the spin-test rotor. Figure 5, is the exciter torque tube assembly showing the cooling tubes and radiant heat shields and the heat leak into the rotor for various helium flow rates is given in reference 6. The design helium flow rate, including leads, is 16 ℓ/hr.

c. Structural Materials Selection

(1) Low Modulus Damping Material

As discussed earlier the superconducting coils will be vacuum impregnated with an epoxy system to form the basic coil module. Each coil will then be positioned on a fiberglass-epoxy composite coil support. Composite covers will be attached with bolts to completely enclose the coil. A final machining operation will qualify the OD of the support structure. This support will then be shrunk inside an

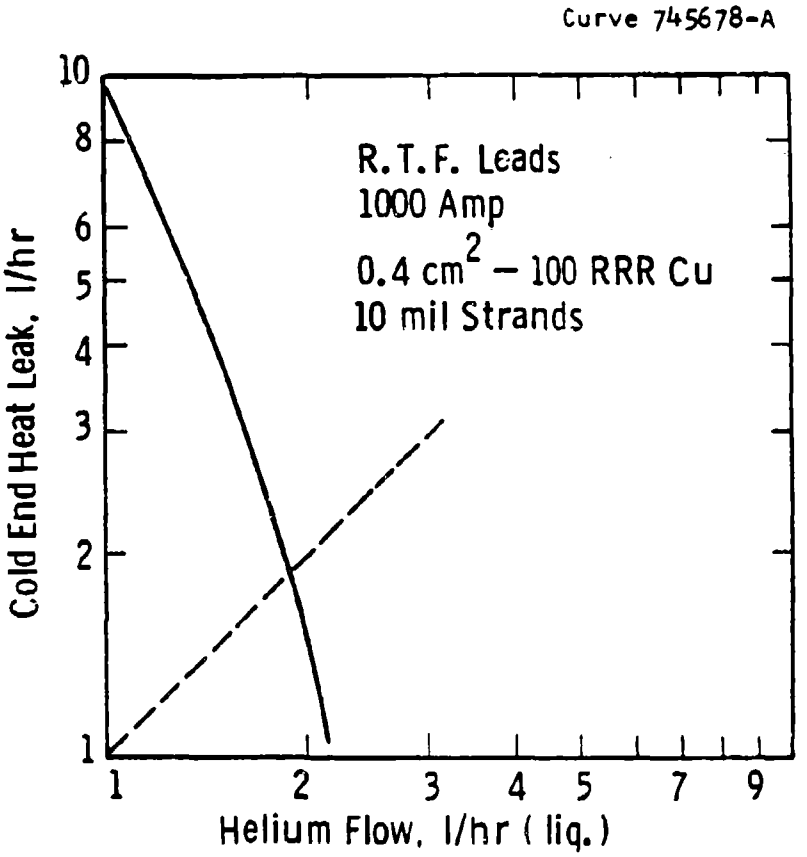

Figure 4. Heat Leak versus helium flow rate for the RTF Power Leads

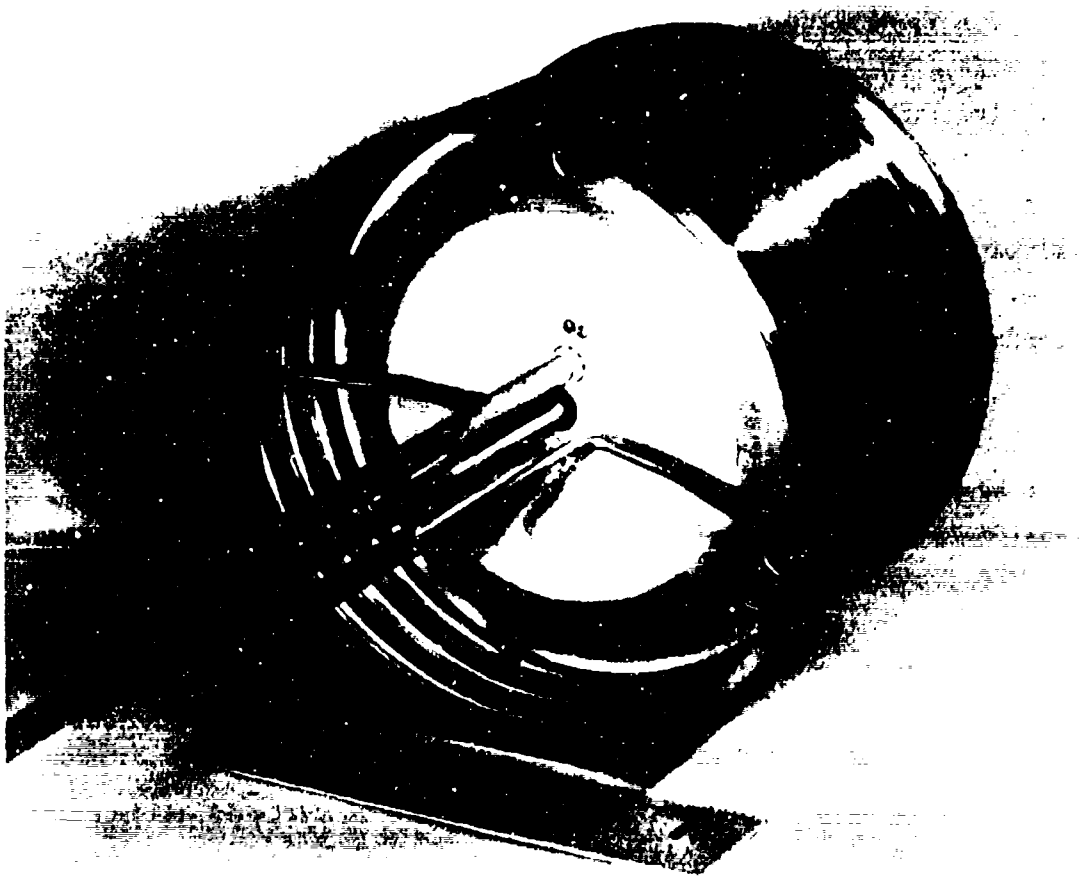

Figure 5. Exciter Cooling Coils and Radiation Shield

Inconel outer shell to provide precompression to the coil and composite support. This precompression is designed to counteract the radial expansion that occurs during rotation which could lead to conductor movement. An inherent feature of the GE advanced rotor design is the use of a low-modulus damping material which is introduced at the coil interfaces to accommodate differential thermal contraction. All relative motion is absorbed as shear strain in the low-modulus interface. This material is basically a low-modulus elastomer like the urethanes, flexible epoxys or unsaturated polyesters. Ordinary polyester Mylar film could possibly provide this low-modulus requirement. A detailed materials analysis however indicates the "urethanes" may be superior to the "polyethylenes."

The low modulus damping film occupies the interface area between the outer winding surfaces and the winding support structure. This film must be able to absorb shear strain due to a combined compression-tension load due to differential thermal contraction, magnetic and centrifugal forces. Pertinent mechanical and physical property information on thin film polymers were identified in References 10 and 11. Based on this study, two materials could be considered, Mylar and Polycarbonate. Mylar or polyethylene terepthalate is a high molecular weight polyester with a relatively high melting point. The polycarbonate is a non-polar, linear polyester of carbonic acid derived from bisphenol A. The significant properties of these two polymers are shown in Table 2. The Mylar film is available from DuPont in various thicknesses. The specific polycarbonate is identified as Makrofol KG and is available from the Mobay Chemical Co. It is a semi-crystalline film biaxially oriented. The pertinent dielectric and tensile properties of these materials at 293^{o}K and 4^{o}K are shown in Table 3. In Reference 11 mention is made that certain polymeric thin films fracture when cooled to 6 to 10^{o}K, while other materials resist thermal fracture consistently. Those materials which fracture readily have elongations only slightly larger than their contractions. Those materials having elong. ions greater by a factor of ten or more always resist fracture.

Table II shows that for Mylar this ratio is 10 and for the Makrofol KG it is 22. In view of the superior elongation properties of the Makrofol KG (polycarbonate) this material should be more effective as a damping interface. For this reason the polycarbonate is selected as the preferred material for the coil winding interface. A polyurethane adhesive (Bostik 7070) was used for afixing the film to the winding surface. The adhesive was applied by diluting the Bostik with methylene chloride. Thermal cycling by rapid cooling in a liquid nitrogen bath did not show any crazing, cracking or lifting of the film

TABLE 2

PROPERTIES OF MYLAR AND POLYCARBONATE

Significant Properties	Mylar	Polycarbonate
Density (295°K)	1.38 gm/cc	1.2 gm/cc
Crystalline Melting Point	538°K	535°K
Molecular Weight	1,200-1,600	50,000-90,000
Crystallinity	Amorphous	Crystalline
Chemical Resistance	Good	Good
Tensile Strength (295°K)	20,000 psi (film) 100,000 psi (fiber)	14,000 psi —
Thermal Expansion Coefficient (295°K)	5×10^{-5} k^{-1}	6×10^{-5} K^{-1}
Dielectric Constant (10^5 Hz, 295°K)	3.05	2.95
Dielectric Constant (10^5 Hz, 295°K)	0.01	0.003

(2) Coil Support Material

Two major criteria were used in the selection of the coil support material, i.e., availability of mechanical and physical property information at 4°K, and resistance to deformation under load. The

TABLE 3

DIELECTRIC AND TENSILE PROPERTIES OF MYLAR AND MAKROFOL KG

Property	Mylar		Makrofol KG	
	293°K	4°K	293°K	4°K
Dissipation Factor (tan $\delta \times 10^6$)	—	200	—	55
Dielectric Constant	—	2.5	—	2.9
Yield Strength ($N/m^2 \times 10^{-7}$)	6.53	19.0	4.93	16.8
Tensile Strength ($N/m^2 \times 10^{-8}$)	1.50	3.48	1.10	2.48
Tensile Modulus ($N/m^2 \times 10^{-9}$)	4.01	4.53	3.48	4.55
Total Elongation, %	114	6.1	72.2	10.8
Thermal Contraction (293-4.2 K), %	0.479		0.474	
Thermal Conductivity (Watts/cm-K)	—	—	6×10^{-4}	9×10^{-5}
Coefficient of Friction, MS	—		0.438	
Elongation/Contraction, %	10		22	

material selected is Spaulding G11 CR industrial glass fabric-epoxy plate. The properties of this material at 4°K are fully characterized at 4°K.[12] Private discussion with Benzinger of Spaulding disclosed that creep tests performed at NBS on both G10 CR and G11 CR laminates showed superior deformation resistance for the G11 CR material. The G11 CR grade thus appears to be more attractive for the Air Force application.

d. Mechanical Design

The RTF mechanical design approach was oriented towards the GE advanced rotor design. A fiber-glass-epoxy composite was utilized for the superconducting coil supports. This support structure contained slots and channels which were interfaced with the coil surface to

provide a liquid helium cooling network. A central cavity in th epole piece was also provided in the pole piece for an additional liquid helium reservoir. A low modulus material was interfaced between the coil surface and support structure. A low modulus material is placed at this interface to abeorb the differential thermal contraction between the coil and support structure. The composite coil support was designed to contain the superconducting leads, terminations and external power leads. The entire coil support was designed to allow a bolted structure which would be final machined to the proper overall diameter. This coil support structure wo' ld then be shrunk into an Inconel outer centrifugal shell to provide sufficient precompression to the superconducting coils. A 500 ft/sec tip speed was established as the design criterion and all material selections were consistent with that peripheral speed.

The outer Inconel centrifugal shell would be attached to new Inconel flanges to allow connection with the rotor stub shafts. These latter stub shafts were removed from the previous spin-test rotor. The excitation and transfer system are also carryovers from the spin-test program. A schematic of the modified RTF is shown in Figure 3.

The outer cryogenic containment for the RTF is similar to the spin-test design. New fiberglass shells were obtained which were assembled into a liquid N_2 container and vacuum enclosure. A dynamic vacuum system was maintained by oil-lubricated face seals and an additional minimum clearance oil seal. A buffer vacuum was used between the two seals to scavenge all oil which leaks past the main face seal.

Consistent with the described design approach a detailed general assembly drawing of the RTF was prepared. The previously determined coil dimensions and coil separation were used as a starting point for the coil support structure. From this general layout the overall rotor sizes — diameter and length, outer shell and all support dimensions could be determined. This overall layout drawing is shown in Figure 6. Detailed drawings on the individual components were then prepared which in turn were integrated into the general assembly drawing.

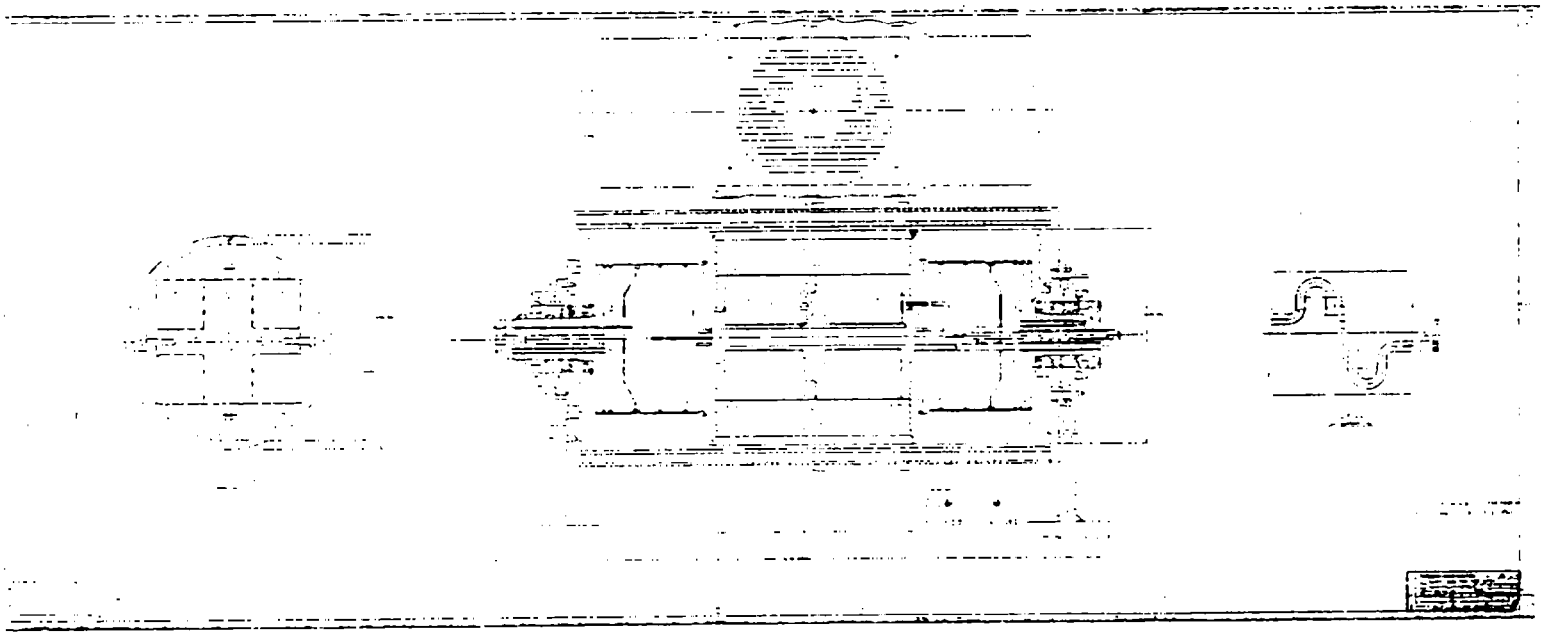

Figure 6. RTF Detailed Schematic

(1) Disassembly of the Spin-Test

The previous "spin-test" was completely disassembled to the base rotor. The rotor was then separated into its original components by machining at the welds joining the thermal transition tubes to the centrifugal shell. The two stub-shaft assemblies could then be easily modified for reuse on the RTF. All of the exciter and helium transfer parts will be reused on the modified RTF.

Following disassembly of the spin-test rotor the desired parts were carefully inspected with metallographic, X-ray and crack detection to evaluate any degradation due to the high speed testing. In addition all of the helium cooling tubes were vacuum leak checked. No problems or leaks were exposed which would prevent reuse of the components.

(2) Coil Support Structure

Similar to the GE advanced rotor design the coil support structure for the two dipole coils was constructed from 611 CR grade glass reinforced epoxy plate. As shown in Figure 7 the plates were stacked oriented glued and pined to allow machining. The x-y plane of the composite with this construction will thus be aligned in the radial direction of the rotor. Thermal contraction of the coils, support structure and outer containment shell are thus nearly uniform. The coil covers and end plates were constructed from the same block as the central coil support.

As detailed in Figure 7 the 611 CR block was sectioned to provide the composite material for fabricating the coil support module and coil support covers. The block for the coil support module was first machined to rough dimensions both external and internal. Final machining for the superconducting coil interface was performed after the coils were wound and vacuum impregnated. The finished coil dimensions could then be accurately transferred for machining the coil support. Figure 8 shows the coil support detail drawing and Figure 9 the final machined coil support.

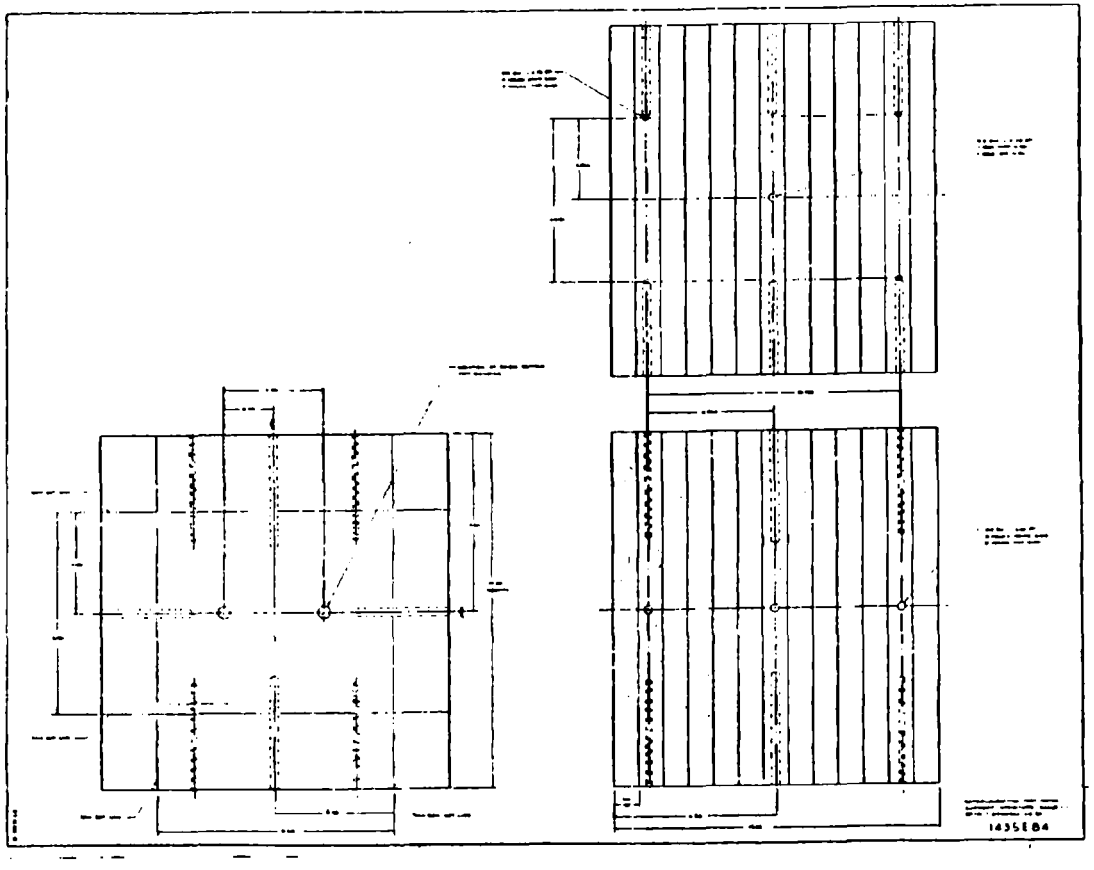

Figure 7. Coil Support GIICR Block

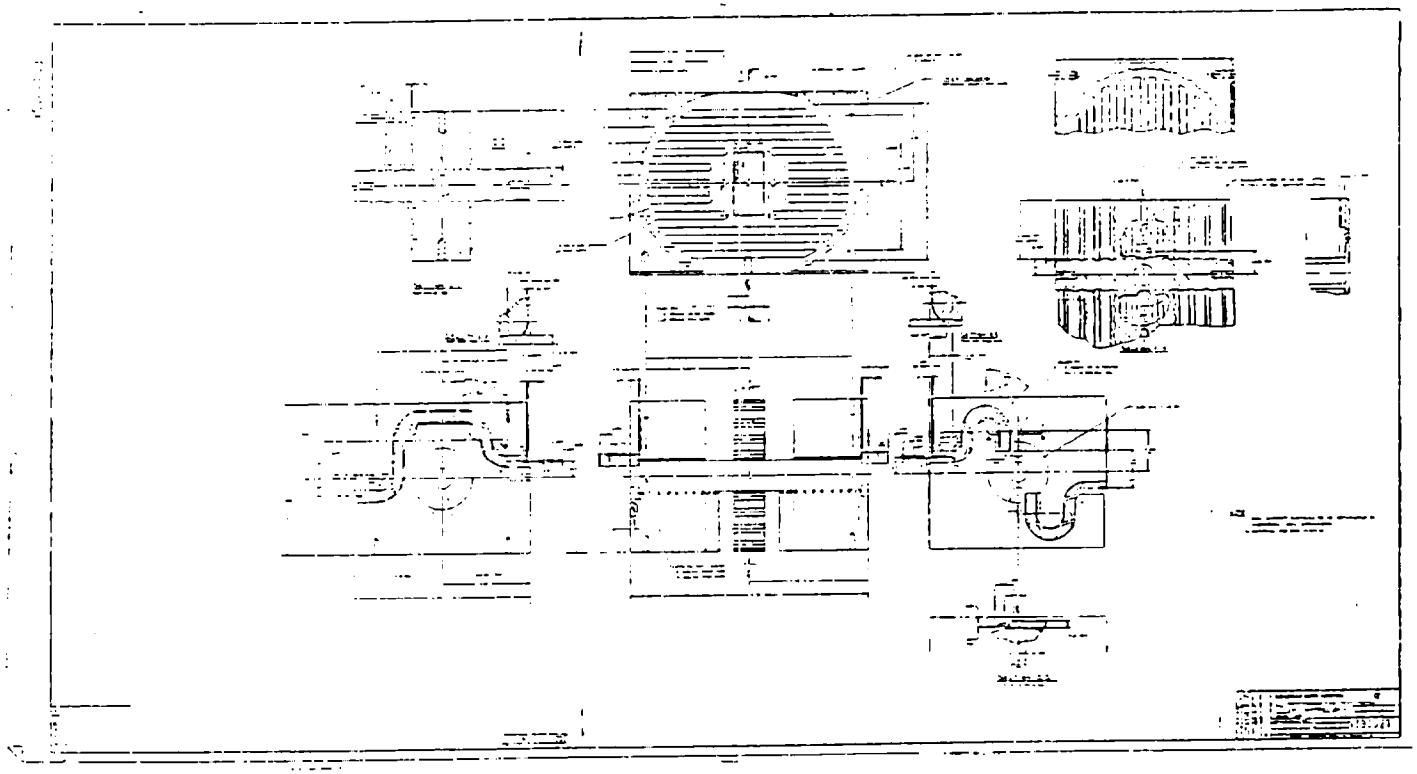

Figure 8. Superconducting Coil Support Detail

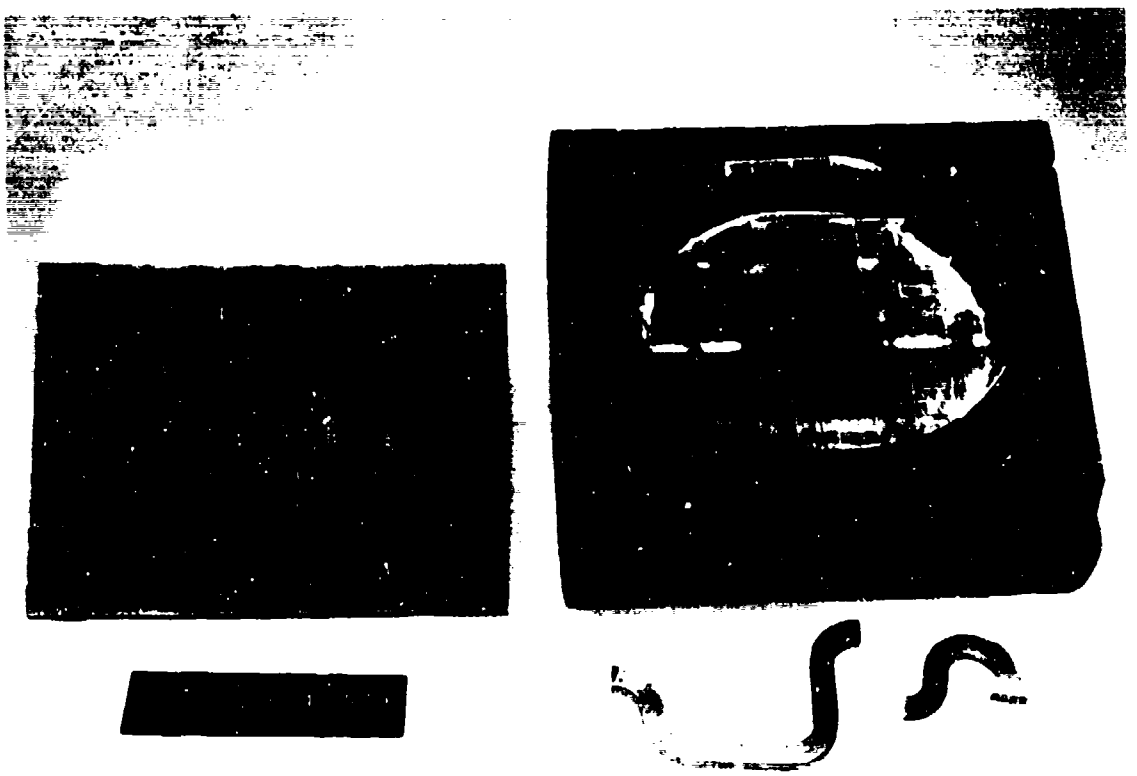

Figure 9. Superconducting Coil Support Structure

(3) Centrifugal Containment Shell

As presented earlier the RTF will experience a combined centrifugal and electromagnetic loading during a one-second spin-up and excitation. As reviewed in references 3 and 6, the centrifugal containment shell must be designed to provide sufficient ultimate strength and in addition some prestress to accommodate the rotational requirements.

An outer shell of Inconel 718 will adequately satisfy these demands.[3,6] The winding and support system Finite element representation (from reference 3) for an outer 718 metallic support shell is shown in Figure 10 for description. Independent analysis conducted during the RTF design phase completely agreed with GE consideration. A properly fabricated 718 shell with a subsequent shrink of the internal coil support structure would provide an adequate centrifugal containment. Inconel 600 flanges could be satisfactorily joined to the 718 material without degradation.

The Inconel 718 shell for the RTF was fabricated by a roll and weld procedure.[6] An Inconel 718 plate was sectioned to the proper size and weld preps prepared on the joining surfaces. The plate was then rolled into a cylinder. Complete NDT testing was conducted on the rolled cylinder prior to welding to evaluate any stress induced cracking. Following this qualification the cylinder was welded and X-rayed in the weld area.

The Inconel 718 shell was then annealed (solution treated) to remove all rolling and welding stresses. The shell was then machined on the OD and ID to the proper dimensions. Following machining the weld area was again X-rayed and crack checked. A final honing operation was performed on the ID to establish the shrink fit outer dimension. The coil support structure will then be final machined to an OD from this dimension. Figure 11 shows the completed 718 outer shell with the Inconel 600 end flange and modified torque tube assembly. The detail drawings for these components are shown in Figures 12 and 13.

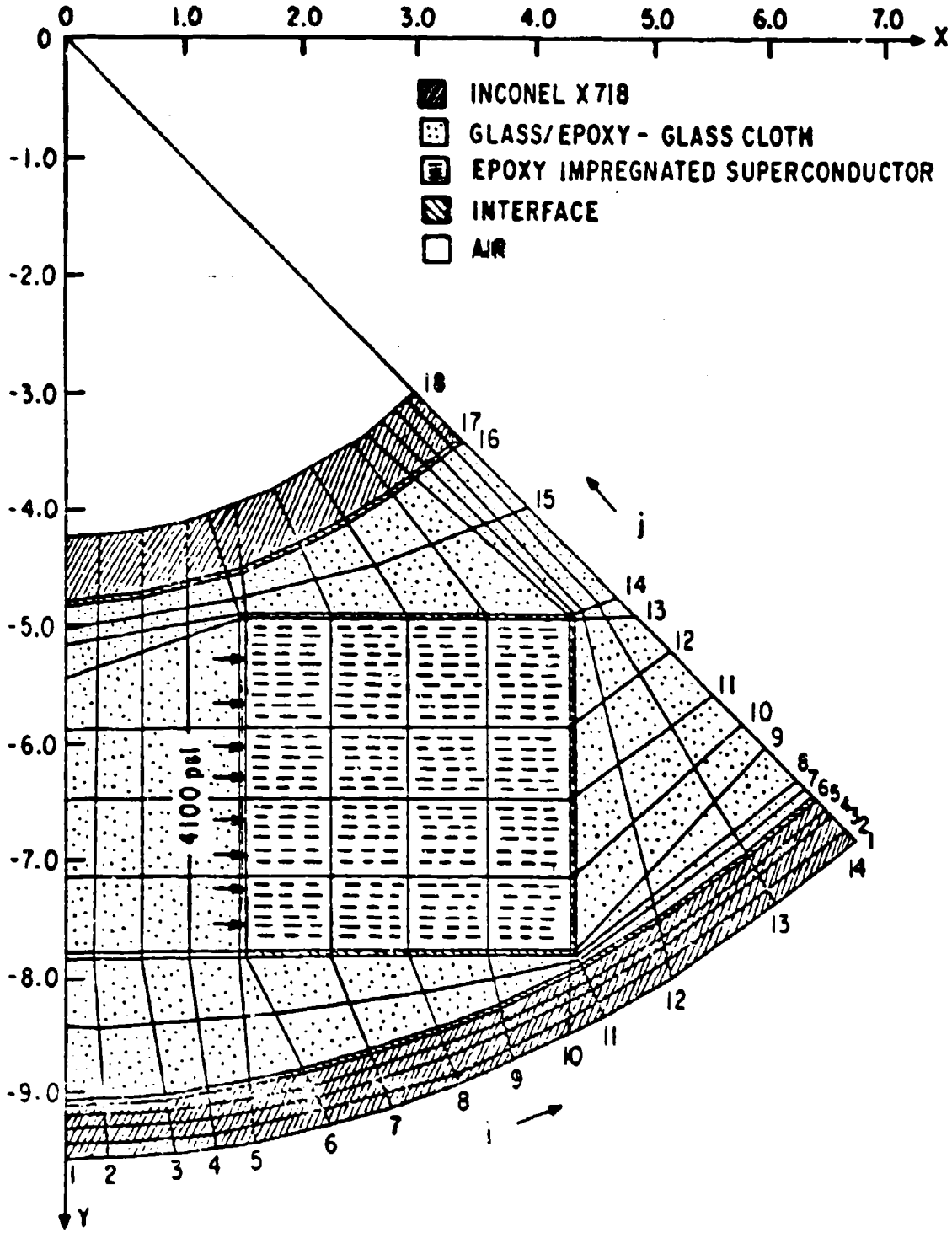

Figure 10. Finite Element Analysis for Winding and Support System (from Reference 3)

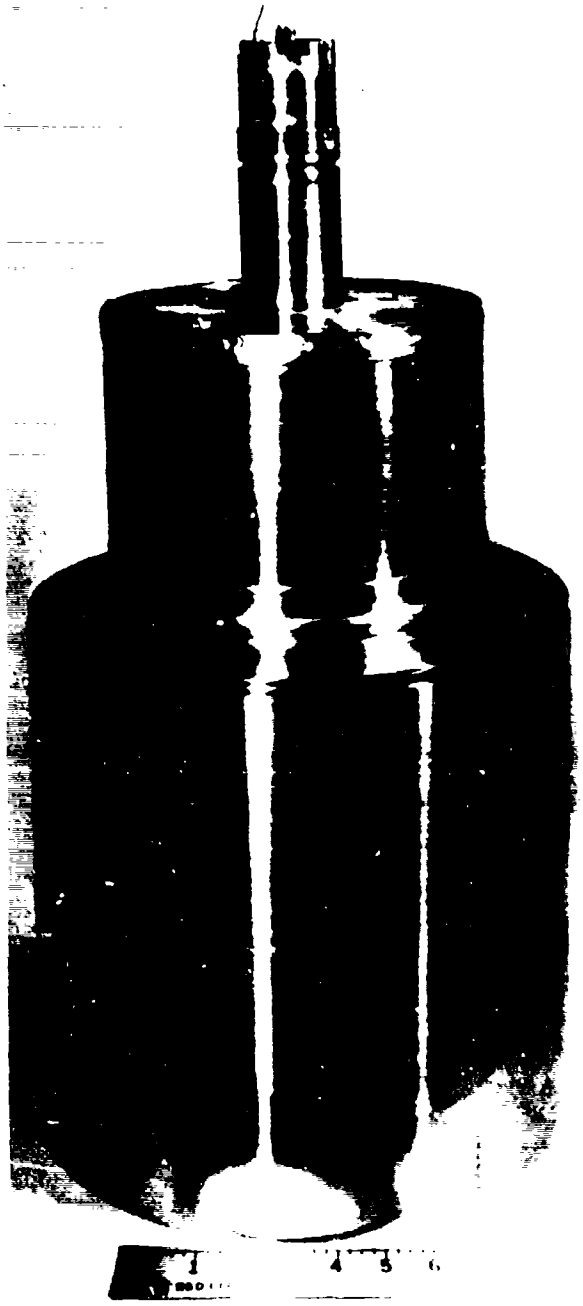

Figure 11. Centrifugal Shell End Flange and Stub Shaft Assembly

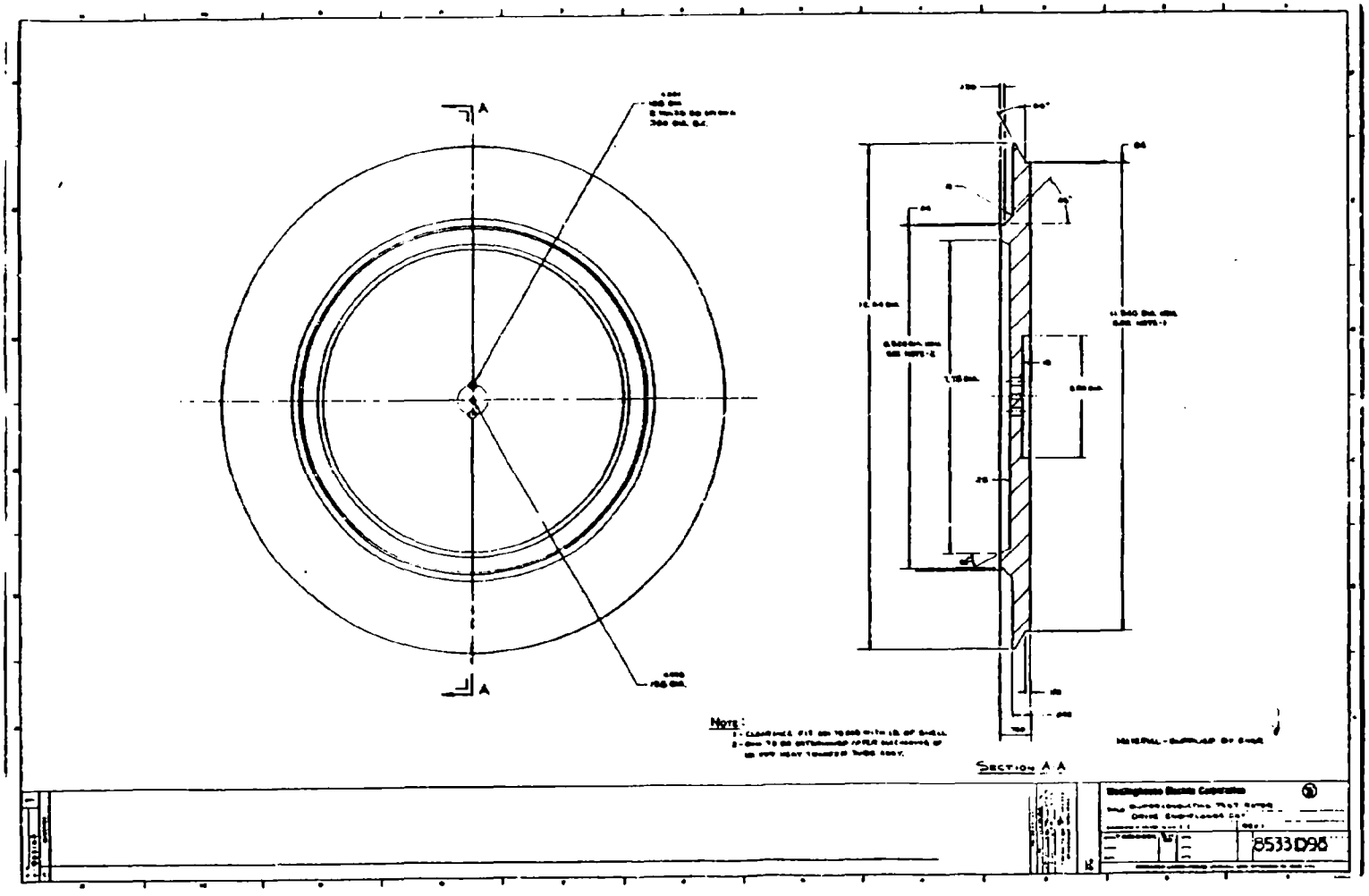

Figure 12. Drive End Flange Detail

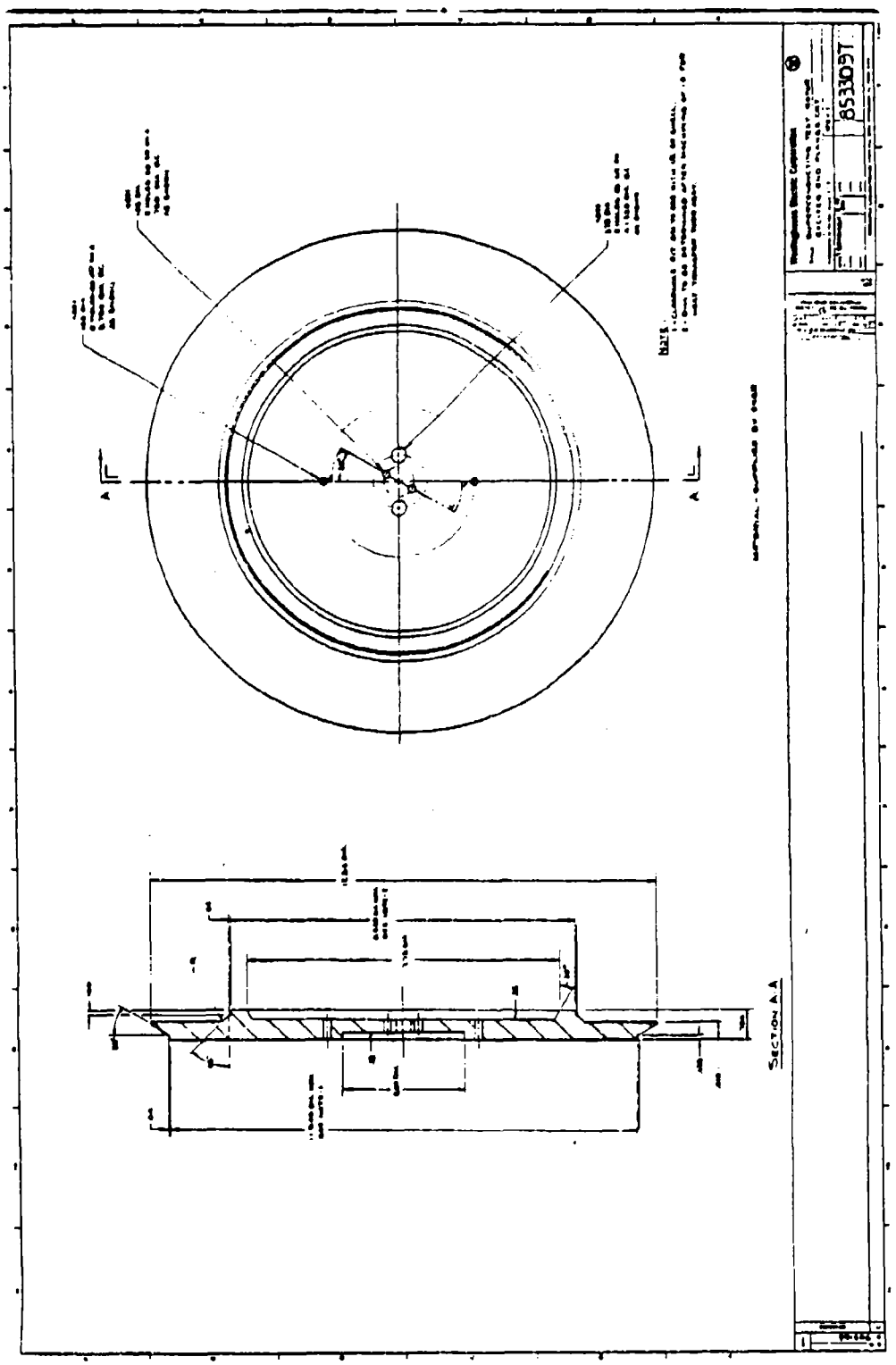

Figure 13. Exciter End Flange Detail

(4) Vacuum Shells

The vacuum isolation for the RTF is maintained by a stationary fiberglass shell supported by the two bearing support stands. Consistent with the earlier spin-test effort a second shell is placed over the inner one to form a "dewar" like configuration. Liquid N_2 can then be placed in the volume between the two shells. The design approach for the present RTF benefited from the past experience with the spin-test. The O-ring seal on the end supports is placed on the inner bore which eliminates any liquid N_2 leakage into the vacuum space.

A detailed drawing for the shells is shown in Figure 14. These shells were filament wound to the desired dimensions, i.e., diameter and thicknesses and the lengths adjusted by machining. To minimize the machining for the end spacers the inner shell was filament wound with a step with sufficient material for adjusting the spacer length and OD.

(5) Exciter Modification

The exciter coil winding slip rings for the previous "Spin-Test" rotor were originally designed for ~ 250 to 300A operation. Modification to this slip ring system is necessary to allow operation at the new design current level of ~ 900A. In addition, the slip rings must be able to obtain even higher current levels to evaluate the Nb_3Sn critical current margin.

Inspection of the slip ring system indicates that higher current operation is presently limited by the copper feed throughs from the outer rubbing surface to the inner bus bar collection. Additional copper feeds must be installed to provide higher current capability. A basic redesign to accommodate the increased current was performed and modifications were made to the slip ring system.

2. Superconducting Dipole Test Coil Design

In Section 2.1.1 the base winding design for the RTF was presented. This design assumed a uniform current density of 1.5×10^4

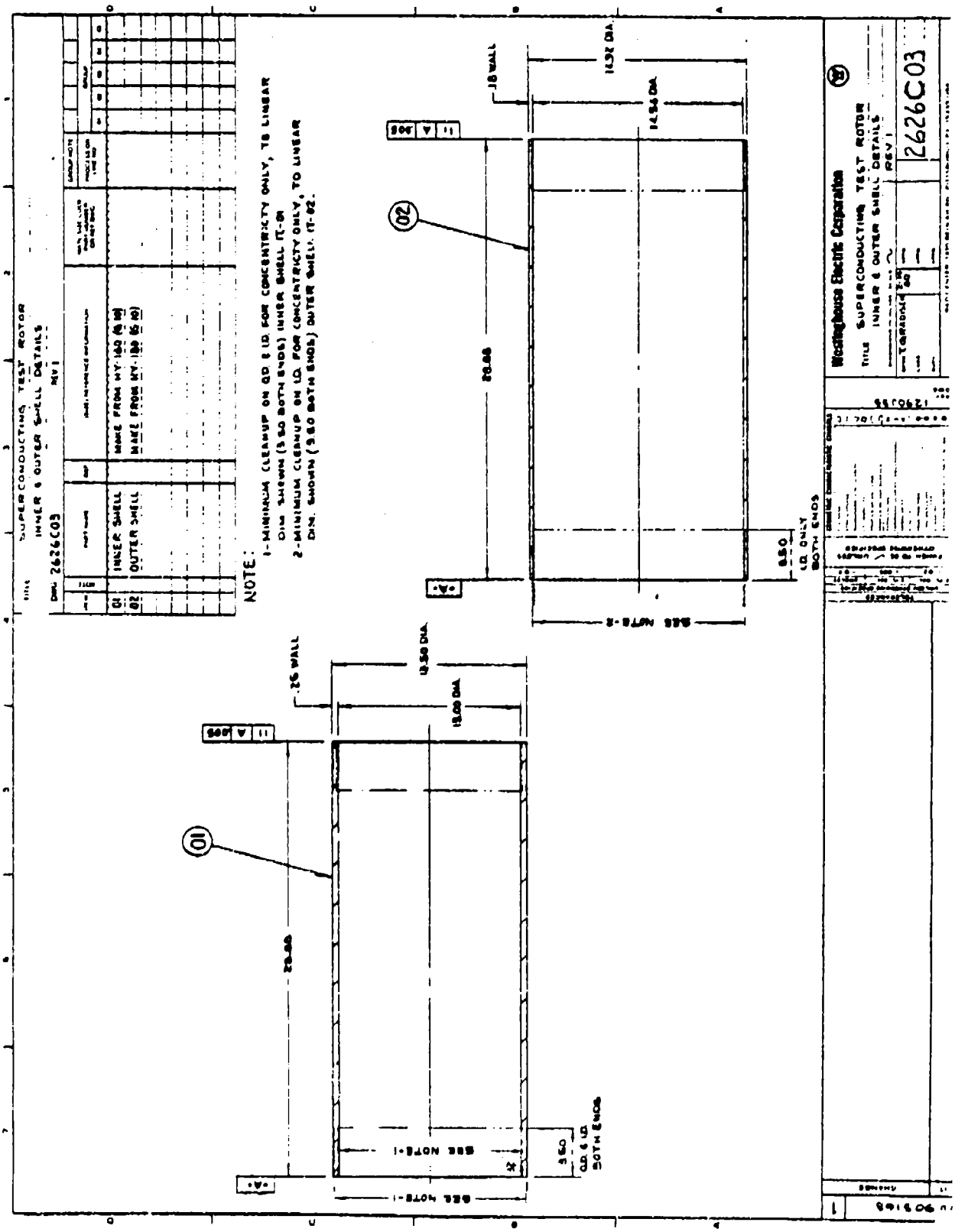

Figure 14. Vacuum Shell Detail

A/cm^2 with a peak field objective of 6.8 tesla. A 2" racetrack coil, with a 2.85" x 2.85" cross section and 10" overall length was selected as the design configuration. The layout drawing for this coil design is shown in Figure 15. In order to satisfactorily fabricate this coil a number of preliminary tests were required.

A specific cross section, i.e., 2.85" x 2.85" can only be achieved if the exact turns per layer and layer build are accurately known. This information can only be obtained by trial winding with a conductor nearly identical to the actual superconductor. In addition the terminations for the start and finish of the coil must be consistent with the winding procedure. Finally the winding fixture and subsequent impregnation process must be experimentally verified. All of these fabrication details can be evaluated by actual winding of a dummy or prototype coil.

Winding trials were thus carried out to produce a circular coil with a cross section at the design value of 2.85" x 2.85". A 6 x 1 dummy conductor was specifically fabricated for these trials. Copper-nickel was used for the strands with molybdenum for the core. A braided S-glass insulation was applied to each strand.

Fabrication of a circular coil would provide the necessary guidance for winding the final racetrack coils. Prior to winding the racetrack coils a second "dummy" coil in the racetrack configuration would be wound and impregnated. This second dummy coil would serve as a final verification of the fixturing, terminations, winding procedures, and impregnation process.

a. Conductor Design

The Nb_3Sn conductor development program carried out at IGC under USAF sponsorship was aimed at providing high current, low loss superconductor for use in airborne generators. The heating in the conductor produced by the fast ramp-up to full field must be minimized in order to maintain the superconducting state. It was recognized

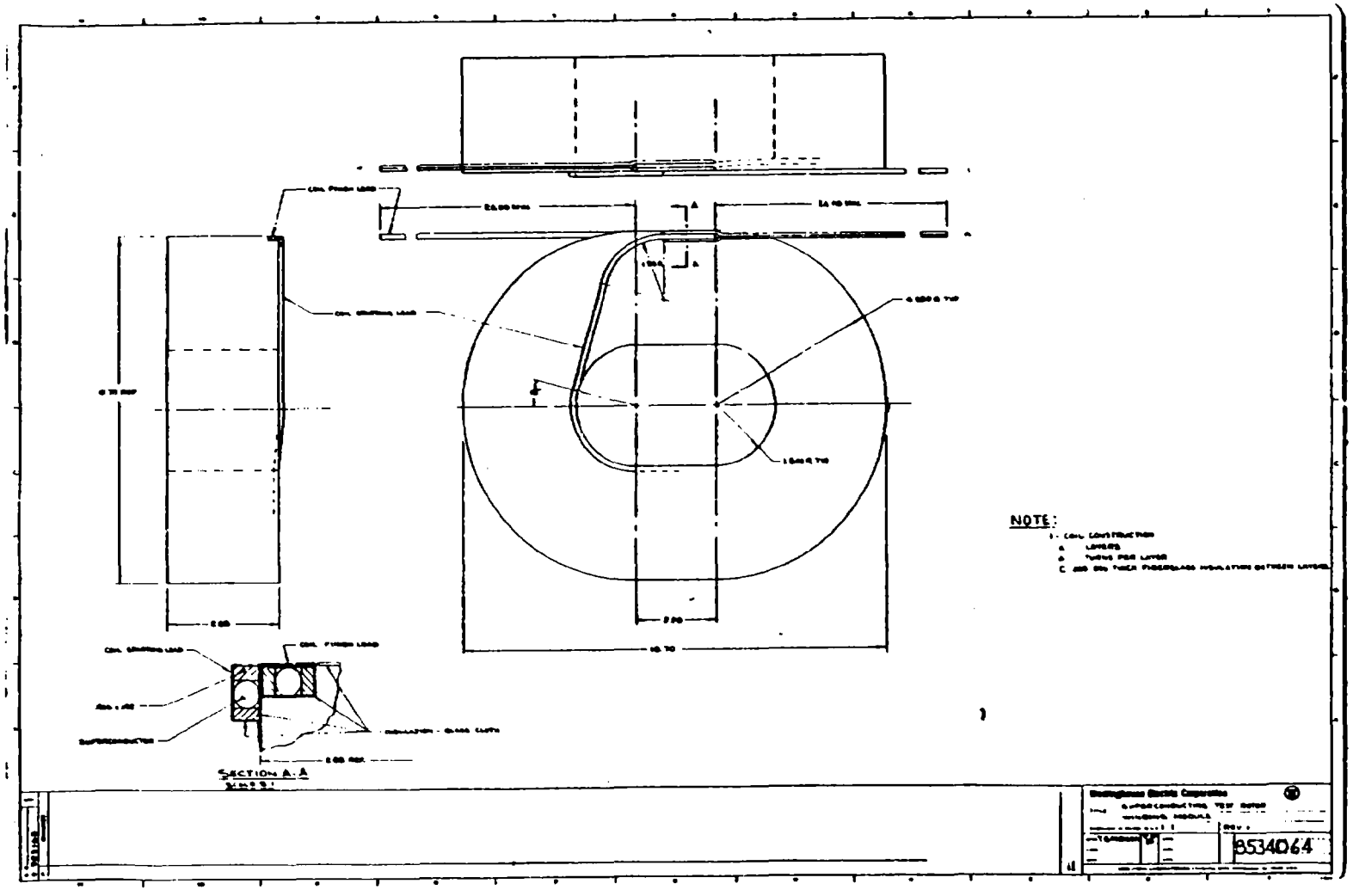

Figure 15. Superconducting Test Coil Detail

through theoretical calculations and experimental measurements that in order for the conductor to have sufficiently low losses at rated current a cable configuration would have to be used. The strands used in making the cable should have fine filaments to minimize hysteresis losses and strand-to-strand insulation is required to reduce or eliminate eddy current losses caused by coupling currents between strands. The cross-section of the strand configuration produced at IGC for this program is shown in Figure 16. The conductor contains 24,480 filaments which are contined n a bronze core surrounded by a tantalum diffusion barrier. The filaments are approximately 2.0 μm in diameter. Outside the tantalum barrier is the stabilizing, high conductivity copper which comprises 48% of the cross-section. The conductor is made by the standard bronze process. The tantalum fins projecting into the copper have the purpose of reducing eddy current losses in the copper sheath. However, it was determined by measurements on a similar conductor that the fins do not affect the losses. IGC elected to retain the fins in the final design for reasons of processing consistency.

The ac losses measured[13] in strands of the IGC Phase 2 conductor indicated that the hysteresis losses may be characteristic of the filament sub-bundle size and not the filaments themselves. The degree of contact between filaments within sub-bundles which leads to the enhanced losses is determined by the degree of reaction. In the Phase 2 strands it was found that a reaction time at 650°C sufficient to convert 80% of a filament to Nb3Sn would not lead to a significant increase in losses. It is expected that these results on Phase 2 strands can be extrapolated to obtain the loss characteristics of the present conductor.

The preferred design of a cable configuration using six superconducting strands around a central molybdenum core is shown in Figure 17. The characteristics given in Figure 17 were for the IGC strand design at the time of the G.E. Phase I report (reference 3) in August, 1977. The conductor supplied for one coil to be made on the present program is the same cable configuration but uses the strand of

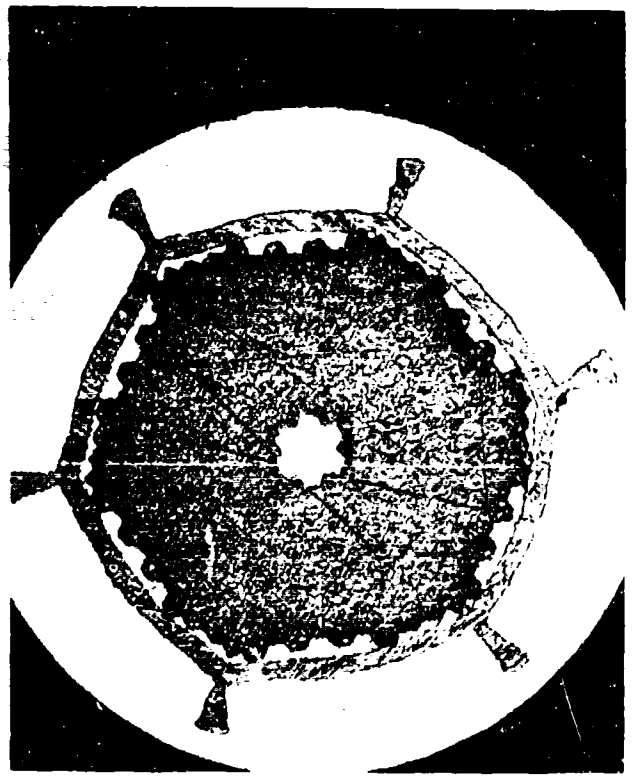

Figure 16. Conductor Cross Section at 100X

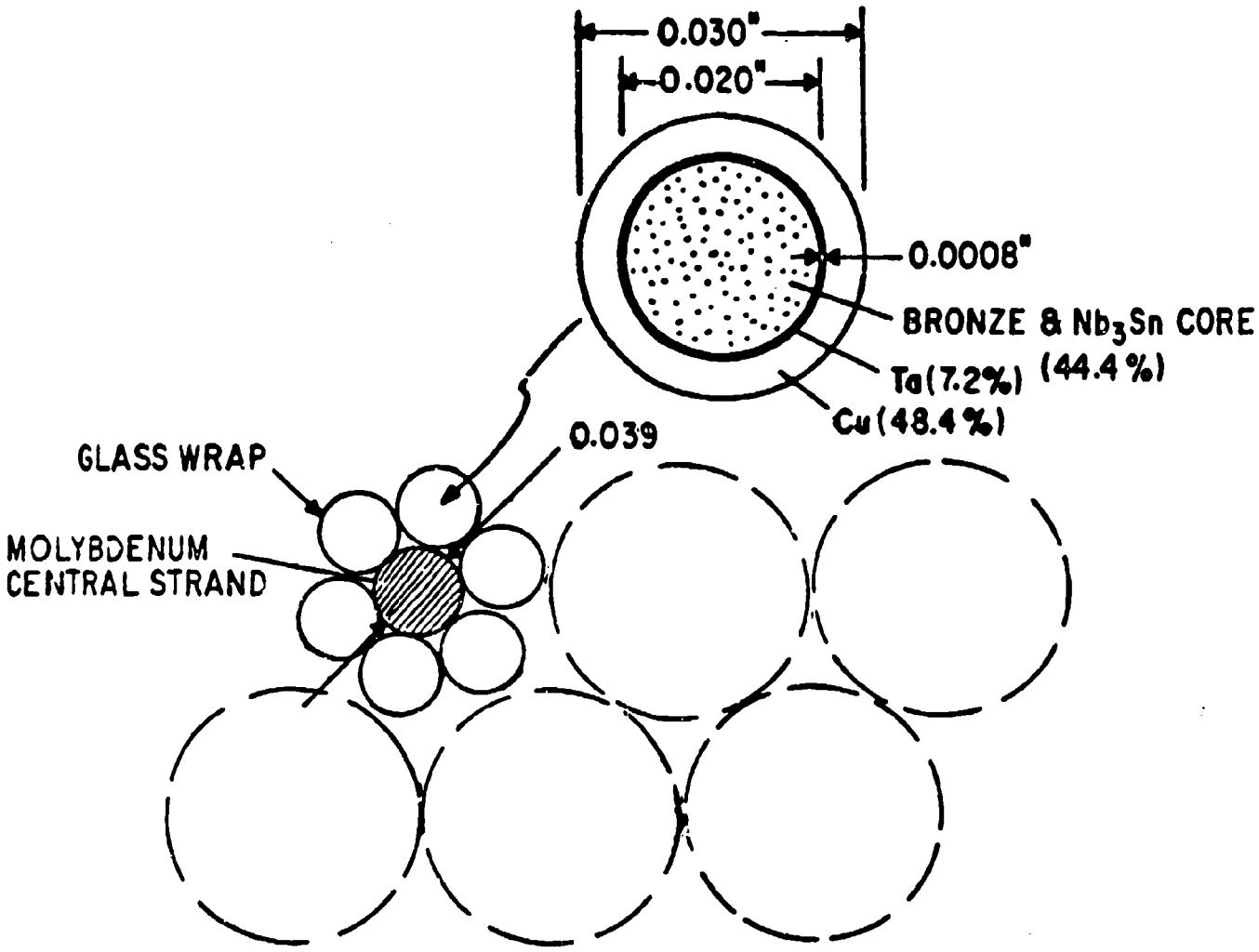

BRONZE AND Nb_3Sn MODULE PACKING FACTOR = 0.211

OVERALL CURRENT DENSITY = 15,000 A/cm^2

BRONZE AND Nb_3Sn CORE CURRENT DENSITY = 7.11×10^4 A/cm^2

T_c = 8.4K (at 6.8 Tesla)
= 9 K (at 6 Tesla)

Cu FRACTION OF THE MODULE = 0.23

CABLE CURRENT = 864.6 AMPERES

LOSSES FOR A ONE SECOND RAMP TO 6.8 Tesla = 24.5 mJ/cm^3 (in the strand)
= 11.75 mJ/cm^3 (in the module)

Figure 17. Cable Design from General Electric, Phase I Report

Figure 16 with 0.038" diameter rather than 0.030". S-glass wrap on each strand is used for insulation as well as over the outside of the cable. Breakage during processing limited the strand lengths so IGC was able to make sufficient lengths of this conductor strand to provide only 690 ft. of cable with no joints. In addition, shorter lengths were produced which were butt resistance welded at Westinghouse and cabled at IGC to produce 670 ft. of cable. (See Appendix E for a description fo the welding procedure and results.) Instead of S-glass, Cu_2S was used as strand insulation and an S-glass wrap was used as cable insulation. This cable was used to construct a second coil.

(1) Conductor Verification

The General Electric specification for current density, listed in Figure 17 for 0.030" strands, translates to a minimum of 254A per 0.038" strand at 10T and 4.2°K. IGC performed heat treatment studies to optimize the current density and provided data that indicated at 10T and 4.2"K the strands would have I_c = 343A when unstrained, I_c = 240A when bent on a 3 inch diameter, and I_c = 328A when bent on a 3 inch diameter and restraightened. These and other data provided by IGC for the 0.038" strands are shown in Figure 18. Also included are data on 0.030" strands. It was expected that the current would not be degraded as much when the cable is bent on a 3 inch diameter, so the projected critical current for the cable configuration should be in excess of the specification.

In order to determine the effect of the butt resistance welded joints on the current characteristics of the strands, we obtained unreacted short lengths of conductor, made welded joints, and reacted the joints along with other short lengths of conductor containing no joints. The reaction procedure was prescribed by IGC before their optimization studies and the critical current was significantly less than shown in Figure 18. The joints were found to be superconducting up to about 25% of the critical current values in the parent wire. Figure 19 shows the values of Ic obtained for the IGC wires reacted at

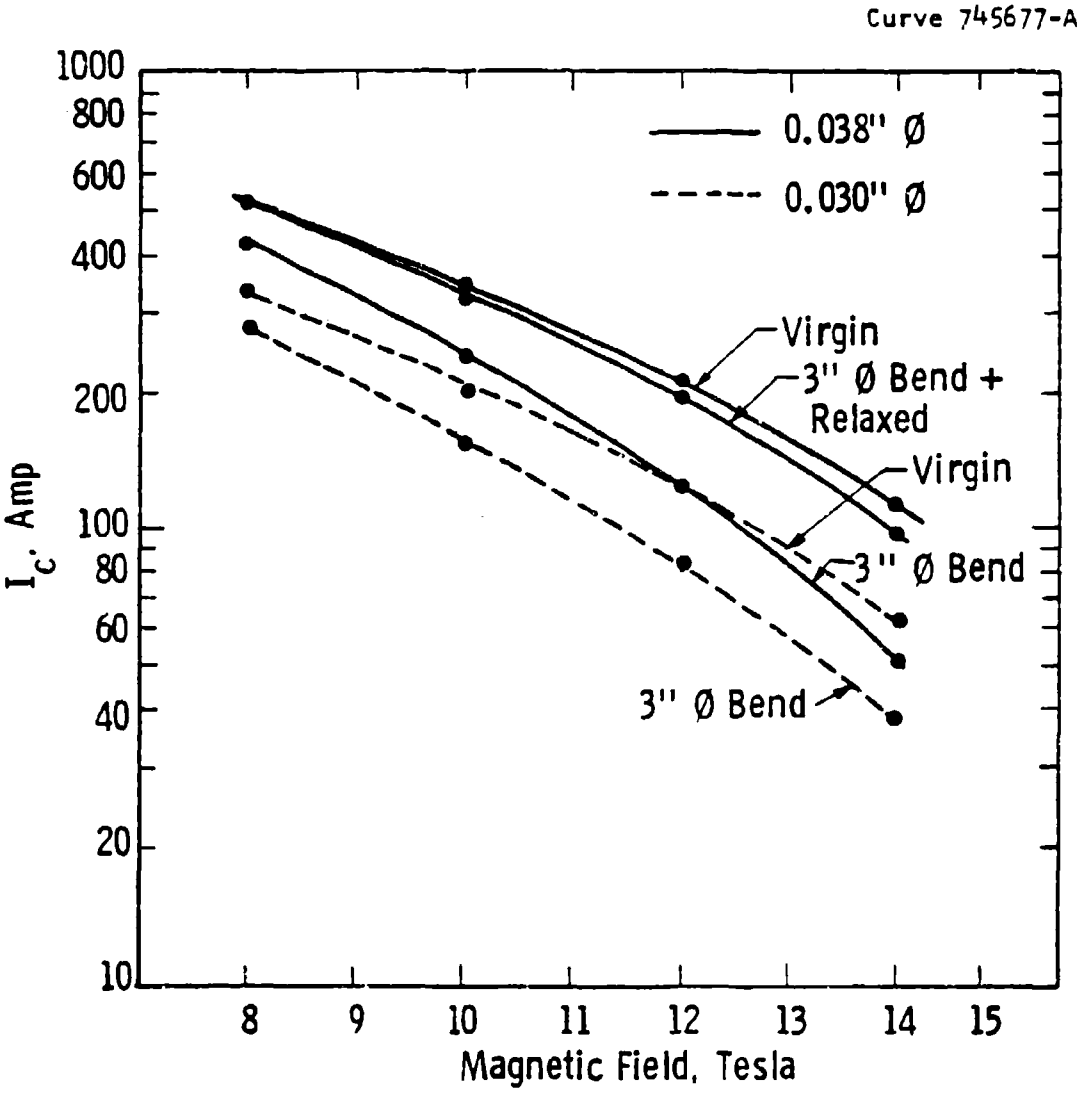

Figure 18. Ic vs H from IGC Data for Optimized Heat Treatment

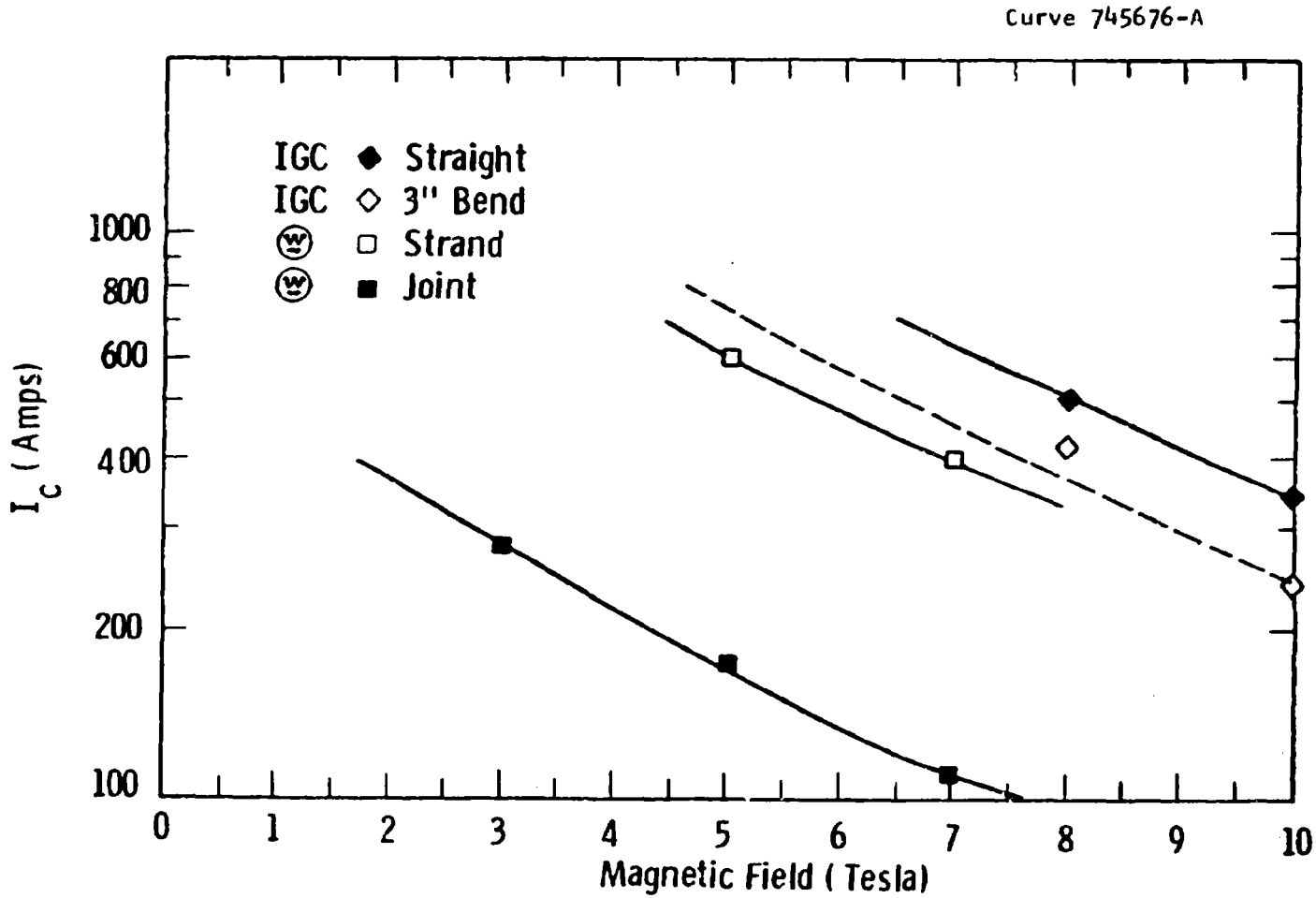

Figure 19. Ic vs H for Strands and Butt Resistance Welded Joints

Westinghouse and the current limit of superconductivity for the joints. For reference we have also plotted the I_c values obtained by IGC on their optimized conductors. At 7T the joint resistance when normal was found to be 1.4×10^{-6} ohms.

The two cables supplied by IGC were tested for short sample critical current at Westinghouse. Samples of 33 cm length were bent around a G-10 disc 10 cm in diameter and 2 cm thick which has copper current contacts attached to the circumference into which 7 cm of each end of the conductor were soldered. The disc was oriented horizontally in a 13 cm bore solenoid which provides a vertical magnetic field with an upper limit of 5T. The field and current were oriented so that the force on the conductor was directed toward the center of the disc. The S-glass was removed from the samples before mounting. In the case of the cable which had S-glass on each strand, this was removed also in order to solder the current leads. The Cu_2S was removed with HCl in the region of the soldered current leads.

At a field of 5T the Cu_2S insulated cable showed a resistive onset which was reproducible, but a quench every time at 0.3 μV/cm and a current level of 4375A. The cable with S-glass insulated strands did not show a resistive onset, but exhibited unstable behavior. Several runs were made and the highest quench current attained was 4425A. Using the data of Spencer et al.[14] and a value of 4400A as an average for the two cable the extrapolated value of current at 7T is 3114A. From Figure 18 we find a predicted cable current at 7T of approximately 3200A using the bent strand data and approximately 3600A for the virgin strands. Our data would indicate that the strands in the bent cables behave very much like bent single strands.

The original design of the two coils to be constructed and tested on this program called for 728 turns to produce 7T at $\approx 10^6$ A-turns. The operating current in the cable would be approximately 1374A. Since the IGC data predicts $I_c > 3200$A at 7T, a large margin would have been available in the coils. In order to produce the same

field with the shorter lengths of cable provided by IGC, which yield only 378 turns, the current requirement is 2645A. Although our data indicates that the coils should be able to produce 7T at this current, they will be operating at 83% of I_c.

The coil wound with the Cu_2S insulated strands has one joint per strand. Figure 19 shows that if the joints are in a field of less than about 1.5T they will remain superconducting at the operating current of 440 A/strand. During winding the joints were placed as far from the center of the coil as possible, but it is not known for sure what field level they will experience. If the joints do normalize, at operating current the heat generated will be 0.27 watts/joint. This will, of course, have some adverse effect on the stability of the coil. However, we expect that current sharing will occur if a joint normalizes and the heating will be less than the maximum.

(b) Circular Coil and Termination Design and Development

The basic approach or desired objective for the termination was to provide a system for anchoring the external lead to the coil module. This mechanical system should be capable of accommodating the thermal contraction and all handling and bending etc. which would occur following the final impregnation. The test coils would be first tested statically and subsequently installed in the coil support structure for the rotating tests. These operations could impose severe stresses to the coil module and without proper support of the termination could lead to possible degradation of the coil current carrying ability.

A number of potential termination designs were thus constructed and tested to evaluate fabrication, impregnation procedures, and resultant mechanical integrity. A special "termination" fixture and impregnation block was constructed for these tests. The selected termination design is shown in schematic form in Figure 20. The 6 x 1 Nb_3Sn cable insulation must be completely removed for the termination

Dwg. 9355A63

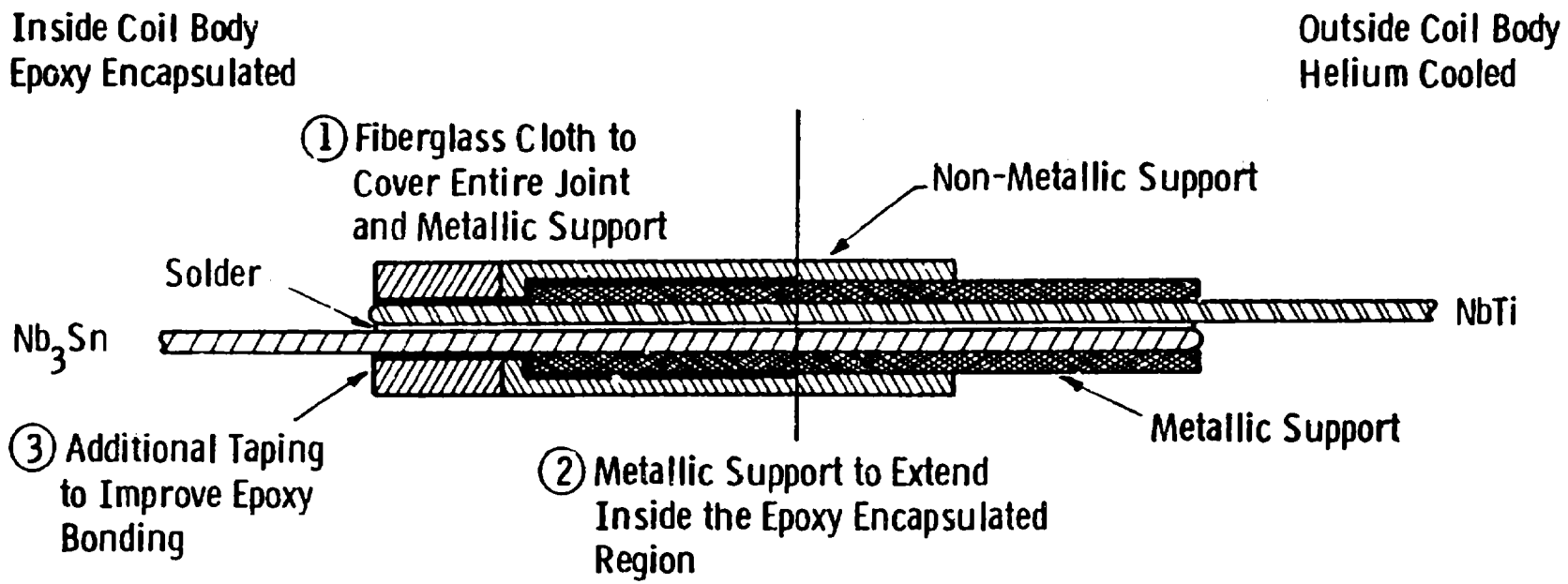

Figure 20. Lead Transition Conceptual Design

tests. The cable is then soldered in a copper channel between two lengths of Nb-Ti monolithic copper stabilized superconductor. This entire assembly is then positioned in a recessed slot in the winding fixture. Fiberglass cloth is first placed in the slot and then wrapped over the joint for additional support. The copper channel is designed to extend beneath the coil surface to provide high mechanical rigidity to the joint. The copper channel also extends into the helium bath in the final coil support structure which provides optimum cooling to the joint region. Following the trial termination tests an actual superconducting joint was fabricated using this design approach and the low temperature resistance measured.

An actual mock-up of the joint concept was constructed using Airco multifilament Nb3Sn conductor. This conductor is basically identical with the Intermagnetic General Corporation Air Force design with respect to strand size, a six-around-one cable, twist and current, and field dependence. The only difference occurs in the insulation system for the overall cable. IGC uses an individual fiberglass wrap on each strand whereas Airco has utilized the Westinghouse developed CuS insulation on each strand. After reaction of the six-around-one cable, Airco then applies a fiberglass wrap over the complete cable. The preparation of the joint requires complete stripping of the insulation system for either conductor.

The joint mock-up was tested in a long dipole coil at transverse fields up to ~ 3T and current levels sufficient to measure the actual resistance of the joint. Ordinary copper blocks were used for terminating the superconductor at each end to deliver the high current. The entire assembly was rigidly mounted on a fixture and immersed in liquid helium.

Figure 21 shows the completely fabricated superconducting joint mounted in the copper channel.

At 3T and a current of 1200A no resistance was detected which indicates with the equipment sensitivity a resistance less than $10^{-9}\Omega$.

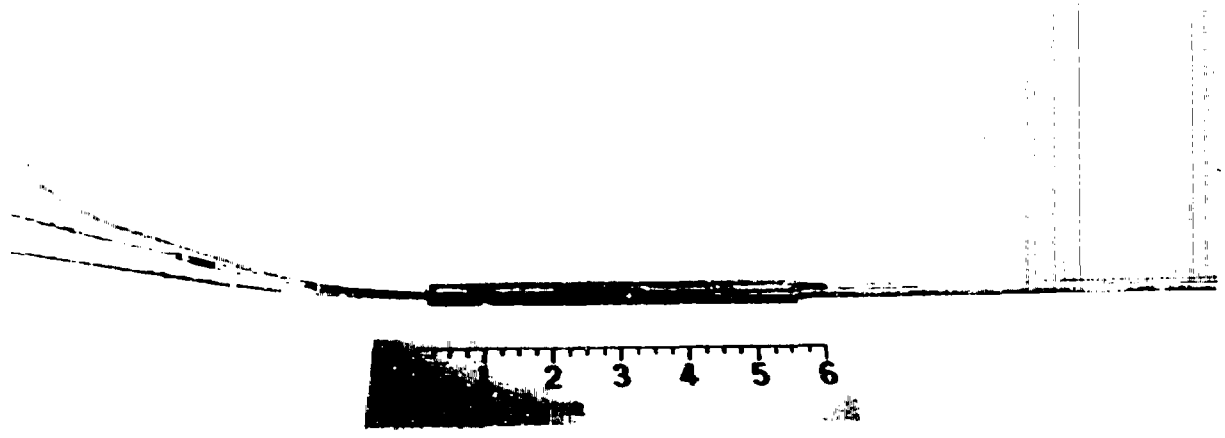

Figure 21. Lead Transition Mock-up

A review of the field calculations indicate at full design current that the field strength in the joint region should be no greater than 2T. Since the proposed joint configuration was tested at 3T at currents in excess of the design current and showed no observable resistance, the joint concept as tested should be completely adequate for incorporation in the final racetrack coil construction.

(c) Circular Coil and Dummy Racetrack Coil Fabrication and Test

(1) Circular Coil

A circular coil was fabricated to evaluate the basic winding question related to the optimum cross section based on the conductor placement during actual winding. These trials showed that the turns per layer and layer build for the final racetrack coil will come quite close to the design cross section of 2.85" x 2.85".

The circular coil was wound using heat treated dummy conductor to evaluate the insulation integrity of the individual strands which were insulated with an S-glass braid. A braiding operation requires an organic sizing on the glass fibers to accommodate the high friction produced during the braiding operation. The subsequent heat treatment to react the Nb_3Sn would decompose the sizing leaving a carbonaceous residue on the braided S-glass. Electrical testing on the circular coil was thus performed to evaluate the effect of the carbonaceous residue on the coil insulation. Since the residue might also affect the epoxy wetting, the coil was subsequently sectioned to evaluate the impregnation process.

The circular coil also included mock-ups of the carbon/carbon-glass thermometers to evaluate lead placement, winding impact and its own potential for compromising the basic insulation system.

The fully impregnated circular coil which was wound with heat-treated dummy conductor was tested for insulation integrity in the following manner.

The resistance per unit length of dummy conductor was measured. Based upon this result, the resistance of the circular coil was calculated to be 1.13Ω. The start and finish leads for the coil were tinned and a resistance of 1.10Ω was observed. This value is quite close to the ideal resistance hence it appears that there are no shorted turns.

Following this test, the tinned portions on the start and finish leads were cut off; the strands separated and the insulation resistance between strands evaluated. These resistance measurements were compared with the ideal strand resistance which indicated that some strand-to-strand shorting was occurring along the length of the dummy conductor. It is clear that this type of shorting will not influence the overall charging characteristics of the completed coil. Inductance measurements of the circular coil basically confirm this conclusion since the measured inductances were consistent with calculated values.

The observed strand-to-strand shorting should only influence the ac loss performance of the conductor. Moreover since the shorting is random, this influence most likely should increase the overall ac losses by only a factor of two. A worst case in which the strands were completely shorted to the core should increase the ac losses an order of magnitude. The anticipated degradation in ac loss performance for the conductor due to random strand-to-strand shorting should not produce any serious problems with respect to cooling the winding under operating conditions.

The thermometer leads basically survived the winding and impregnation process. The coil handling during the electrical tests however showed the leads to be mechanically weak with at least half of them breaking off at the coil interface. The thermometer leads were supported by several different methods: Teflon tubing, fiberglass tubing, additional parallel copper conductor and a small spring like enclosure. Of these methods the Teflon tubing appeared to offer the

most promise. An improved design will be attempted for the dummy racetrack.

(2) Dummy Racetrack Coil

The remaining effort on the test coil design was directed at the winding and impregnation of a dummy racetrack coil. All of the fixtures and procedures for winding this coil were derived from the circular coil fabrication. The dummy racetrack coil included mock-ups of the thermometers as discussed in the previous section. The selected design configuration or the Nb_3Sn cable termination was also incorporated into this winding.

A full-size dummy racetrack coil was wound and fully impregnated. This coil thus represents the last step in evaluating the winding procedure, lead concept, and conductor insulation system. The fully impregnated coil with the Nb_3Sn-NbTi lead transition is shown in Figure 22. Figure 23 shows the opposite face of the coil which features the sensor leads.

After removal from the potting fixture, the coil was examined for bubbles, epoxy crazing or any other visual problem. This examination indicated the winding and epoxy system to be in excellent condition. The coil was then cycled to liquid nitrogen temperature and reexamined. Minor epoxy crazing was observed after thermal cycling on the inner bore surface along the racetrack. This crazing was attributed to a high build-up of epoxy in that region without sufficient fiberglass reinforcement. Additional fiberglass will be placed in this region in the final coil winding which should eliminate any crazing of the epoxy. This overall problem, i.e., lack of fiberglass, was related to a natural bow in the conductor caused by the short racetrack length. Some difficulty was observed during winding with maintaining a completely straight section along the short racetrack length. After the first layer, even with high tension, the wire was observed to naturally bow out along the straight length. Additional tensioning and fixturing was

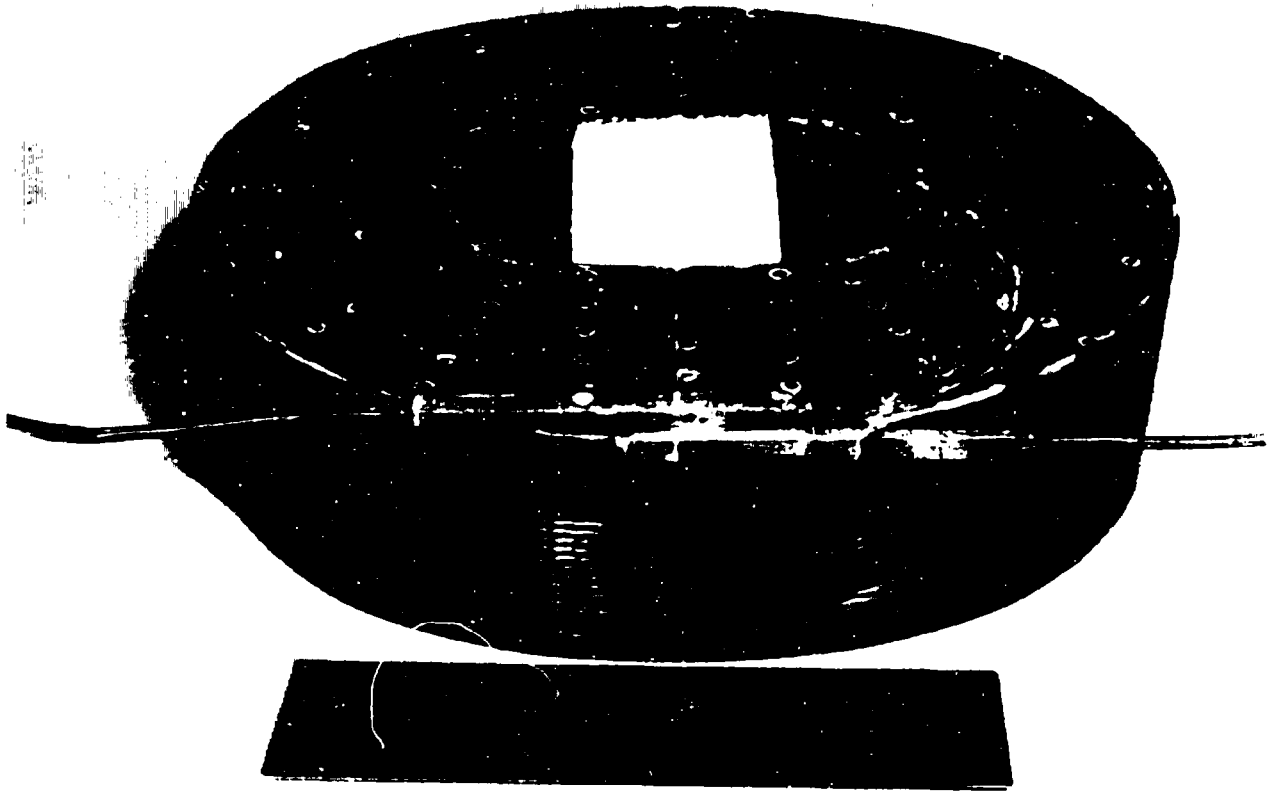

Figure 22. Dipole Test Coil - Lead Transition Face

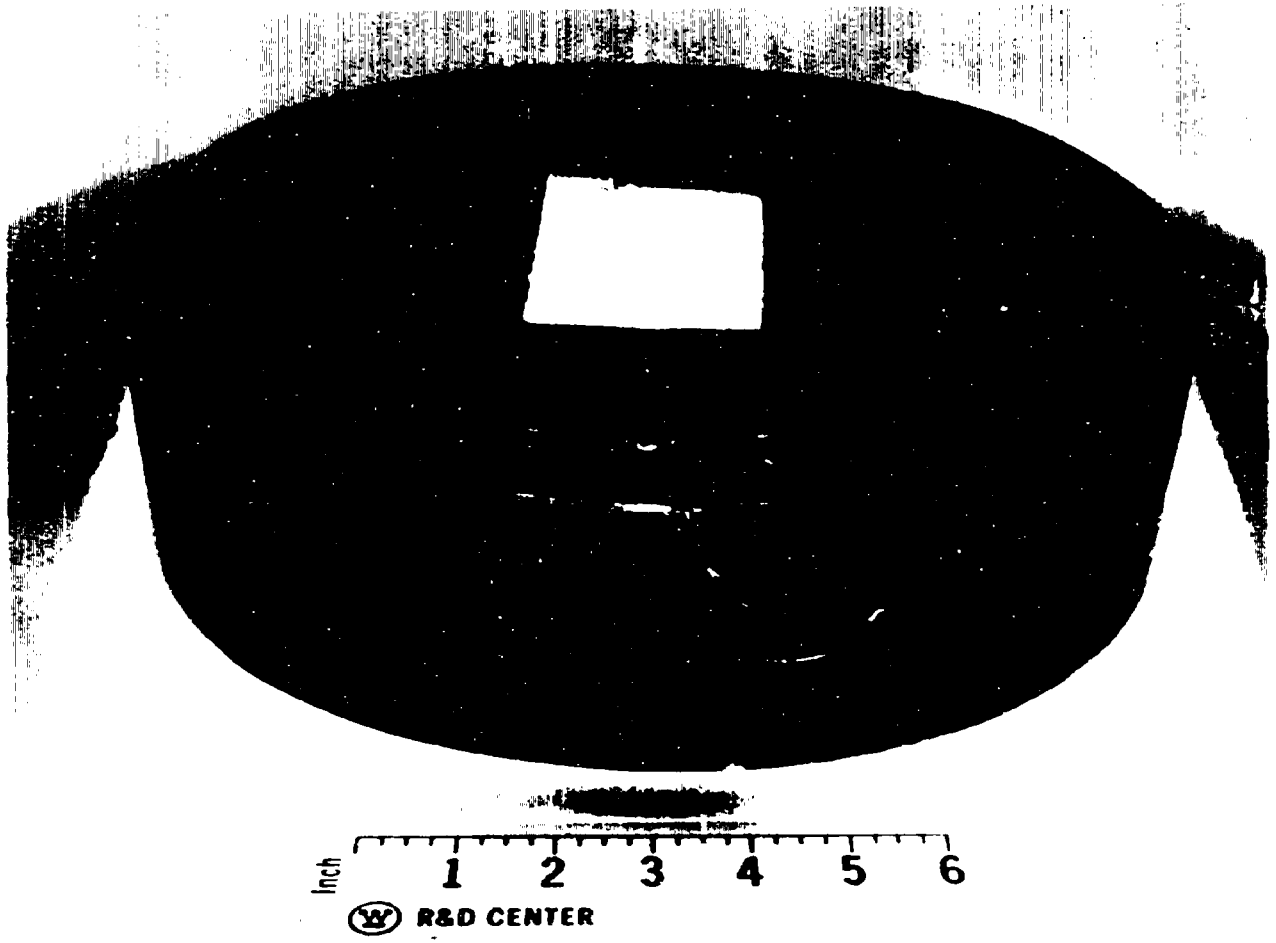

Figure 23. Dipole Test Coil - Sensor Face

not practical, hence the resulting slightly oval configuration was accepted. The final oval shape resulted in an approximately 0.080 per side additional build along the racetrack which will be accommodated by relieving the side covers of the coil support structure.

Detailed tests were then performed on the coil/conductor insulation system as a function of temperature and the coil field profile was also measured. The field profiles as measured are shown in Figures 24, 25, and 26 which were obtained with a sensitive gauss-meter at low current excitation (~ 3A) in the dummy coil. It is clear from these observed plots that the coil is showing field profiles characteristic of a racetrack coil. The slightly oval configuration thus does not appear to markedly influence the desired racetrack field configuration.

The resistance and inductance of the coil was then measured from room temperature to helium temperature. These measurements were compared with theoretical values for the dummy conductor which in turn would provide some insight into the basic insulation system on the cable conductor.

A measurement of the dummy conductor showed the following values:

Room Temperature - 0.01218 Ω/ft.

Liquid Nitrogen - 2.29×10^{-3} Ω/ft.

Liquid Helium - 7.0×10^{-4} Ω/ft.

These above resistance values were obtained on a length of dummy conductor by soldering current and voltage leads to two ends of the cable. The resistance values were then multiplied by the total length of conductor in the dummy racetrack (1,357 ft.) to obtain the theoretical resistance for the coil. These theoretical values are compared in Table 4 with the actual measured resistance of the coil.

Curve 745673-A

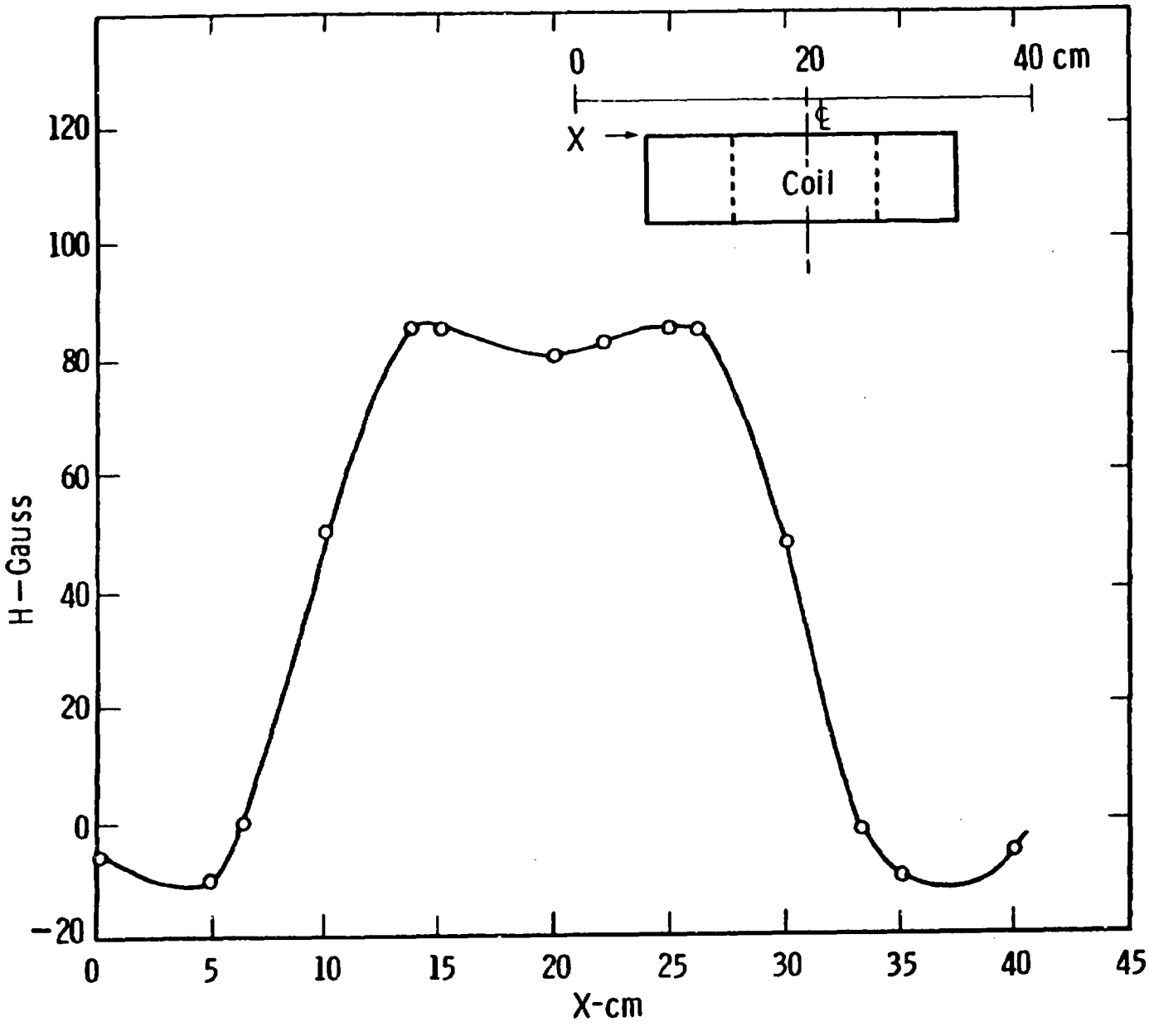

Figure 24. Dipole Test Coil Field Profile - Longitudinal

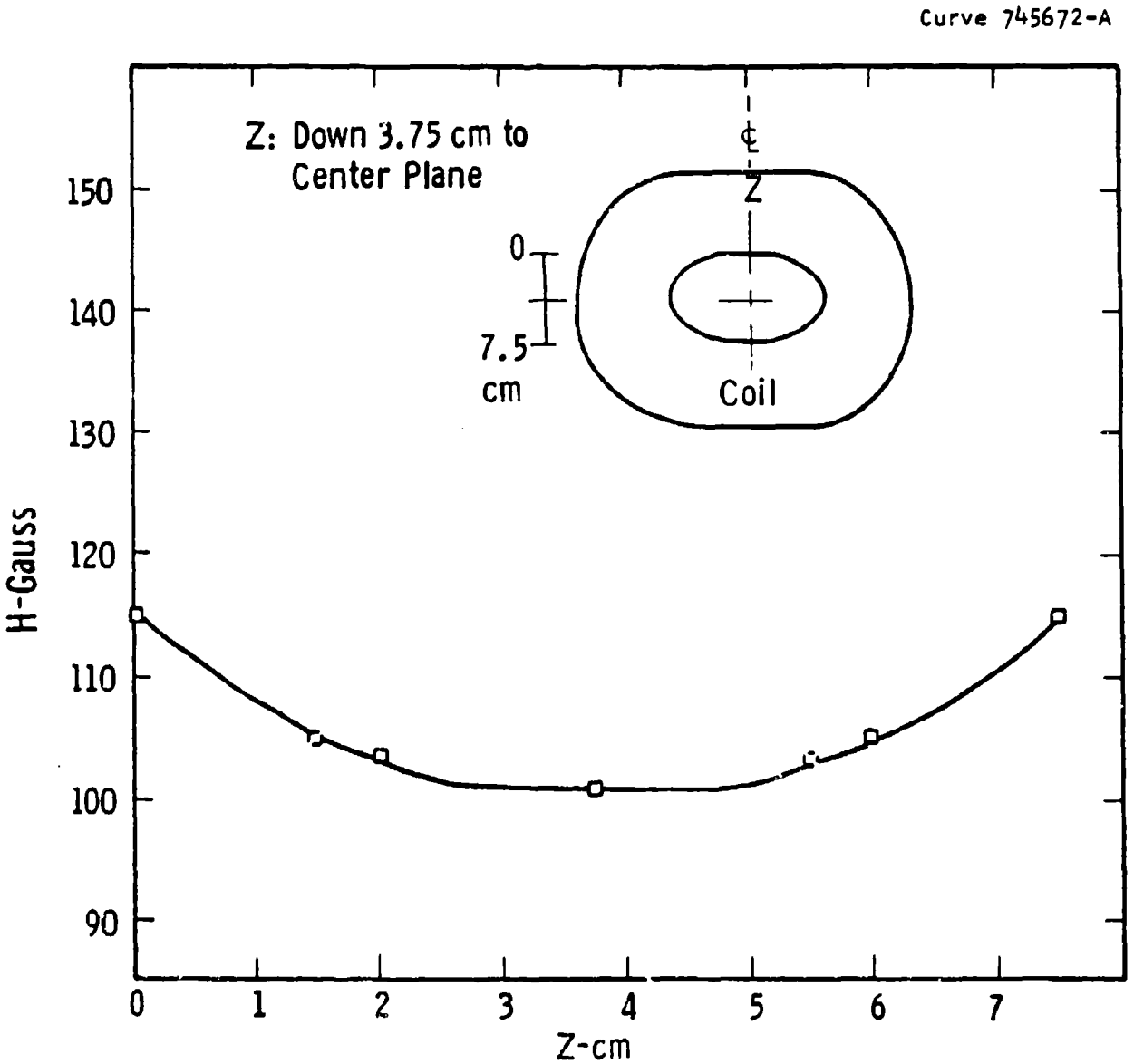

Figure 25. Dipole Test Coil Field Profile - Vertical

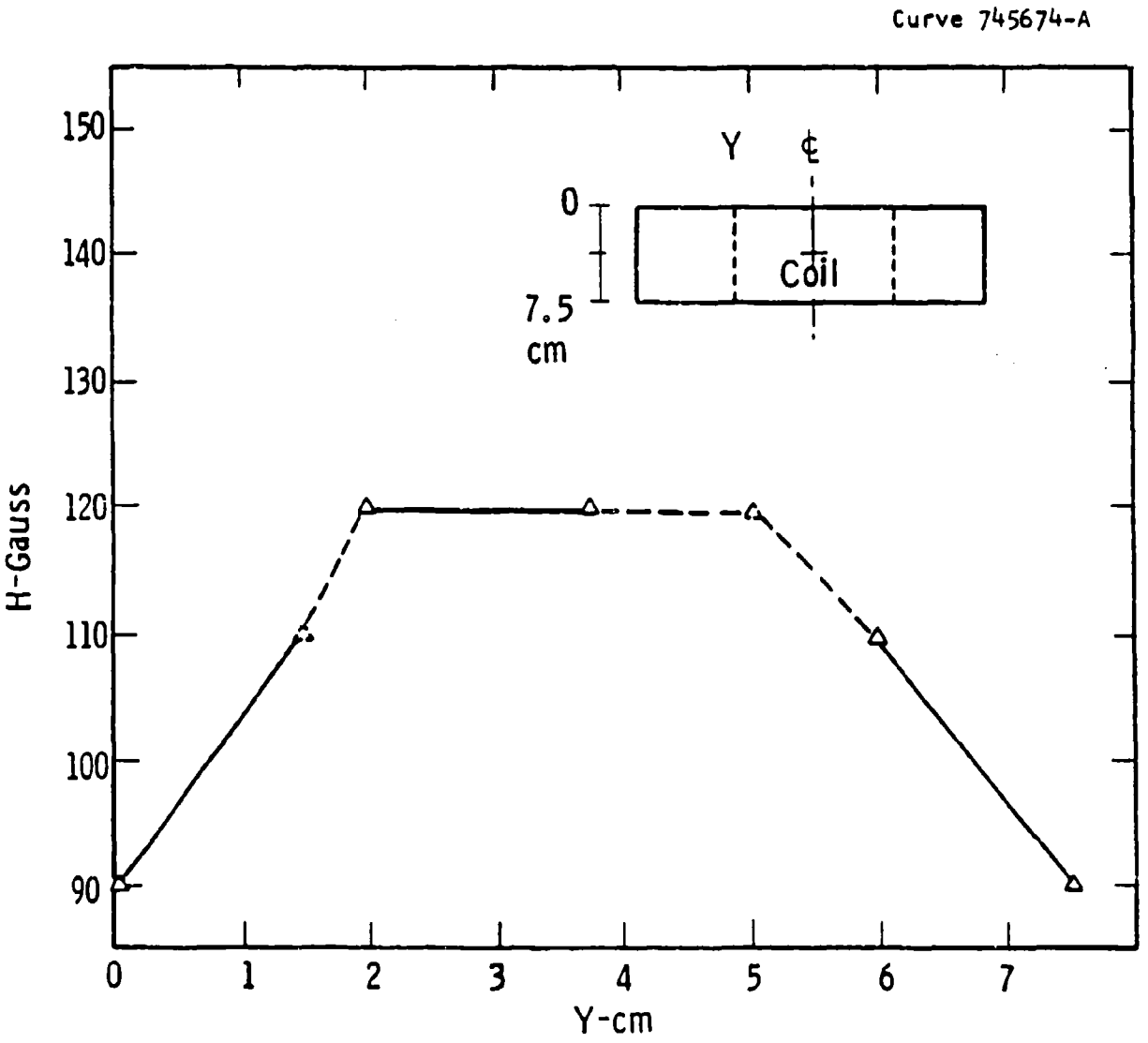

Figure 26. Dipole Test Coil Field Profile - Bore

Table 4 also presents measured values for the coil inductance which provides additional information on the insulation and winding integrity.

TABLE 4

TEST COIL ELECTRICAL MEASUREMENTS

Temperature	Theoretical Coil Resistance	Measurement Coil Resistance	Measurement Coil Inductance
Room Temperature	16.53*	1. 13.556* 2. 12.96 3. 13.02	1. 1.62 mh 3. 2.72 mh
Liquid Nitrogen	3.11	2. 3.03 3. 3.66	2. 41.5 mh
Liquid Helium	0.95	3. 1.17	3. 41.7 mh 4. 13.6 mh

1. Initial measurement.
2. After thermal cycle to 77°K and warm up.
3. After warm up and thermal cycle to 4.2°K.
4. After 1-1/2 hours at 4.2°K the coil inductance dropped to this value.

The observed changes in resistance and inductance are attributed to two possible sources.

- o Carbon layer on the S-glass filament winding on each strand of the conductor cable.
- o Penetration of the strand through the braided S-glass.

Previous concern was expressed about the carbonaceous layer produced upon reaction of the S-glass insulation system (during the 700°C reaction anneal for the Nb_3Sn). This carbon layer could produce a conducting mechanism for shorting the coil on a turn-to-turn basis. Any observed shorting due to the carbon should be more pronounced at room

temperature and reduced at helium temperature, since carbon is a semiconductor and shows a higher resistance at helium temperature.

The observed resistance changes indicate that the carbon layer is in fact influencing the measured coil resistances due to the closer agreement in resistance as the temperature is decreased.

The observed changes in inductance also show an increased number of turns at the lower temperature. A carbon shorting mechanism as the only insulation problem is not completely clear since the inductance changed dramatically to a lower value after aging at 4.2°K. This latter result could only be attributed to penetration through the S-glass layer due to thermal contraction allowing a large number of turns to be shorted.

The most likely situation which is consistent with the present results is a combination of the two mechanisms, i.e., carbon layer and penetration through the conductor.

The inductance of the dummy racetrack can be approximately calculated using an inductance formula due to F. W. Grover. The inductance of a circular coil with square cross section represents the closest approximation to the present short racetrack. Using this inductance formula a value of ~ 54 mh is obtained. The ~ 41 mh inductance values measured on the initial cooldown thus are close to the calculated value. The 1 to 3 mh values are most likely representative of heavily shorted conditions.

The dummy racetrack coil was then sectioned to provide a detailed inspection of the impregnation process. In Figures 27A and 27B are shown two metallographic views of this section at different magnification. Excellent impregnation and apparent complete wetting of the winding was observed. No voids or cracks could be detected. As a result the expressed concerns with respect to the carbon layer and its possible influence on the impregnation process has not developed into any obvious problem.

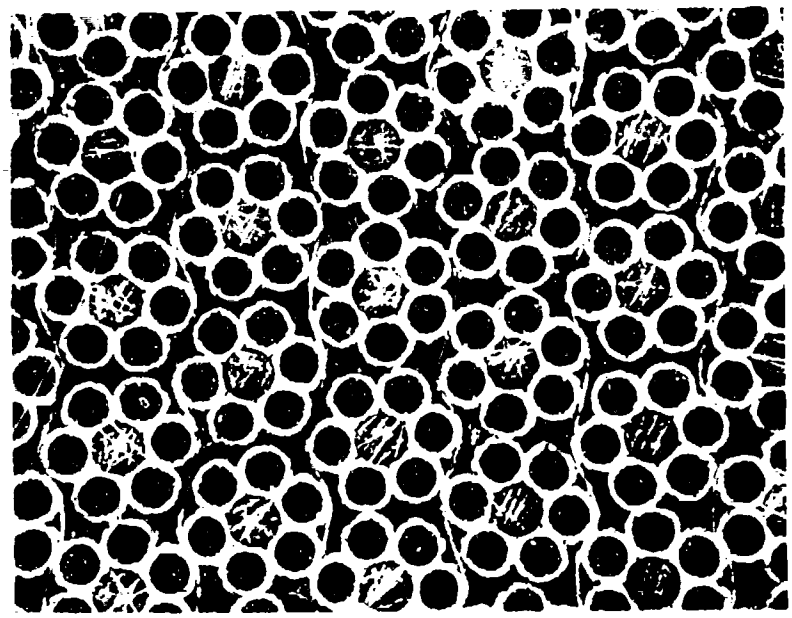

(A)

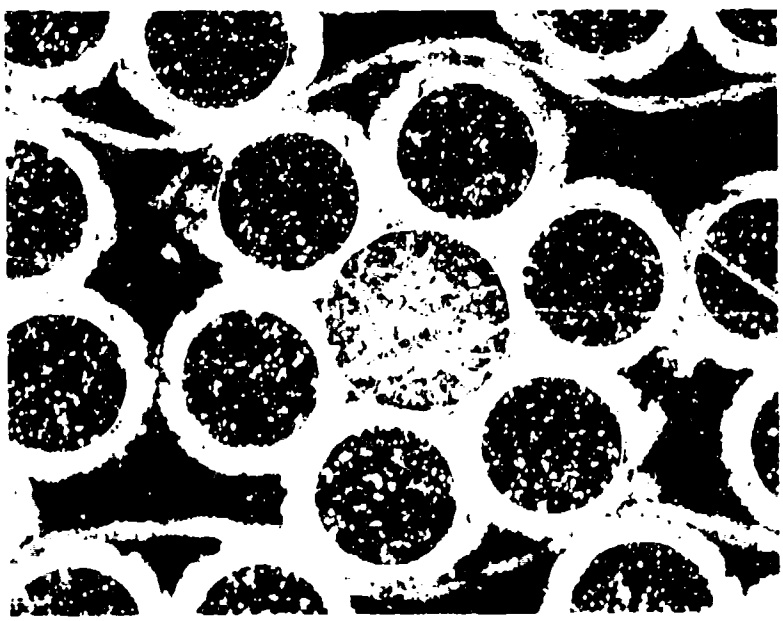

(B)

Figure 27. Metallographic Examination of Dummy Racetrack Section A./X, B.25X

SECTION III

FABRICATION OF THE Nb_3Sn TEST COILS

1. Coil Fixture and Mold Design

The final 6 x 1 Nb_3Sn cable which was insulated and reacted was received from IGC. This final conductor turned out to be different in diameter, length, and insulation system than the design configuration. In addition the racetrack winding fixture developed under this program by IGC was not available to Westinghouse for final coil winding. As a result a new winding fixture was designed, fabricated, and preliminary winding trials conducted.

The coil winding fixture was fabricated according to the revised conductor dimensions, i.e., shorter length and larger diameter. This fixture incorporated a three-piece collapsible mandrel which facilitates removal after impregnation. Two end plates were attached to the mandrel with one end serving as a mounting plate to the coil winder. The end plates contained a system of tapered holes for ease in impregnation of the coil through these plates. Following machining the fixture was thoroughly cleaned and treated with a release agent. The fixture was then mounted on the coil winder and a mockup prepared using 0.090" stranded copper cable with fiberglass between layers. This mockup provided preliminary winding experience with respect to placement of the fiberglass on the winding fixture side plates, pole piece and between layers. In addition the turns per layer and layer build was confirmed and methods established for completing each layer and the transition to the next layer. Following these winding trials the dummy cable was removed and a small test coil was wound using ~ 400 ft. of Airco 6 x 1 Nb_3Sn cable. This Airco cable is similar to the received IGC cable

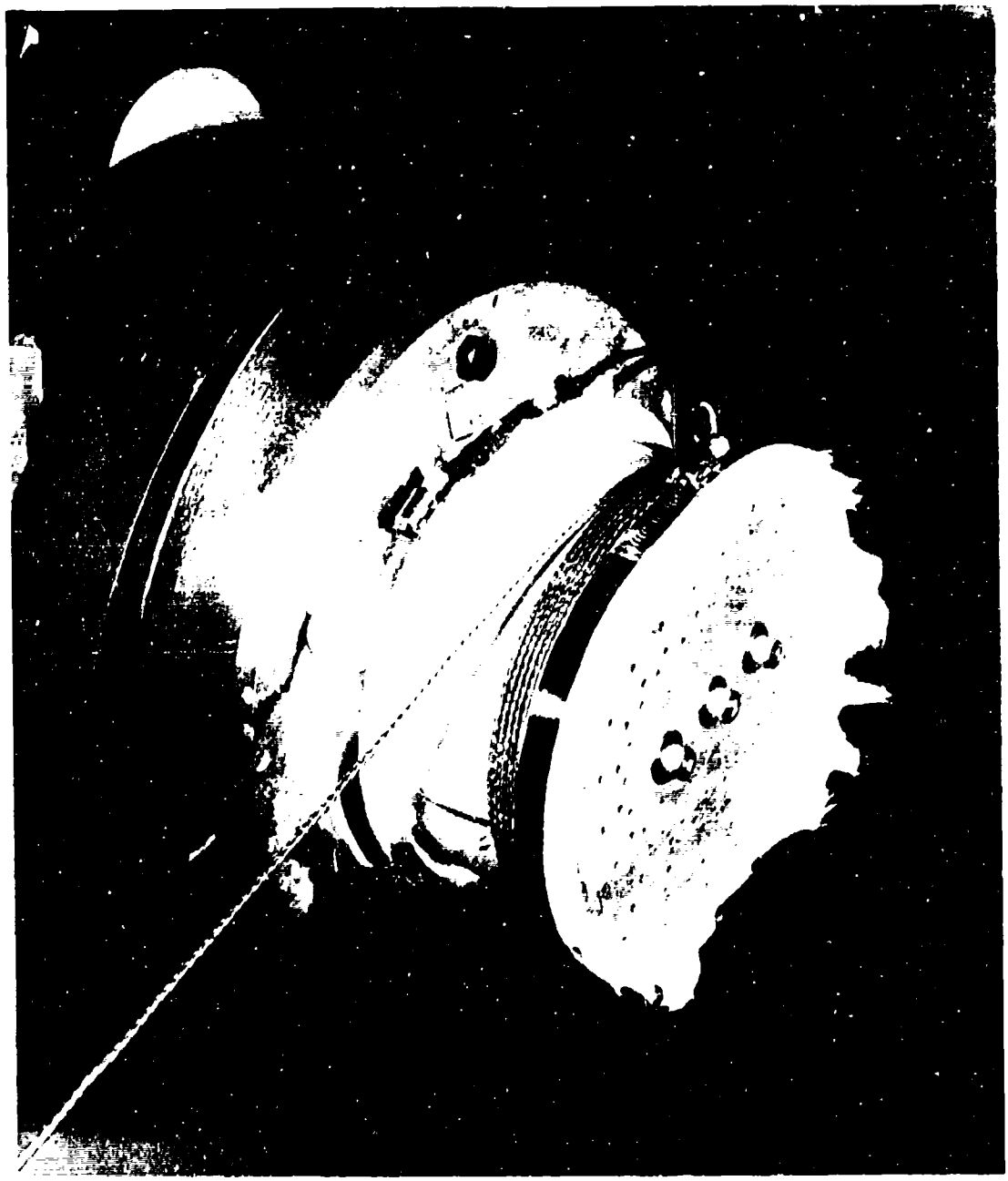

Figure 28. Test Coil During Winding

insulated with Cu_2S. Figure 28 shows the winding operation during the winding of this test coil. After the test coil was wound it was impregnated to evaluate the impregnation process.

Upon completion of the winding additional fiberglass cloth is wound around the outer winding surface, a metal strip is then attached which serves as the outer mold. The winding fixture is removed and horizontally placed on a base plate. The bottom end plate is offset ~ 1/4" above the base plate to permit easy access of the impregnating resin through the bottom end plate as well as the top. Basically the impregnation mold consists of this outer metal strip, which conforms to the desired race racetrack shape, and the two end plates. A silicone rubber dam was used to seal the end plates and outer metal strip. The completed test coil and mold fixturing is shown in Figure 29 prior to vacuum impregnation. This fixture as shown is then placed in the impregnation chamber and filled with resin as shown schematically in Figure 30.

A full-size mockup coil was then wound and fully impregnated. Following impregnation, the coil was thermally cycled to LN_2 with minor cracking observed on the outer surface. This cracking occurred in a region that apparently did not have sufficient fiberglass reinforcement. The final winding with the superconductor will be adjusted to accommodate additional fiberglass which should prevent any such occurrence. In addition the impregnation containment will be adjusted to minimize any chance for unsupported epoxy areas to occur.

The mockup coil was subsequently sectioned to evaluate the impregnation process. There was no evidence of voids or any other problem. Complete impregnation across the entire coil surface was observed.

2. Impregnation System and Procedure

Commercial magnet manufacturers such as IGC who produce epoxy impregnated superconducting coils do not present or release details

Figure 29. Test Coil in Potting Mold

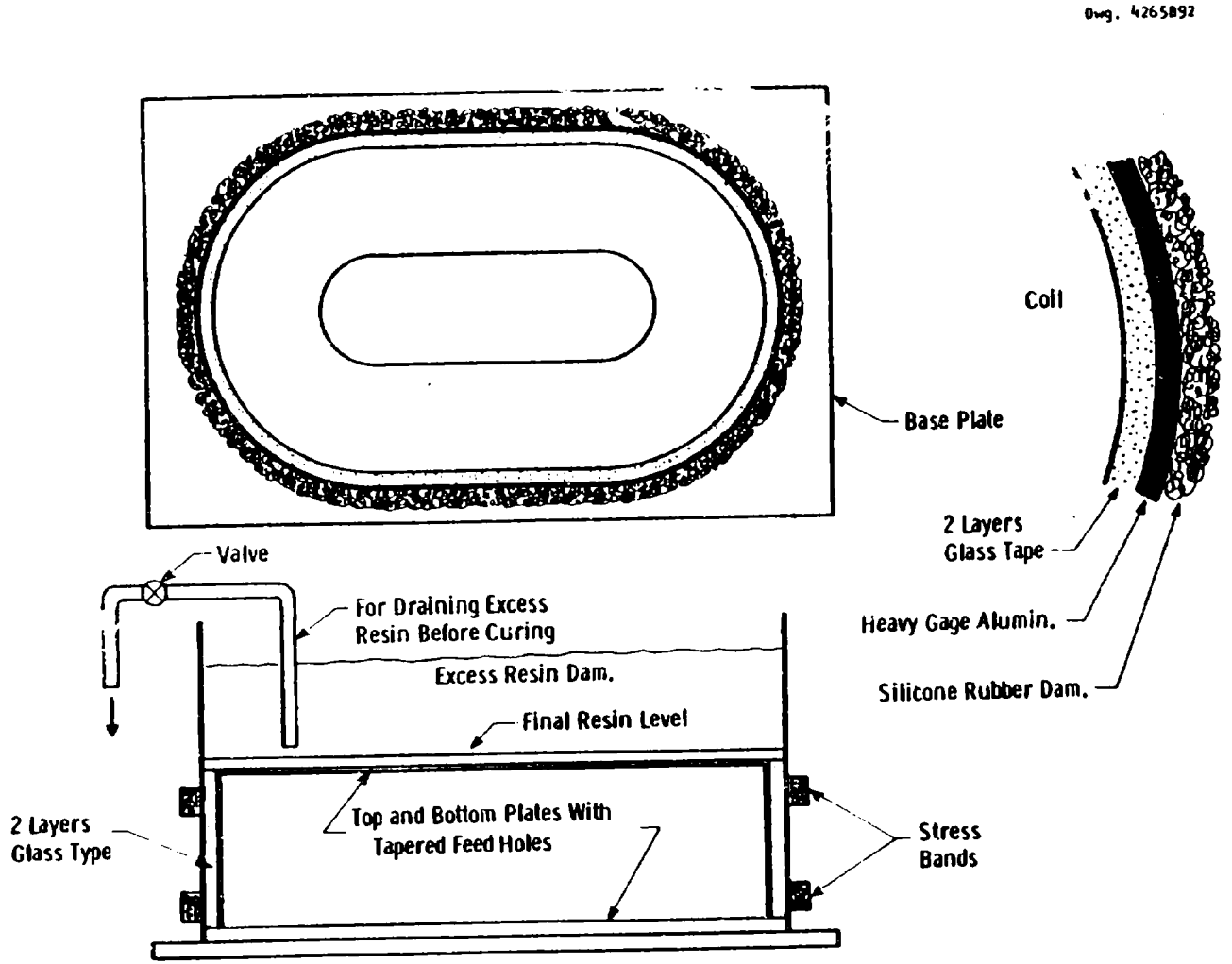

Figure 30. Schematic of Impregnation System

concerned with their impregnation process or resins utilized in their construction. It was possible however to inspect the dummy racetrack coil produced by IGC for this program.

A literature search was also conducted directed at published data on superconducting impregnated coil development. The following resin requirements resulted from this investigation:

- The need for 100% penetration of the coil substructure and the fiberglass layer insulation and conductor insulation.
- High mechanical integrity of the resulting coil consistent with low temperature stability.
- Long working life to permit good vacuum and pressure exposure.
- Smooth thermal conversion with minimal exotherm and low chemical shrinkage.

With these requirements in mind and based on past experience derived from previous programs related to superconducting coil construction a selection of resin and hardener was made. The materials selected for the impregnation process were:

- Epoxy Resin - DER 332 (lowest viscosity undiluted resin)
- Epoxy Diluent - Heloxy 68 (used to lower viscosity even further).
- Anhydride Hardener - HN2200 (a low viscosity liquid coreactant).
- Accelerator - Tertiary amine or metal complex (for controlling the rate of chemical reaction).

(a) Impregnation Procedure

All parts of the mold were seasoned with a silicone release agent. Care was taken to remove any excess release compound through buffing the surfaces after treatment and by cleaning out all through-holes.

A commercially designed impregnator tank was used for the process. The mold containing the coil was placed in this equipment and vacuum and heat were applied to degas the coil. This was accomplished at 65°C using 0.8 torr for a minimum of 16 hours.

The impregnating resin was degassed in a separate operation using a temperature of 45°C and < 1.0 torr vacuum for about 40 minutes.

The degassed resin was then introduced into the impregnator tank without breaking the vacuum on the coil. Sufficient resin was used to provide at least a 2-inch liquid head above the mold. A vacuum of 1-1.2 torr was employed for two hours with the resin temperature at 60 to 65°C.

The pressure inside the tank was normalized to atmospheric pressure then increased to 50 psig. The coil was held at this pressure on the resin at 65°C for about 30 minutes.

After this VPI process the pressure was normalized, the tank was opened, and the excess resin on the top of the mold was removed. The door on the impregnator was closed again and the pressure increased to 50 psig. The heat input was then adjusted to level off at 155°C for a minimum of 16 hours.

After dropping the pressure to atmospheric, the mold was removed from the impregnator and then immediately disassembled so as to remove the excess cured resin surrounding the coil fixture while it was at a high temperature. The high temperature is above the glass transition of the resin and, therefore, it is relatively easy to remove unwanted resin on the outside of the mold. The complete coil was then removed from the flanges (end-plates) and collapsible mandrel.

3. Superconducting Coil Fabrication

The first superconducting coil was wound with the larger diameter cable, i.e., each strand insulated with fiberglass. Nb-Ti to Nb_3Sn joints were implemented as described in Section 2.2.2. Upon

completion of the next to last layer (17th layer) it was determined that insufficient wire remained to complete the final layer. An accurate measurement of the conductor utilized up through the 17th layer amounted to 605 feet. The remaining conductor on the spool was approximately 15 feet for a total spool length of 620 feet. The IGC shipping memo indicated 690 feet which would have been sufficient to allow completion of the last layer. Due to the unexpected short cable length of 620 feet it was decided to wind only to the 17th layer which caused a decrease of 21 turns for this coil. The lead configuration with respect to the finish location had to be changed since winding to the 17th layer would place the start and finish lead at the opposite faces. Originally the leads were at same location on the bottom surface of the coil. A check of the conductor length of the second spool (with Cu_2S insulation) indicates that this conductor length is in fact close to the IGC shipping number of 670 feet. The second coil will thus be wound to the full 18 layer level. The first coil was then impregnated as described in the previous section. Figure shows the completed first coil. The first coil was lightly sanded to remove all residual epoxy to allow proper placement of the interface material. As described in Section 2.1.3.1 the low modulus material was interfaced to the coil surface. Detailed measurements of the completed coil were then taken which were used for final machining of the coil support structure. The final machined coil support structure is shown in Figure 9.

Coil #1 was wound, impregnated, surface prepared and support structure machined for proper placement during low temperature tests. Following the previously described sequence the second coil was also wound and impregnated. The final impregnated coil is shown in Figure 31. The second coil contained thermometers mounted at the coil midplane on both sides of the racetrack. An improved method was devised for lead routing and lead protection. This system worked successfully compared to earlier attempts by IGC on sensor lead protection which resulted in virtually all the sensor leads breaking off during handling. Electrical

Figure 31. Nb_3Sn Dipole Test Coil (Coil #1)

check of the sensors for the second coil indicated all leads were intact.

In Figure 32 both coils are shown with the low modulus material attached to coil #1.

4. Instrumentation

The RTF is an experimental rotor for investigating the cooling mechanism and stability of racetrack type superconducting coils in high 'g'-fields. For this reason, it is essential that instrumentation be provided for evaluating the rotor performance. This instrumentation should evaluate as a minimum the overall cryogenic performance, the magnetic field response, and superconducting coil sensitivity to stress during cooldown, rotation, and ramped field.

Cryogenic Performance. The cryogenic performance will be evaluated by carbon-glass or carbon resistance thermometers located at various positions throughout the rotor. This thermometry will measure the overall temperature distribution within the winding: the inlet flow temperature, temperature rise after transients, and power lead performance. Carbon based resistors are extremely attractive for low temperature thermometry in a superconducting rotor. They offer high thermometric sensitivity in the range of interest, i.e., 3 to 100°K. In addition, they possess low heat capacity, small physical size, and relative insensitivity to magnetic fields. (At 4T, the magnetoresistance correction is approximately 2% of the zero-field resistance.) If properly mounted with provision for lead placement they offer a fairly high degree of reliability compared with other forms of thermometry instrumentation. In Figure 33 the winding and coolant thermometers are identified as T_{c1} and c_g respectively.

Stress-Strain Measurements. A high-speed superconducting rotor presents an internal low temperature structure which may comprise a number of diverse materials with respect to thermal contraction characteristics. As a result, high differential contractions may

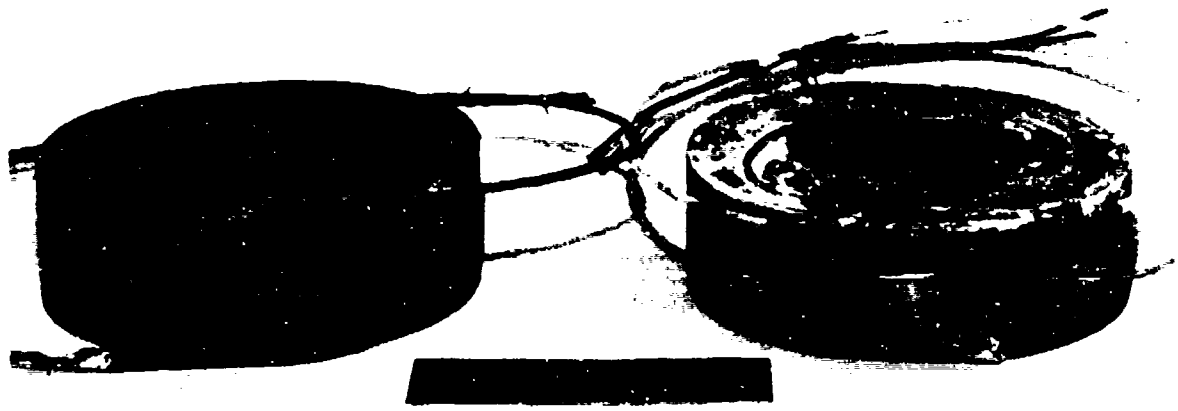

Figure 32. Nb_3Sn Dipole Test Coil (Coil #1 and #2)

produce pronounced strain effects. These effects plus the overall rotational stress would be evaluated by strain measurements. Strain gauges locations on the winding are shown in Figure as s_{f1} and s_{g2}.

Magnetic Field Measurements. The steady-state and ramped magnetic field behavior can be evaluated by the placement of magnetoresistance probes on the low-temperature structure. These probes, which require four leads, have been used at 4.2°K with great success. The probes have demonstrated extremely fast time response which should easily follow the ramping and quench characteristics of the field coils. An external search coil can be used for evaluation of the overall ac or dc field changes relative to the rotor.

5. Data Acquisition and Reduction

The recording of large quantities of data from an experiment can be done today with a dedicated microcomputer. To this end, the Westinghouse R&D Center has implemented a laboratory data acquisition and reduction system for use with superconducting rotating experiments. This system is based upon a 8-bit microprocessor - the Zilog Z-80 which operates at 4 MHz. The system consists of two central processors, 65,536 bytes of random access memory storage, three minifloppy disks (each capable of over 100K of mass storage), and several input/output ports which can handle either digital or analog data in either serial or parallel formats. This data acquisition/reduction system would have been used in the RTF related experiments. This apparatus should have been an excellent tool to monitor the total performance of dipole coils under test in the rotating test facility.

A description of a rotor telemetry system also developed for the task of data acquisition on rotating experiments is briefly described in Appendix D.

The data acquisition and reduction systems have been fully tested to operate at 3600 rpm as part of the EPRI/Westinghouse 300 MVA generator development program. The equipment has been used to collect

heat transfer data both under steady state and transient conditions. In both cases, the rate of data collection and storage was not limited by the processor speed. However, real-time data reduction was severely limited by processor speed. This was circumvented by post-experimental data reduction followed by data display. We anticipate no major difficulties in using these tools for rotor speeds up to 12,000 rpm.

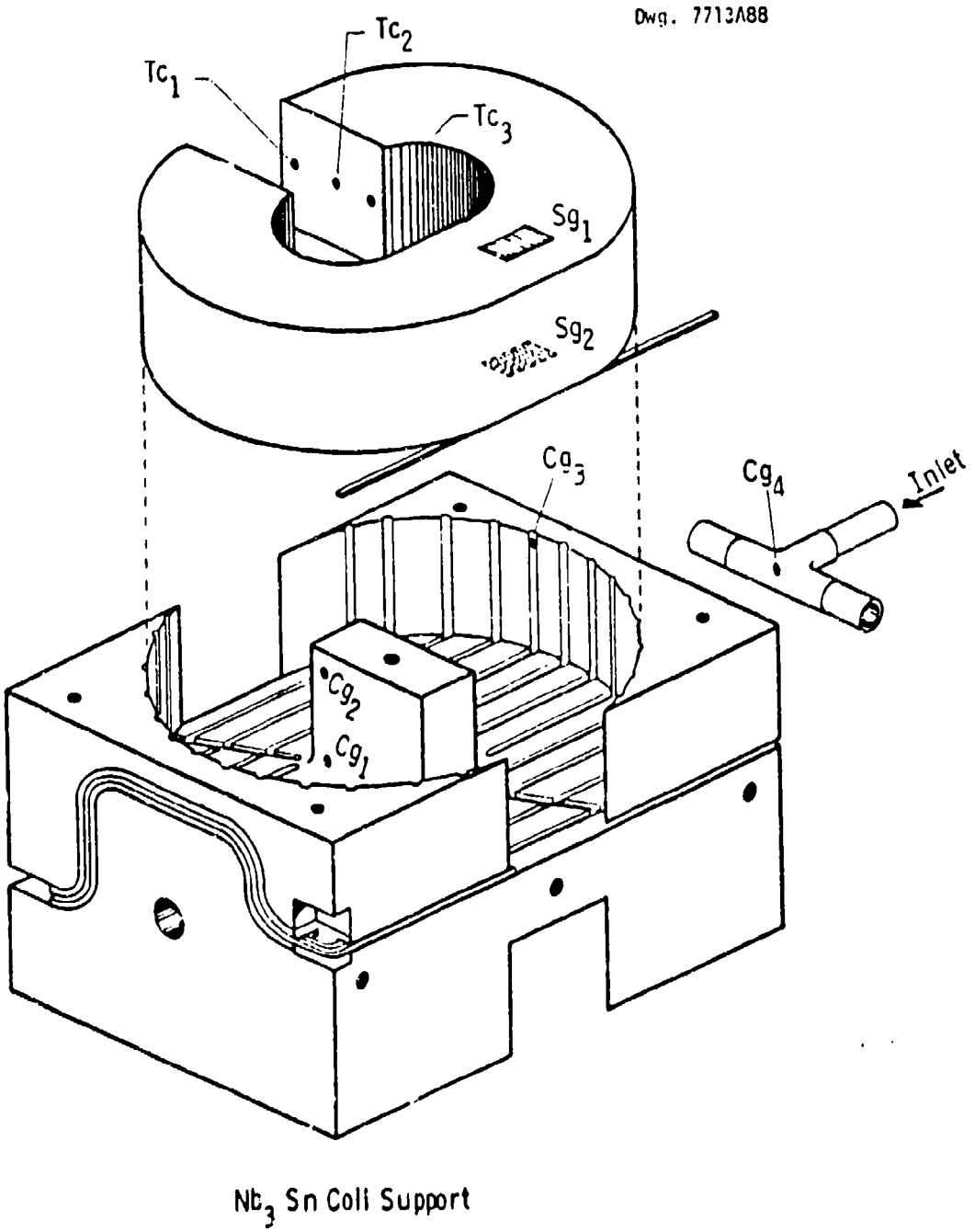

Figure 33. Nb_3Sn Coil Support with Instrumentation Sensors

SECTION IV

CONCLUSIONS AND RECOMMENDATIONS

The Superconducting Rotor Dynamics Program has demonstrated that the essential mechanical and electrical features of a superconducting generator can be modeled in a test rotor. This test rotor or Rotating Test Facility (RTF) can be designed to reproduce the transient electrical and mechanical conditions that impact most heavily on a generator design. The superconducting coils in a rotating field configuration must operate in a difficult environment. Time-varying magnetic fields, shock, vibration, Lorentz forces, and centrifugal loading all impose potential temperature fluctuations which may degrade or even normalize the supercurrent operation.

These same loads also impact on the cryogenic cooling scheme through thermohydraulic effects which are currently under investigation in separate programs. These latter thermohydraulic cooling transients may of themselves be sufficient to compromise an overall generator design and operation.

A RTF design and test of a specific generator approach can be carried out at a much smaller [illegible] than required for a full generator construction. The RTF approach to future advanced generator considerations should therefore be on integral part of the planning and should in fact precede commitment of a new generator construction.

APPENDIX A

CHRONOLOGICAL RECORD OF EVENTS

The period of performance for this program spans the four years from September 1979 to September 1983. Included in this section is a brief chronological summary of the significant accomplishments under this contract.

September 1979 to October 1979

(a) A field calculation was made to evaluate the influence of coil cross-section racetrack length and spacing between two coils on the overall field strength. A racetrack coil with a cross section of 2.85" x 2.85" and a racetrack length of 2" was selected. The corresponding peak field was shown to be 6.5 tesla for a two-coil series linking configuration.

(b) The definition of work and the preliminary schedule for the Phase I subcontract effort by IGC was determined and accepted.

October 1979 to November 1979

(a) A tentative design of a self-regulating helium flow system for the RTF was established. It included a 1" helium pool, an insulated "T" tube and a vapor trap with spin-up vanes.

(b) G-11CR glass reinforced epoxy plate was selected for the basic support structure material.

(c) To accommodate the shear load during thermal contraction between the coil and support structure, two candidate low modulus

materials, polycarbonate film and mylar have been selected for further evaluation.

(d) Sixty pounds of superconductor were projected to be required for the proposed racetrack coils.

(e) A dummy cable comprised of copper-nickel and molybdenum strands was ordered to evaluate the winding design.

(f) To evaluate the proposed lead support system and provide guidance on winding a circular coil mock-up was determined to be necessary.

November 1979 to mid-December 1979

(a) The best location for the "T" tube inlet was determined to be in the vacuum space.

(b) To avoid thermosiphon instabilities, the coil module cooling channels were modified to communicate with the central pool.

(c) The best configuration for the composite coil support structure was determined to be G-11CR glass reinforced epoxy plates that were stacked, oriented, glued and pinned. The best orientation for the x-y plane of the composite was determined to be in the rotor's radial direction.

(d) Inconel 718 was selected to be the preferred material to construct the outer containment shell and support flanges. Inconel 600 was determined to be a suitable substitute for the end-flange material.

(e) A general layout and assembly drawing for the RTF was begun.

(f) The dummy conductor constituent materials were received.

(g) The circular coil forms for the lead mock-ups were designed.

Mid-December 1979 to February 1980

(a) The modified RTF design and proposed instrumentation was presented to the Air Force in a design review.

(b) A central gas plenum to collect boil-off gas was added to the design.

(c) Torque tube cooling feed tubes and the power lead configuration was evaluated and included in the layout drawings.

(d) G-11CR plate, the necessary adhesives and the "low modulus" interface materials were ordered.

(e) Layout drawings were completed.

(f) The dummy cable was under fabrication.

(g) The fixtures to evaluate the leads were designed and fabricated.

February 1980 to March 1980

(a) Thermohydraulic design was completed with exception of power lead optimization.

(b) All RTF structural materials were received.

(c) Three hundred feet of prototype prototype Nb3Sn cable for evaluation and inclusion in the lead mock were received from Airco.

(d) Spin-up and excitation tests of the Nb-Ti Spin-Test Rotor at speeds up to 12,000 rpm were performed. (see Appendix A for details).

(e) The RTF was removed from its test stand and disassembled in preparation for the proposed modifications.

March 1980 to April 1980

(a) Optimization of the power lead design centered on a 0.4 cm^2 cross section to be consistent with the existing stub shaft penetrations.

(b) The order was placed for the 718 to fabricate the containment shell.

(c) The G-11CR plates were prepared for bonding.

(d) All detailed layout drawings were completed.

(e) The dummy conductors for lead mock-up and winding the circular coils were completed.

(f) The parts of the disassembled RTF were crack checked and helium leak tested.

April 1980 to May 1980

(a) The two end flanges were completed (excluding penetrations).

(b) The G-11CR plates were bonded to form a block.

(c) Lead joint mock-ups confirmed the need for a copper channel around the Nb_3Sn-NbTi transition to offer the best support.

(d) The circular coil fixture was fabricated.

May 1980 to July 1980

(a) The thermal analysis of a 0.4 cm^2 cross section power lead comprised of 4.5 mil copper strands confirmed its suitability.

(b) The G-11CR block was sectioned to form the composite material for fabricating the coil support module and covers.

(c) The bearing support caps were completed.

(d) The orders for the fiberglass shells were placed.

(e) Lead mock-ups with copper channels and glass cloth wraps were prepared and tested.

(f) Circular coil winding trials indicated that the racetrack cross section should be close to the 2.85" x 2.85" design approach.

July 1980 to September 1980

(a) The fiberglass vacuum and liquid nitrogen containment shells were completed.

(b) The Inconel 718 centrifugal containment shell was ultrasonically inspected for cracks and welded and dye-checked for cracks. No cracks were observed in either case.

(c) The inner coil support blocks were machined to the approximate racetrack coil dimension.

(d) Modifications to the "Spin-test" rotor slip rings for operation at near 900A were begun.

(e) The 2 kA high current test rig for testing the Nb3Sn joints was prepared for its first tests.

(f) The first circular coil was wound, impregnated, heat treated and tested for insulation integrity. The coil resistance measured was very near the calculated value indicating no shorted turns stand-to-strand insulation tests were made indicating some shorting but inductance measurements confirmed that these should not influence the coil charging characteristics.

September 1980 to November 1980

(a) The end spacer design for the fiberglass dewar was reviewed with Owens Corning, and changes were suggested to minimize vacuum leaks.

(b) The Inconel 718 centrifugal shell was machined to approximate dimensions, and the X-ray tests of the welds indicated minor porosity, while using " " a superficial surface scratch was located for burnishing and grinding.

(c) The end flanges and outer rotor containment flanges were completed.

November 1980 to January 1981

(a) The copper leads support structure and power lead termination were fabricated.

(b) The major RTF structural elements were assembled to verify mating and to determine the welding procedure.

(c) Tests of the lead mock-up for currents up to 1200A in fields up to 3 tesla indicated a resistance of less than 10-9 to 10-10 ohms.

(d) Tests of the dummy racetrack coil were made. The inductance tests showed significant shorting probably through the carbonaceous layer of the S-glass insulation system.

January 1981 to April 1981

(a) The end spacers for the vacuum shell were filament wrapped and bonded to the inner shell.

(b) The maximum length of cable which could be fabricated without joints was projected by IGC to be 740 feet using a strand size of 0.038". Since the coil design required around 1400 feet of cable using 0.030" strands, the racetrack coil might only reach 85% of the designed performance.

April 1981 to August 1981

(a) All work on the RTF modifications was halted due to the changes in the program scope.

(b) Short sample tests on the 0.038" Nb_3Sn strands indicated an I_c of 450A at 7 tesla. At this critical current level, the generated field in the racetrack coil should be very close to the desired level.

(c) Evaluation of butt-resistance joining to form a long cable indicated that if the joints are place in a 5 tesla a lower field than the cable with joints should be able to carry the same current as a cable without joints.

August 1981 to January 1982

(a) Twelve lengths of the 0.038" Nb_3Sn material were butt welded to form six strands of 600 to 650 feet with one weld per strand.

(b) Each strand was coated with Cu2S insulation by vapor deposition.

(c) IGC cabled the six strands around a molybdenum core, applied an S-glass braided overwrap to the cable, and reacted the material to form the Nb_3Sn.

January 1982 to May 1982

(a) Two lengths of reacted Nb3Sn cable were received: (1) 690 feet of 0.133" diameter cable with S-glass insulation applied to each strand and (2) 670 feet of 0.125" diameter cable with Cu_2S applied to each strand and S-glass insulation applied to the cable.

(b) IGC reneged on delivery of the coil winding fixture which they fabricated for the Air Force program due to their concern that the fixture contained proprietary information about the IGC impregnation process. The charges related to this fixture were agreed to be refunded and Westinghouse began designing a new fabrication fixture for coil assembly.

Note: Refund was never received from IGC.

(c) The impregnation system and procedures were identified for impregnating the racetrack coil. From information available in the literature, the technique proposed is similar and may be identical to the techniques used by IGC and GE.

May 1982 to June 1982

(a) For the received cables, the racetrack coil height was determined to be 2.870" when 21 turns and 18 layers of cable were used. This dimension was so close to the 2.850" requirement for the RTF that the original coil structure should readily accommodate the racetrack coil.

(b) The coil winding fixture was fabricated and tested with a copper cable using 0.090" strands.

June 1982 to August 1982

(a) Short sample measurements of the IGC cables were performed at 5 tesla. The S-glass insulated cable had a critical current of 4100A and the Cu_2S insulated cable had a critical current of 4400A.

(b) A small test coil using the Airco cable was wound and impregnated to evaluate the resin system.

August 1982 to October 1982

(a) Lead placement in the coil support structure was laid out for machining.

(b) The test fixture for the coil tests were designed and construction was initiated.

(c) A full size coil mock-up was wound and impregnated. The coil was sectioned to evaluate the impregnation process. Complete impregnation across the coil was observed.

(d) Winding of the first Nb_3Sn coil, using the S-glass insulated cable, was completed. An accurate measurement of this conductor indicated that 620 feet (not 690 feet) of conductor had been provided by IGC necessitating changing the coil design from 18 layers to 17 layers and relocating the coil termination.

October 1982 to January 1983

(a) The first Nb_3Sn coil was fully impregnated, and the surface mold marks and excess epoxy removed to produce a smooth outside surface.

(b) Attachment tests on the "low modulus" inface materials were made on the impregnated dummy coil. The first test using a 3M adhesive spay to attach the "low modulus" material were unsuccessful. The next test using a polyurethane adhesive was successful when thermally cycled to liquid nitrogen temperature.

January 1983 to April 1983

(a) The coil support structure for the first superconducting coil was completely machined and ready for final placement and test.

(b) The second Nb_3Sn coil, using the Cu_2S insulation, was wound and fully impregnated. This coil contained thermometers mounted at the coil mid-plane on both sides of the racetrack. The method of lead routing was determined to be successful based upon electrical continuity measurements.

APPENDIX B

"ACCELERATION TESTS ON A MODEL SUPERCONDUCTOR ROTOR"

R. D. Blaugher, P. W. Eckels, and A. Patterson

ABSTRACT

The use of superconducting field windings in ac generators offers a reduced size and weight, increased efficiency, higher output voltage, and lower synchronous reactance compared to conventional machines. Increased output power can also be obtained by operating the generator at very high speeds. The U. S. Air Force has supported research and development programs directed at lightweight, high-speed airborne superconducting generators in the 10's of megawatt power range. These programs have involved prototype rotor[1] and complete generator construction[2,3] and advanced superconductor fabrication.[4] The operational requirements or system interface has also been addressed.[5] The system analysis indicates that the generator may require a simultaneous spin-up and excitation to rated speed and power in a time frame as short as one second. This requirement imposes extremely large mechanical, electrical and thermal transients which may limit the performance of the superconducting field winding. In addition, a rapid spin-up may create hydrodynamic instabilities in the helium system which may influence the ability to cool the winding. This latter problem has not been directly studied to date. It is fairly apparent that hydrodynamic instabilities such as interrupted helium flow could completely dominate the rotor performance during a rapid spin-up.

The presently reported tests are directed at an investigation of rotor cooling under operating conditions representative of high-speed generators in a rapid spin-up mode. We initiated exploration of the

influence of acceleration and current excitation on superconducting coils in a series of rotor-winding tests. Both field ramping and rotor spin-up and spin-down were performed independently (and simultaneously).

The following sections review the mechanical and cryogenic description of the "Spin-Test" rotor. The acceleration and current excitation results of two test series are discussed in terms of quench current and thermodynamic performance of the cooling system. These tests present strong evidence for hydrodynamic instabilities in the helium cooling system which occur under acceleration. Analysis and identification of various spin-up problems are identified. No spin-down problems were encountered.

INTRODUCTION

The analysis of the Air Force system requirements[5] suggest the most severe heating and disruption of the cooling system of a superconducting generator would occur during a rapid spin-up and excitation. Simultaneous spin-up and coil excitation produce severe, coexisting mechanical, electrical and thermal transients whose adverse effects are compounded by possible instabilities in the helium cooling system.

The rotor is either directly connected to a turbine as shown in Figure 1 and accelerated to speed or the turbine is coupled, at rated speed, through a clutch arrangement. Either method imposes a high mechanical acceleration transient of the order of 10^4 g's for approximately one second.[6] Moreover after application of the driving power the generator must be fully loaded otherwise the rotor will overspeed with resultant shut down of the turbine. For this reason the field winding must be fully excited prior to or during application of the prime mover. The latter condition would impose an additional ramped field loss and temperature rise to the field winding.

The R&D Center under Air Force contract has been studying the impact of rapid acceleration on the performance of superconducting

coils. A "Spin-Test" facility was designed, constructed and tested to evaluate mechanical and electrical transients on superconducting rotor coils. The rotor and coil configuration was specifically designed to reproduce the geometry, mechanical and thermal conditions which occur in a high-speed superconducting generator. Tests were conducted to evaluate the behavior of the helium management system under acceleration. A review of these recent tests is presented which shows evidence for hydrodynamic instabilities in the helium cooling system.

"Spin-Test" Rotor

The "Spin-Test" rotor shown in Figures 2 and 3 is a liquid helium cooled rotor mounted within a stationary vacuum enclosure. Two "racetrack" superconducting windings are enclosed by a shrink fit Inconel 718 cylinder in a two-pole winding configuration. The Inconel cylinder which provides the winding centrifugal containment is welded at both ends to thin walled thermal transition shells. Each thermal transition shell is cooled by two spiral wound stainless tubes which were copper brazed to the inner wall. Inconel 600 stub shafts were attached to each end of the rotor. The power leads, instrumentation leads, and all inlet and exit helium flow tubes were fed through the stub shafts.

The end bells which support the rotor and outer stationary dewar also house the oil lubricated bearing and vacuum face seals. The double-walled fiberglass dewar is filled with liquid N_2 which maintains a 77°K ambient for the inner helium cooled rotor.

The superconducting rotor coils shown in Figure 4 were wound with rectangular Nb-Ti multifilamentary monolithic copper matrix superconductor. The copper-to-superconductor ratio is 2:1. Spacers were inserted between layers of the step structure racetrack to provide radial paths for the helium to flow. Additional spacers in the end turn region provided access for longitudinal helium flow through the winding

DWG. 7752A17

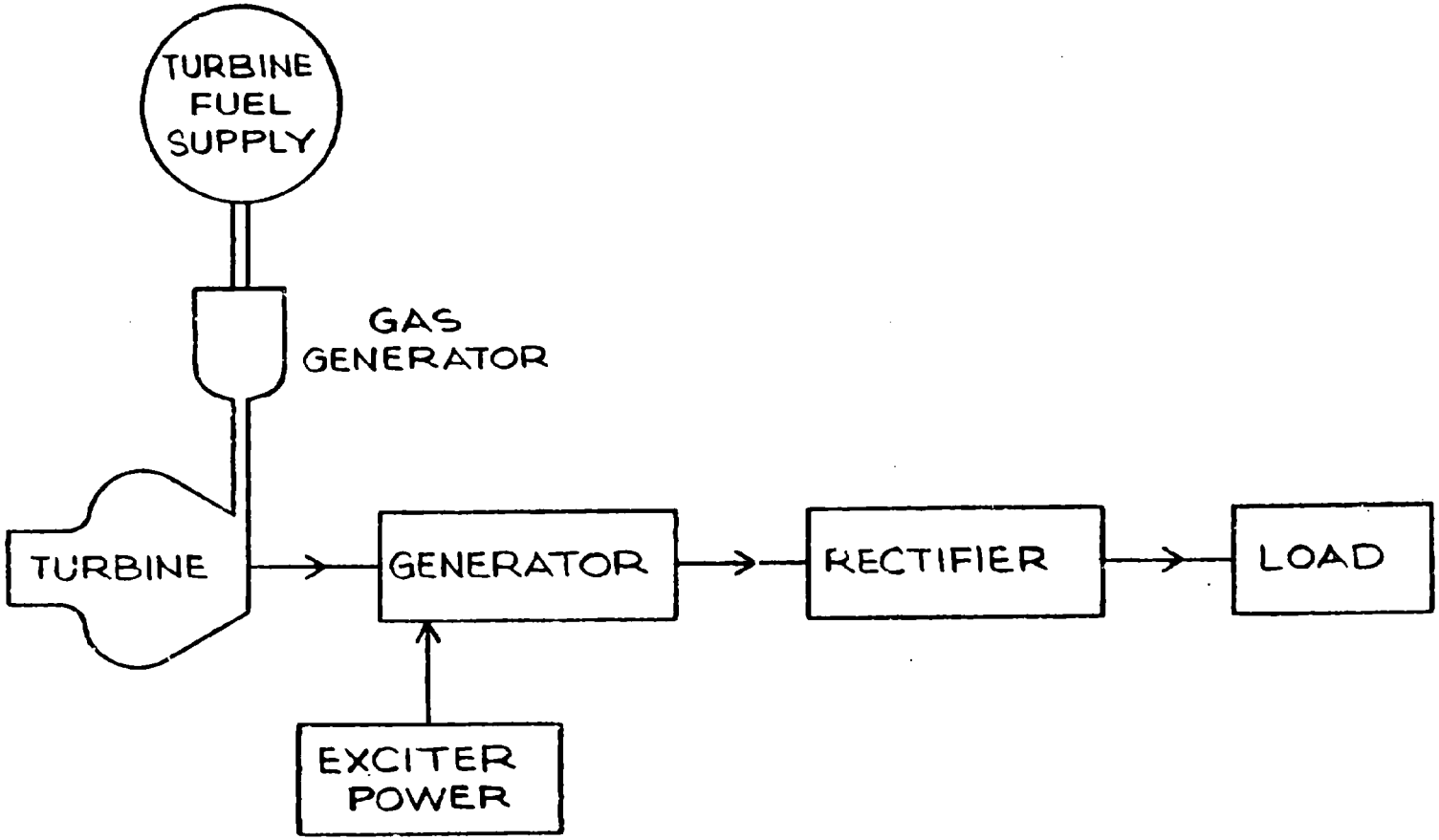

Figure B-1. Generalized Airborne System

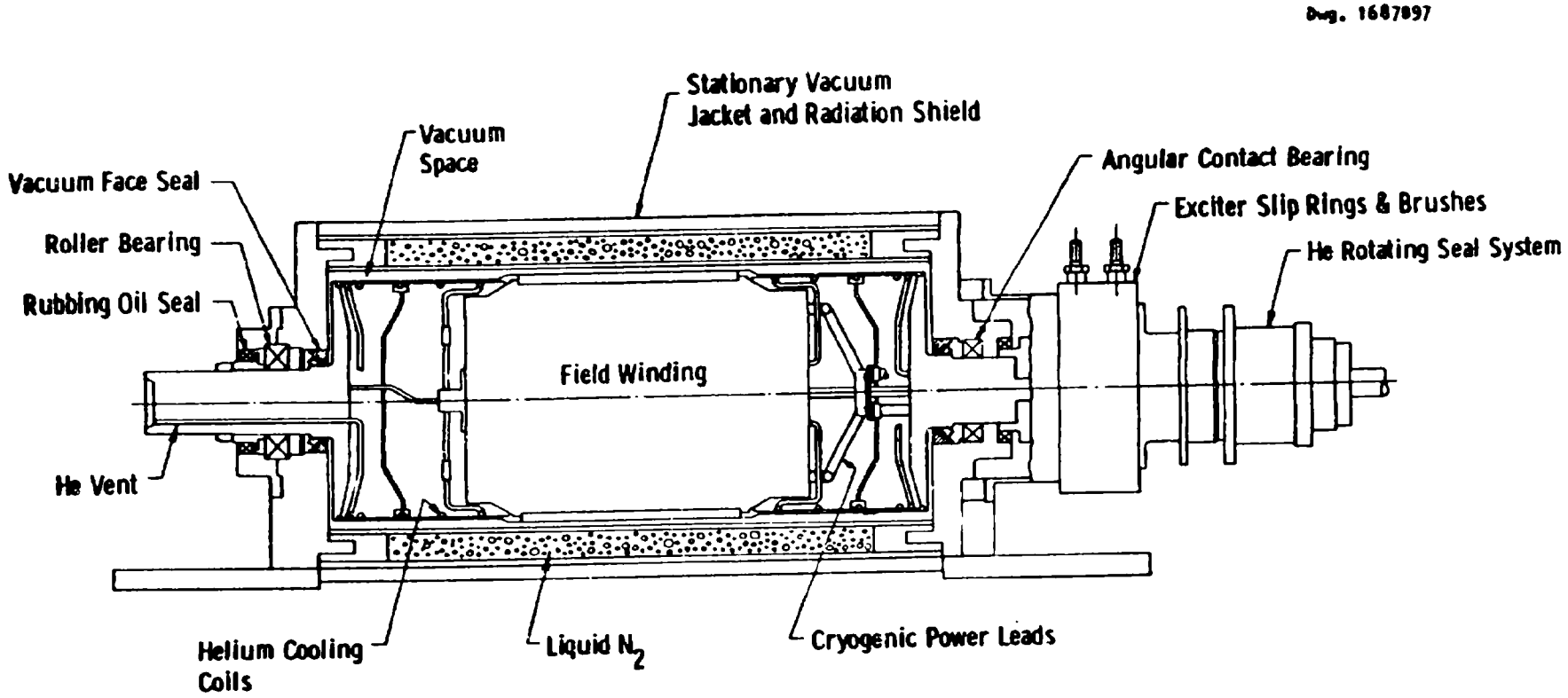

Figure B-2. Schematic of Spin-Test Rotor

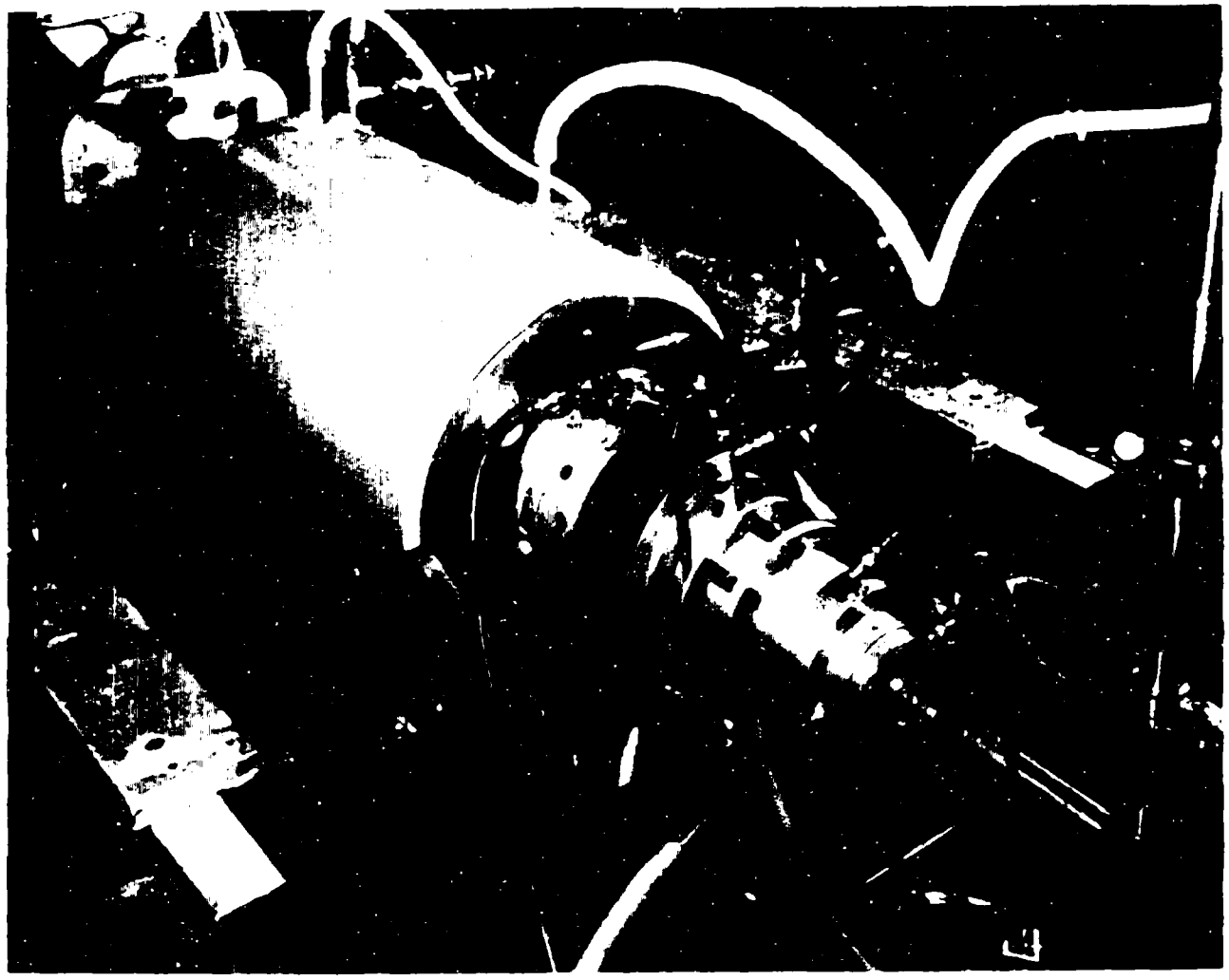

Figure B-3. Spin-Test Rotor Installed on Test Stand

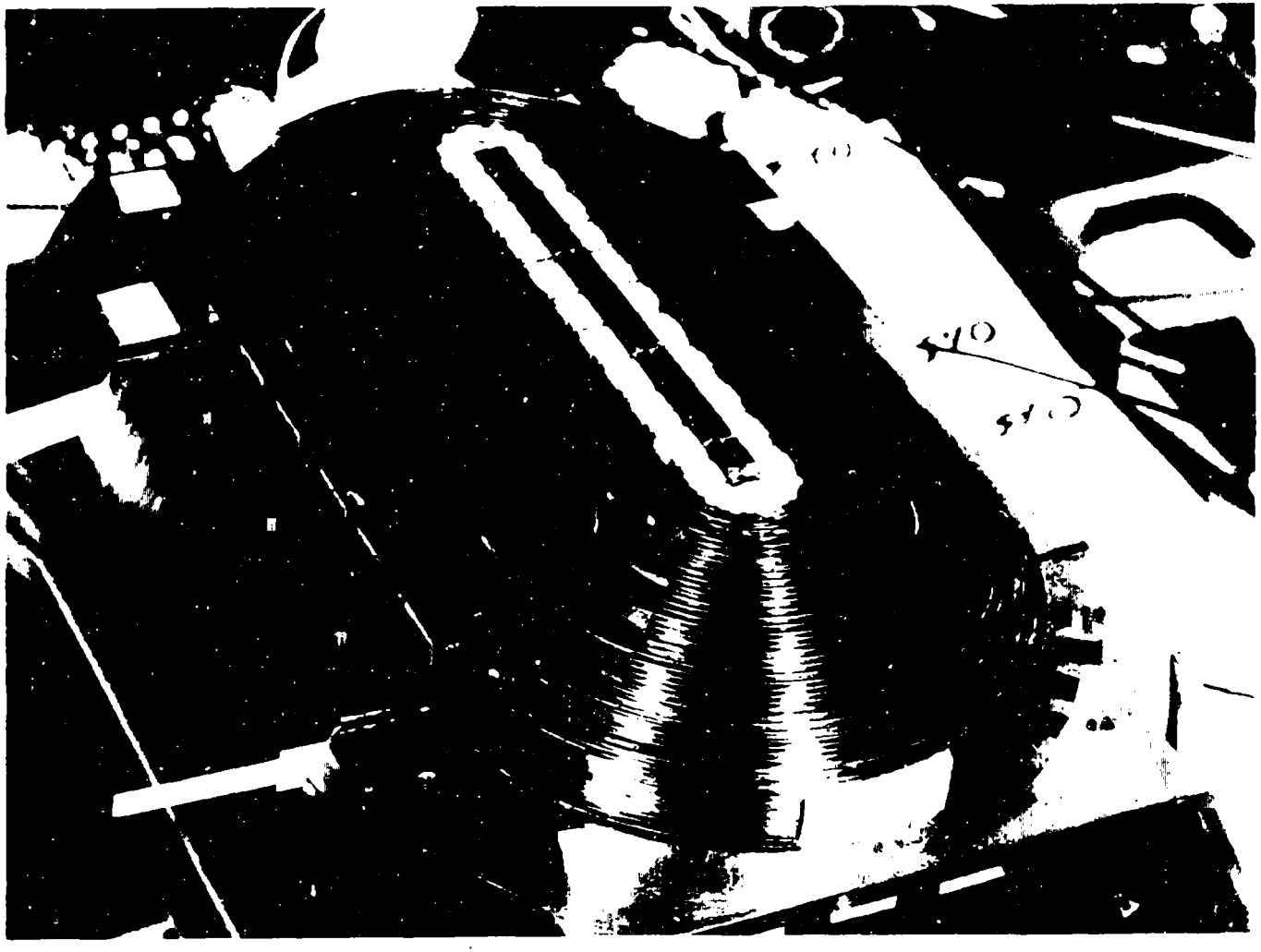

Figure B-4. Superconducting Coils Mounted on Support Structure

interstices. These interstices are created by the turn-to-turn placement of the rectangular conductor.

The entire mechanical design for the "Spin-Test" was capable of steady-state operation at 12,000 rpm and acceleration levels of 12,000 rpm/sec.

"Spin-Test" Helium Flow Description

The helium flow stream is supplied to the "Spin-Test" by a helium transfer system which provides the stationary to rotating interface. This transfer system, described in detail in an earlier publication,[7] incorporates the helium seals, the inlet bayonet and locating bearings.

A calibrated carbon thermometer was mounted on a small copper block soldered to the inner flow tube of the bayonet. Thermally conductive adhesive was used to glue the thermometer into a hole drilled in the copper block.

The helium flow circuit within the "Spin-Test" rotor is shown in Figure 5.

The helium stream upon entering the rotor from the bayonet encounters a copper impeller at A which rapidly accelerates the fluid to rotor speed and provides nearly complete phase separation. The dense liquid is diverted outward B through a hollow copper finned heat exchanger shown in Figure 6 located in the center or pole of the winding. The copper fins, central copper core and impeller basically constitute the main heat exchanger which is specifically designed to remove the heat produced by compressional processes. The heat exchanger is shown mounted within the winding in Figure 4. The heat absorbed in the fins flows radially inwards to the cold copper core producing gas due to liquid boil-off. This gas combines with the inlet gas and flows outward C through radial tubes to cool the drive end thermal transition shell. This gas then returns on-axis and exits the rotor through orifices mounted on the stub shaft.

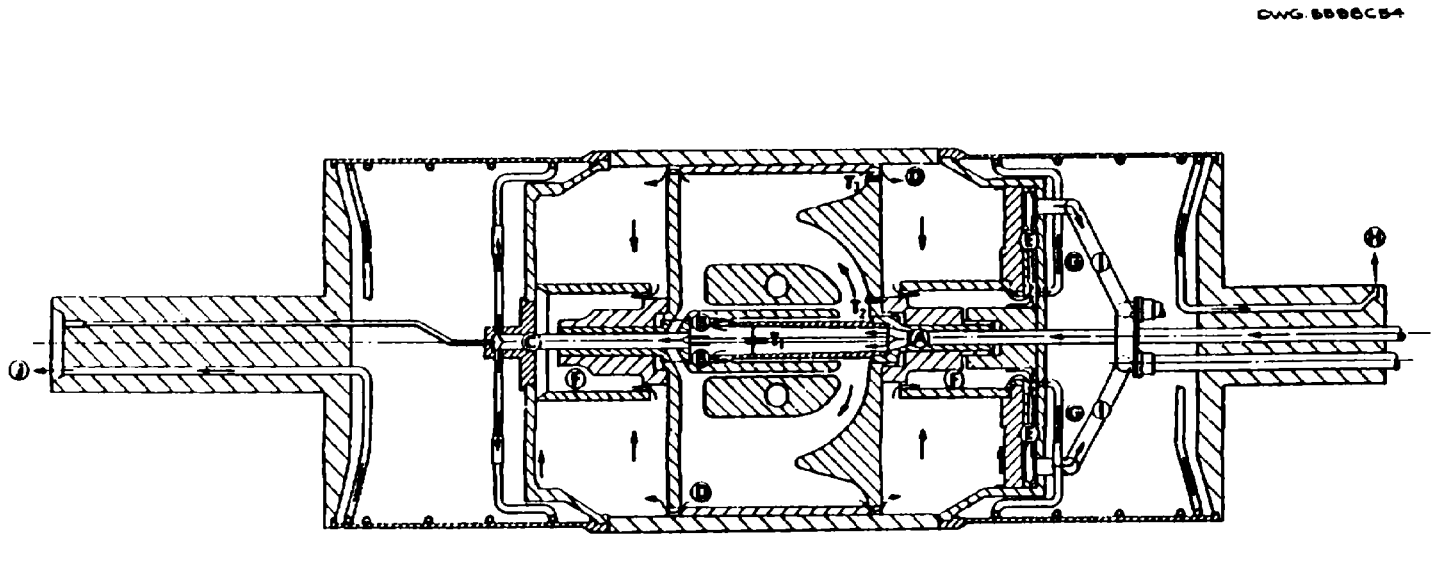

Figure B-5. Spin Test Helium Flow System

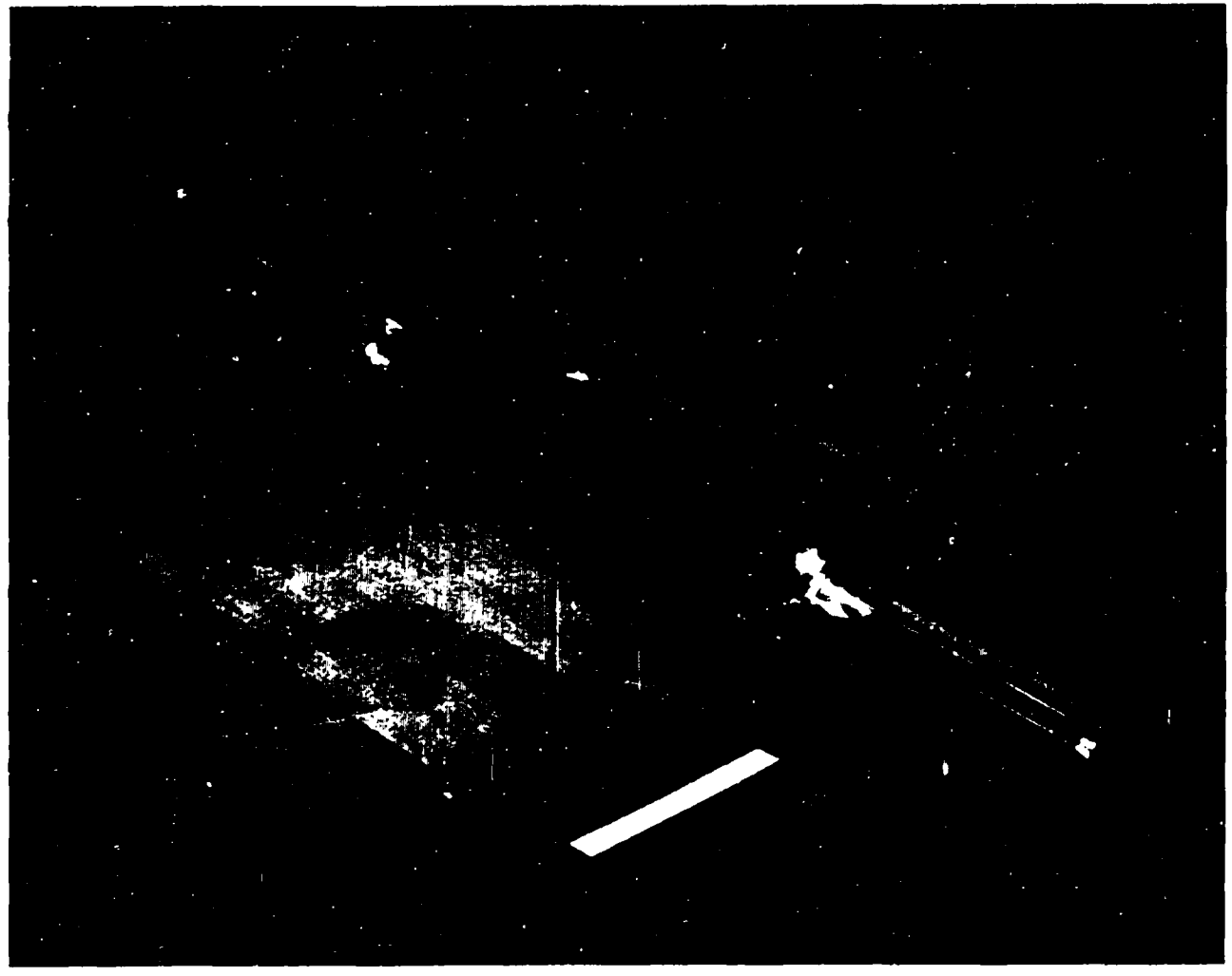

Figure B-6. Copper Heat Exchanger

The helium liquid flowing off-axis exits the hollow copper fin D at the winding OD (see also Figure 6) and then moves radially inwards providing added cooling due to decompression. The liquid level within the winding is controlled by a dam E which also feeds a helium pool to cool the electrical leads. The lead cooling I is essentially self-regulating with added heat producing increased flow to the lead. The winding also incorporates an auxiliary heat exchanger which is thermally connected to the main or central heat exchanger at the core ID. This auxiliary heat exchanger provides additional capability for heat removal from the helium contained in the winding. During a rapid spin-up mode, the helium isolated in the winding will experience compressional heating. This heating will produce high convective flow velocities in the radial passages and around the auxiliary heat exchanger which should reduce the temperature rise in the winding.

The heated helium produced in the winding moves radially inwards to a gas plenum F located near the axis of rotation. The gas in this plenum is directed through tubes G to cool the anti-drive thermal transition shell J. The cooling tubes return the gas on axis where it exits through the exciter drive shaft to orifices located on the slip ring flange H.

This cryogenic scheme should minimize the temperature rise in the winding during the mechanical transients and the associated compressional heating for a rapid spin-up condition. A fast current excitation of the order of one second with the present copper stabilized Nb-Ti conductor would impose an unacceptable heat load which most likely would quench the winding.

Carbon resistance thermometers were mounted on the heat exchanger so that they projected ~ 1.0 mm into the helium flow. These thermometers are identified in Figure 5 as T_1, on the impeller at the rotor axis, T_2, on the base of the copper heat exchanger and T_3, on the outer tip of the heat exchanger fin.

The external helium supply system to the rotor was also monitored during all running tests. A subcooling heat exchanger (CTI) was located between the supply dewars and the rotor inlet bayonet which provided control on the helium inlet temperature and pressure. The CTI allowed subcooled (below 4.2°K) helium to be introduced into the rotor.

"SPIN-TEST" ROTOR COLD DYNAMIC TESTS

The main test objective for the "Spin-Test" Rotor was concerned with the acceleration influence on excited superconducting coils. Previous tests on the earlier four-pole rotor[1] showed superconductor normalization under fairly modest speed changes of ~ 2500 rpm/min. when starting from low speeds. This normalization was attributed to conductor movement which generated sufficient heat to initiate a quench.[5] The speed increase also produced a slight temperature rise due to helium compression. This temperature increase however was very small (~ 0.1°K) and certainly not serious enough to quench the winding.[1]

The "spin-test" rotor as presented in the earlier discussion was cooled down, at low speed, to liquid helium temperature. The cryogenic flow conditions were then adjusted to obtain a minimum temperature on the rotor centerline thermometer, T_1. Different temperatures at the rotor centerline could be obtained by a pressure-temperature balancing procedure between the rotor and the external helium supply. The complete helium flow system showing the external supply and the test rotor is shown in Figure 7.

The external flow conditions to the rotor are established by pressurizing the supply dewars, P_{s_1} or P_{s_2}. The CTI heat exchanger located between the supply dewar and rotor conditions the flow stream to allow lower temperature helium to be inputed to the rotor. Typical dewar supply pressures of 10 to 15 psig would raise the helium temperature to ~ 4.8 to 5.0°K. The additional transfer and line losses would thus produce an unacceptable helium inlet temperature near 5°K or above. The CTI thus allows subcooled helium to be introduced to the

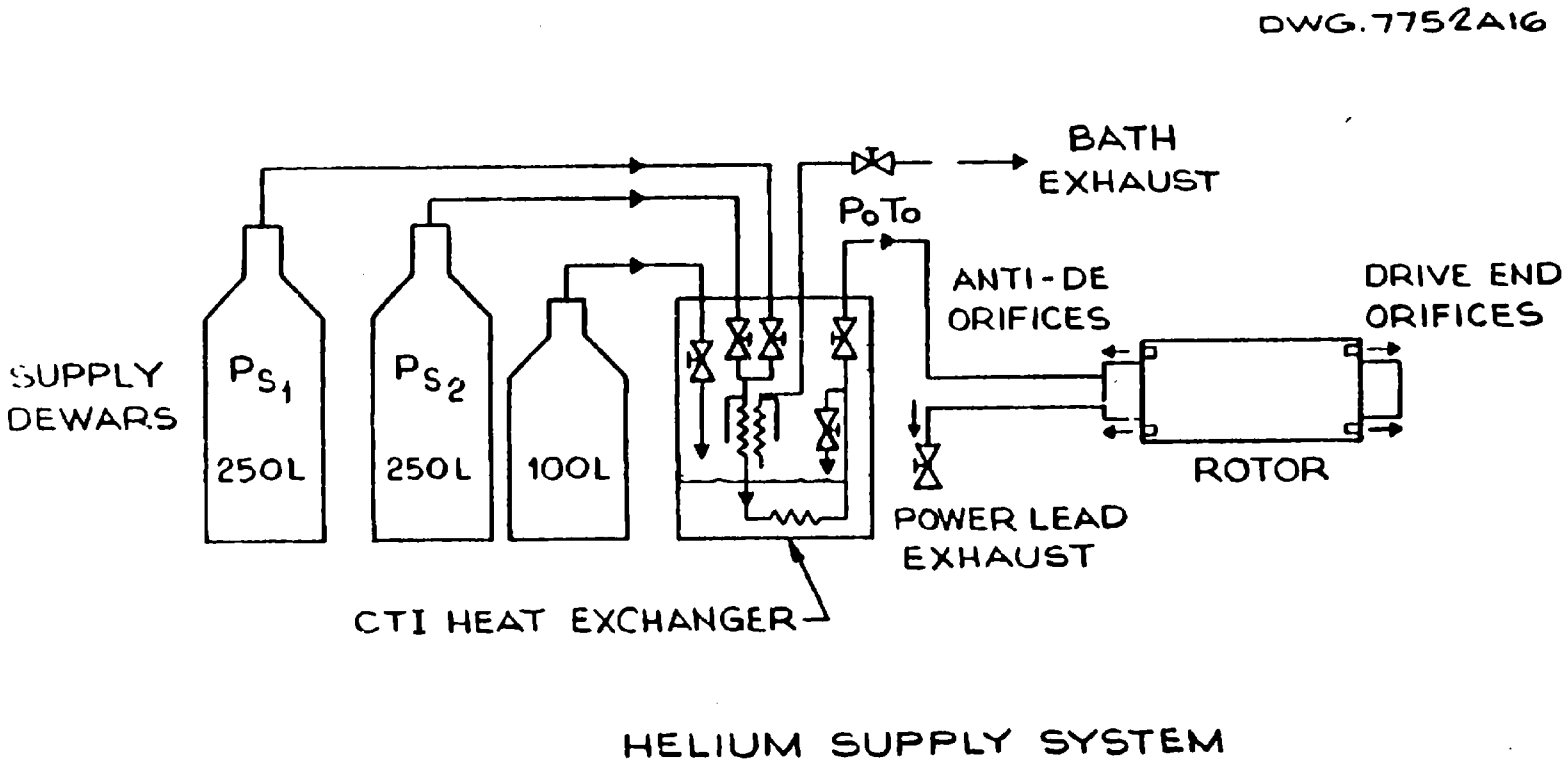

Figure B-7. Helium Supply System

rotor in a highly controlled manner. The CTI system is capable of supercritical operation, i.e., pressures above the 2.30 atm. critical with subcooling as low as 3.0°K. The outlet pressure and temperature from the CTI, P_o and T_o, thus establish the inlet conditions to the rotor. The actual inlet temperature at the bayonet is also monitored to precisely define the inlet conditions. The mass flow rate and the quality of the inlet helium can thus be fairly well defined by this experimental procedure.

Current Excitation Tests

A series of current excitation tests on the superconducting coils were initially performed to evaluate the maximum current level and ramping capability. These excitation tests were conducted at a constant rotor speed of ~ 1000 rpm. The helium flow conditions were: supply dewar pressure P_s = 1.68 atm, rotor vacuum 2μ, CTI outlet P_o = 1.56 atm. and T_o = 4.4°K, and inlet bayonet T_B = 4.5°K. The average mass flow rate was essentially the same throughout these and subsequent tests at ~ 40 ℓ/hr.[6] The inlet flow quality was quite low as inferred from the observed inlet pressures and temperatures. The maximum current excitation levels obtained under these cooling conditions is identified in Table 1. Also included is the maximum current level obtained with pool-boiling conditions at fast and slow ramp rates.

The ramping behavior of the superconducting coils at different speeds and temperature conditions provides some insight into the effective rotor cooling. The ramping capability of any coil is limited by the heat generated due to conductor movement and the ramping loss in the superconductor itself. For a specific coil system the temperature rise and resulting coil performance is influenced by the ability to remove this heat. The cooling system thus provides a major role in establishing the overall performance limits.

The ramping data obtained in test I provided a reference level for the ramping capability of the coils under rotation. These slow

speed results should be comparable to the pool cooled static test values. At low speeds the centrifugal force is minimized with respect to its influence on conductor movement and the helium flow system. The inlet flow conditions moreover present helium properties which are similar to the pool-boiling environment.

The Test I and static results, for low ramp rates can be compared if we adjust for the temperature difference. At low ramp rates the heat generated due to conductor movement is more easily dissipated due to the longer time constant. This argument of course only applies to gradual or frictional type heating of the conductor. The thermal conditions for slow excitation thus tend to be nearly isotropic with the maximum current limits related to the coil temperature.

The "spin-test" thermometry did not provide for temperature measurement of the winding region. The helium temperature at the rotor OD and the winding itself should however be reflected by T_3, the OD heat exchanger thermometer. For this reason, the rotor ramping data is correlated with the T_3 temperature which is listed in Table 1. The inlet conditions also influence with the winding temperature hence T_o, the inlet temperature is also listed for comparison.

If we take the 4.2°K static quench current of 325A as the maximum two-coil critical current, the ramping results can be normalized using the temperature vs field behavior shown in Figure 8. The maximum quench current at slow speed was 305A which is 94% of 325. A two-coil current of 305A produces close to 4.5T as determined from the load line.(6)

The 305A quench current thus corresponds to a winding temperature of ~ 4.4°K which is close to the 4.6°K value for T_3. It is immediately apparent that the higher ramp rates up to 255 A/min. for Test I degrade the quench current. Moreover, static, pool-boiling conditions allowed a ramp rate of 720 A/min. without a quench. The Test I results thus indicate even at low speeds that the cooling capability of the rotor may be degraded compared to static pool boiling.

Table B-1

Quency Current for Different Ramp Rates, Cooling and Speed

Test	Speed (rpm)	Ramp Rate (A/min)	Quench Current (A)	T_3 (^oK)	T_o (^oK)	Remarks
I-10	850	12.4	298	4.7	4.47	
I-17	850	24.0	305	4.6	4.46	
I-7	1000	110.0	220	4.7	4.44	
I-6	1000	255.0	140	4.7	4.42	
	Static	720.0	(15 → 315)	(4.2)	(4.2)	did not quench
	Static	36.0	325	(4.2)	(4.2)	pool boiling
II-3	4000	2.50	200	4.8	4.18	
II-8B	4000	16.0	260	4.6	4.23	
II-8A	1200	64.0	190	4.80	4.25	
II-11	1200	64.0	280	4.25	3.58	
II-10	6000	72.0	240	5.00	3.20	
II-13	8000	64.0	220	5.15	3.84	

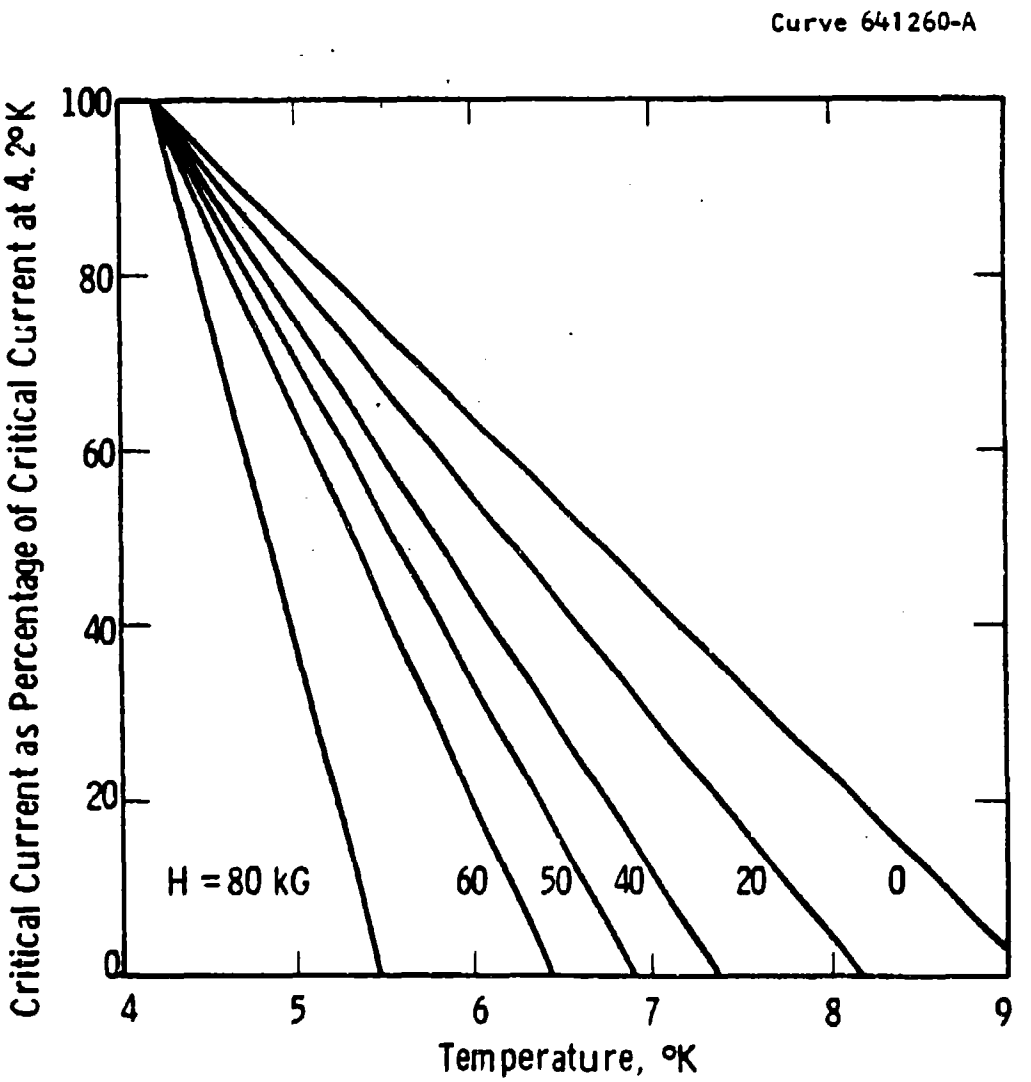

Figure B-8. Magnetic field and temperature degradation of the current carrying capacity of Nb-Ti conductors

Additional ramping data was obtained at higher speeds under different cooling conditions. This data identified as Test II evaluated the influence of speed and reduced inlet temperature on the ramping capability. As listed in Table 1 the ramping value for Test II-8A @ 1200 rpm basically agrees with the previous Test I results. The quench current for Test II-3 @ 4000 rpm (T_3 = 4.8°K) appears to be slightly degraded. Test II-8B (T_3 = 4.6°K) also @ 4000 rpm shows improved ramping, close to Test I results, which may be due to the lower temperature. The inlet temperature T_o for these three tests was ~ 4.2°K. The latter 4000 rpm data did not conclusively demonstrate any cooling degradation as a function of speed. A series of three additional tests were then conducted at essentially the same ramp rate as a function of speed. The inlet temperature T_o was also reduced to evaluate this effect on the ramping capability.

A comparison of II-8A and II-11 @ 1200 rpm for the same ramp rate shows a dramatic increase in quench current for the reduced T_3 of 4.3°K. This value however is still degraded compared to the static result. Test II-10 and II-13 at 6000 and 8000 rpm respectively show improved ramping capability, i.e., higher quench current, even with the increased T_3 temperature of 5.0 to 5.2°K.

The centrifugal force tends to reduce the conductor movement as the speed is increased. At 8000 rpm, for example, the OD centrifugal force is increased by almost two orders of magnitude. The ramping performance at high centrifugal speeds should be less influenced by conductor motion. The winding temperature and conductor cooling would thus dominate the observed excitation behavior. This relationship is consistent with the 8000 rpm result of II-13. A ratio of quench current gives 220/325 = 0.68. Reference to Figure 8 (for ~ 3.5T)[6] indicates a temperature of 5.3°K for 68% which is close to the T_3 temperature of 5.2°K.

These latter tests thus indicate improved ramping capability compared to the earlier low speed results. The improved performance for

Test II-11 can be mainly attributed to the reduced temperature. The high speed (II-10) and (II-13) improvement is more likely related to the increased centrifugal loading which restricts the conductor motion. In addition, at high speeds, improvement in the helium heat transfer coefficient can also be expected.

Current Excitation and Ramping Discussion

The current excitation and ramping data which was studied as a function of speed and temperature presented some general trends which impact on a rapid spin-up cooling and winding design.

The spin-test helium system did not provide adequate cooling as the speed was increased. Steady-state operation at 8000 rpm indicated OD and winding temperatures above 5.0°K. This temperature rise which was measured at the heat exchanger OD did not appear to be significantly reduced due to heat exchanger. Even at low speeds the heat transfer or helium cooling was degraded compared to the pool-boiling environment. Improvement in low speed performance could be obtained by reducing the inlet temperature. Reduced inlet temperatures appeared to influence the winding cooling even for the higher speed conditions.

Higher centrifugal loading tended to improve the ramping performance. This result indicates acceleration followed by excitation would be desirable as compared to simultaneous spin-up and excitation. A highly supported conductor, as obtained in a fully impregnated coil may provide the necessary support to allow spin-up and excitation. The overall performance may be improved by high T_c conductors such as Nb_3Sn. This material would still require rigid conductor placement due to the attendant problems from conductor motion.

The spin-test "open winding" design allowed helium in intimate contact with the conductor. The performance, with respect to heat removal, should have been improved due to the helium circulation and its high specific heat.

The open structure, however, allowed significant coil degradation since proper conductor support was not obtained. The maximum current level was only 71% of short sample.[6] Moreover the high helium content also produced higher compressional heat loads resulting in increased winding temperature.

An open winding design for rapid spin-up and excitation does not appear to be an optimum configuration. Rigid conductor placement as offered in an impregnated coil is indicated along with a minimum in the off-axis helium.

Rotor Acceleration Tests

A series of acceleration tests were performed to evaluate the stability of the superconducting coils and helium flow system to various spin-up conditions. In these tests, the influence of acceleration rate, start and finish speed, helium flow conditions and coil excitation were investigated.

As reported in the earlier "spin-test" final report[6] a series of acceleration tests were performed on excited superconducting coils. The coils were energized, at ~ 1000 rpm, to current levels as high as 80% of the ~ 300A low-speed quench current. The speed was then increased in steps to a maximum of ~ 25,000 rpm/min. to evaluate coil stability. An upper speed of ~ 4000 rpm was selected due to the observed performance of the helium cooling system. Initial gradual spin-up tests to 4000 rpm (@ 400 rpm/min.) indicated essentially no change in the inlet flow conditions and rotor temperatures.

The helium distribution, within the rotor, was adjusted to improve the flow through the winding. Small diameter (0.76 mm) orifices were installed in the drive end with larger diameter (1.52 mm) in the anti-drive end. Both sizes are less than the cooling tube diameter of 4.8 mm. The power lead exhaust flow was also increased to reduce the possibility of lead overheating during the acceleration changes. The inlet temperature, T_o, during these tests was close to 4.5°K.

The centerline temperature T_1 was observed to increase as the acceleration level was increased. At a 25,000 rpm/min. rate the centerline temperature rose to nearly 100°K and recovered after 30 sec. to ~ 4.5°K. The heat exchanger OD thermometer T_3, gradually increased to ~ 5°K during the same time frame and then decreased to the ~ 4.6°K initial temperature. A 240A current level in the winding was maintained with no observed variation in current.

Since the speed change did not produce a quench, it is apparent that the observed temperature rise was confined to the centerline or core of the rotor. The temperature at the OD, T_3, of ~ 5°K also indicates that the warm gas on the centerline did not propagate out into the winding.

Additional tests were performed to further evaluate the influence of acceleration on the stability of the helium flow system. In these tests the speed was again ramped in increasing steps to 4000 rpm. Identical 1.52 mm orifices were installed at both ends of the rotor. The winding current was not energized for these tests and the inlet temperature T_o was 4.2°K.

A gradual spin-up to 4000 rpm at ~ 700 rpm/min. showed no change in the inlet or rotor temperatures. A spin-up at 5300 rpm/min. again showed no temperature variation. At 13,300 rpm/min., however, the centerline T_1 and OD temperature T_3 both rose, to 4.8 and 5.5°K respectively. After ~ 20 sec., for a constant speed of 4000 rpm, the temperature recovered to the initial conditions.

The inlet temperature T_o was then reduced to 3.8°K and the rotor spun-up to 4000 rpm at 16,300 rpm/min. This spin-up showed only a minor change in the rotor temperatures with T_1 (start) = 4.0 to (final) 5.0°K and T_3 (start) = 4.3 to (final) 5.2°K. This acceleration test is shown in Figure 9. A reduction in the inlet temperature thus reduced the OD temperature rise from 7.6 to 5.2°K.

Additional spin-up tests to 6000 rpm were performed at 4.3°K inlet temperature for speed changes in excess of 25,000 rpm/min. A wide

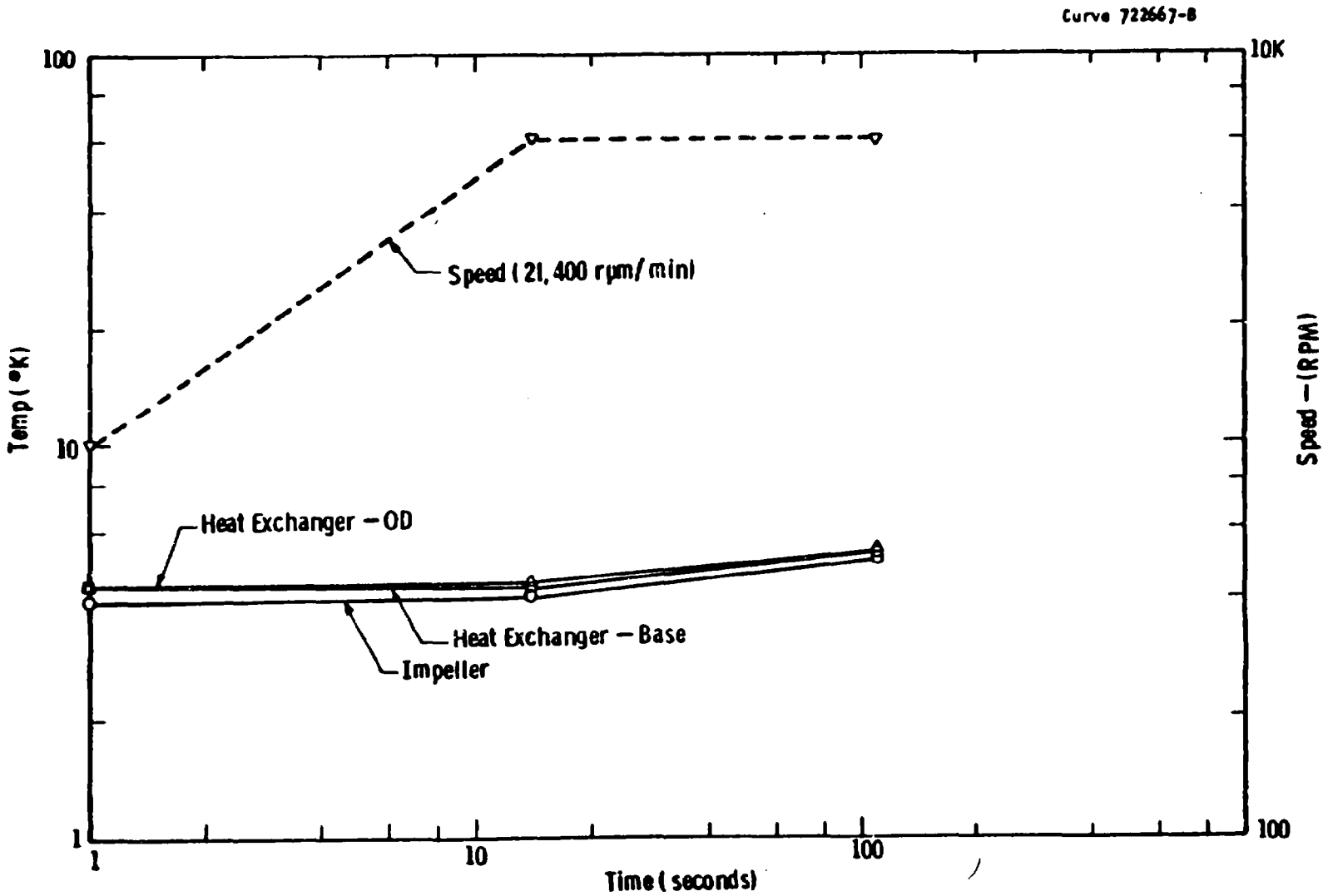

Figure B-9. Acceleration Test with Sub-cooled Inlet Conditions

variety of flow and orifice combinations was attempted. These acceleration tests showed a consistent dumping of the helium reservoir in the winding with a resulting T_3 temperature of 15 to 18°K. Attempts to cool the winding or refill the winding reservoir were unsuccessful at steady-state speed. The winding could only be recooled to the initial ~ 4.5°K by reducing the speed to the 500 to 1000 rpm.

A final test was run where the rotor speed was increased in steps to 8000 rpm. The resulting temperature changes due to the acceleration influence is shown in Figure 10. The inlet condition for this test was again subcooled to 3.8°K.

Acceleration Test Discussion

The centerline temperature pulses observed on the first series of acceleration tests was apparently related to a backflow of gas from the drive end cooling tubes to the centerline. A warm core of gas was momentarily collected which was cleared away after ~ 25 sec. and the temperature restored to the initial condition. It was originally suggested in the spin-test final report[6] that this flow reversal might be related to an inertial influence on the exit stream. A calculation of the pressure change due to the acceleration influence is not sufficient to counteract the high centerline pressure of ~ 1.6 atm. A more likely explanation was developed by careful review of the flow effects created by the different orifices and the power lead exhaust.

It is suspected that a pumping action was produced by the anti-drive end cooling tubes which lowered the winding and centerline pressure. The restriction on the drive end orifices allowed gas from these tubes to backflow to the centerline due to this reduced pressure. The increased flow into the rotor which should also occur was diverted outwards by the impeller through the heat exchanger fin to the winding. Over cooling of the base of the heat exchanger at T_2 should result which was indicated by the temperature measurements. During the acceleration change T_2 in fact showed the lowest temperature.

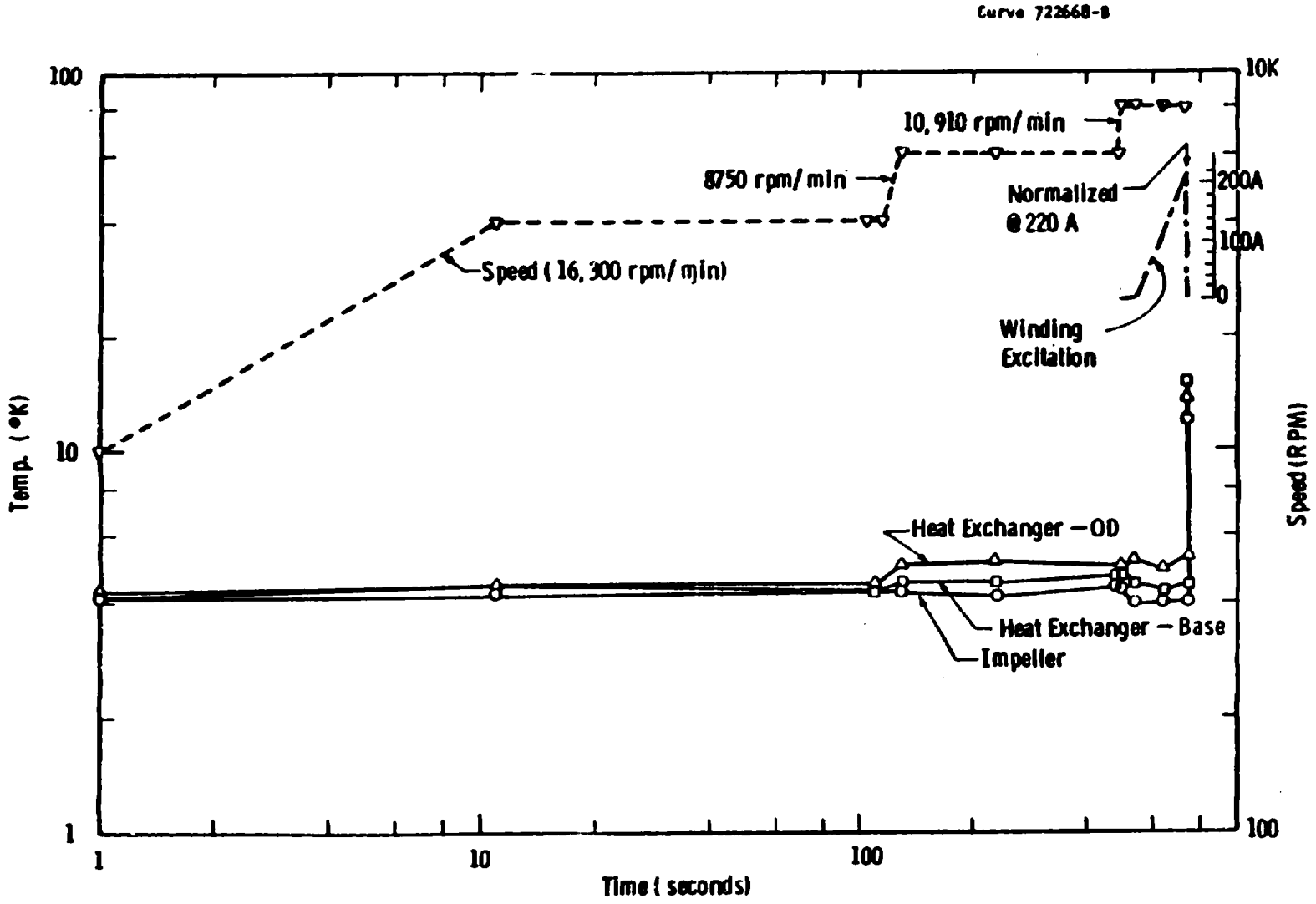

Figure B-10. Superconducting Coil Excitation at 8000 rpm

When the drive end orifices were increased to 1.52 mm which reduced the exit restriction, the high centerline temperature pulse disappeared.

The pumping action on the winding region was dramatically shown in some of the additional spin-up tests. The orifices for these tests were either removed entirely or a 1.52 mm diameter installed. A rapid spin-up to 6000 rpm for inlet temperatures of 4.2°K allowed the winding region to be entirely purged of its liquid reservoir. Attempts to refill the winding with cold centerline liquid at speed were not successful. The inability to refill the warm winding with cold liquid, at steady-state speed, is extremely baffling and represents one of the least understood results. It is possible that some form of an acoustic interaction or impedance is created by the warm outer winding reservoir. Liquid moving off-axis flashes instantly and warms immediately to the OD temperature.

The ability to maintain the winding reservoir with liquid is enhanced by subcooling the inlet flow stream. Inlet conditions of 3.8°K and below produce a dense single-phase liquid which allows an off-axis cold flow to be maintained. These latter subcooled conditions produce OD or winding temperature which are in line with compressional heating.

REFERENCES

1. R. D. Blaugher, T. J. Fagan, Jr., J. H. Parker, Jr., J. M. Wells and J. L. McCabria, Proc. Fifth Int. Cry. Eng. Conf. (1974), p. 143.

2. R. D. Blaugher, J. H. Parker, Jr. and J. L. McCabria, IEEE Trans. on Mag., Vol. MAG-13 (1977), p. 755.

3. B. B. Gamble and T. A. Keim, Adv. in Cry. Eng., Vol. 25 (1979), p. 127.

4. G. R. Wagner, S. S. Shen, R. E. Schwall, M. S. Walker and A. Petrovich, IEEE Trans. on Mag., Vol. MAG-15 (1979), p. 228; M. S. Walker et al., IEEE Trans. on Mag., Vol. MAG-15 (1979), p. 80.

5. H. L. Southall and C. E. Oberly, IEEE Trans. on Mag., Vol. MAG-15 (1979), p. 711.

6. R. D. Blaugher, Technical Report, AFAPL-TR-77-39 (1979).

7. A. Patterson and R. D. Blaugher, Adv. Cry. Eng., Vol. 23 (1978), p. 132.

APPENDIX C

EXAMINATION OF STICK-SLIP MOTION IN SUPERCONDUCTING DIPOLES

J. H. Murphy
Westinghouse R&D Center
Pittsburgh, Pennsylvania 15235

ABSTRACT

The energy released due to stick-slip motion of a conductor in a superconducting dipole winding is calculated. Stick-slip motion of a conductor has for years been postulated to be the primary source of premature normalization of superconducting windings. Formulae are presented which presume knowledge of the mechanical and electrical properties of the conduction and the state of the conductor before and after the event occurs. Example calculations are made of superconducting dipoles to illustrate the magnitude of temperature rise which can be anticipated. Among the examples considered are dipoles of the size the Air Force Spin Test Rotor and the 300 MVA Superconducting Generator. A comparison of dipole windings and solenoidal windings shows the relative difficulty involved in designing a mechanically stable dipole winding.

1. INTRODUCTION

The present memo is one in a series of memos devoted to the analytical examination of mechanical stability in superconducting windings.[1] In this memo, we examine the mechanical stability of a superconducting dipole winding which is constrained until the frictional force retaining the conductor is smaller than the Lorentz force acting on the conductor. The conductor subsequently slips and continues to

move until either the conductor impacts an immovable surface or the conductor strain increases sufficiently to offset the Lorentz force. The present model assumes the conductor acts like a string subjected to a Lorentz force, therefore only the effect of axial strain has been considered.

2. THEORY OF MECHANICAL STABILITY

Many applications of superconducting magnet technology require the magnet configuration to be in the form of a racetrack winding or dipole winding. This configuration is generally characterized by two semicircular sections connected by two rectangular sections. These straight sections have the greatest potential for conductor movement as the following analysis demonstrates.

As with the solenoid, let us begin to examine this mechanical stability problem by investigating the thermodynamic relationships which govern the behavior of a conductor which in this case is anchored at two ends and subjected to a Lorentz force. Initially, it is assumed that this conductor is mechanically constrained by the adjacent structures through frictional forces. Where practical, the general case is considered where the conductor has some initial curvature and initial stress. The initial stress in the conductor is assumed to be insufficient to restrain conductor motion. Once the Lorentz force becomes large enough to overcome the static frictional force between the conductor and the structure, the conductor will move. Work will be performed on the conductor until the conductor comes to rest. It is assumed that these events occur very rapidly, therefore the conductor temperature will rise under essentially adiabatic conditions.

The analysis of the mechanical stability in a dipole depends upon the final state of the conductor. Two limits can be calculated; the case of a conductor self supported and the case of a conductor externally supported are examined.

Case I - Final State — Conductor Self Supported

The mechanical stability model appropriate for analyzing a conductor which is self supported in the final state is illustrated in Figure 1.

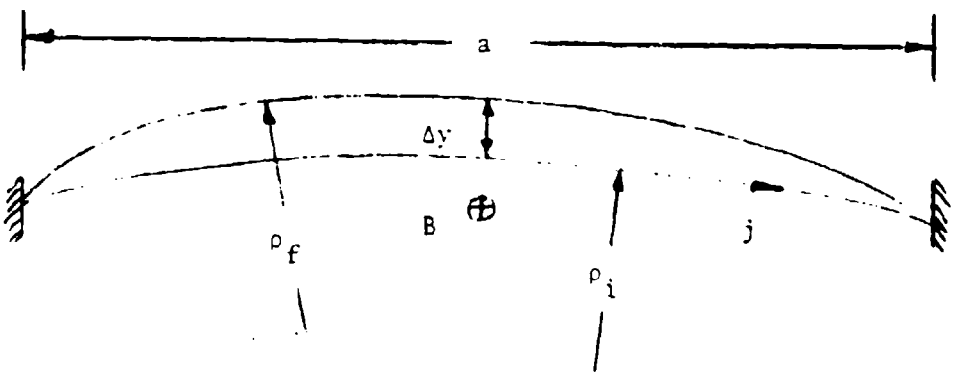

Figure C-1. Mechanical Stability Model for a Self Supported Conductor in a Dipole Winding.

In this calculation, the conductor thickness, t, is assumed to be very small in comparison to the distance between tie points, a. The conductor is subjected to a body force due to the interaction of the conductor current density, j, with the local magnetic field, B. The initial strain in the conductor is ε_i and the final strain is ε_f. The force per unit volume acting on the conductor, f, is given by

$$\underline{f} = \underline{j} \times \underline{B} \qquad (1)$$

Since the conductor is assumed to be self-supporting when it finally comes to rest, the final strain in the conductor is directly related to the Lorentz force and can be found from

$$\varepsilon f = Bj\rho_f/E \tag{2}$$

where E = Young's modulus of the conductor. Furthermore, the final strain can be found from the geometry of the winding, accordingly, it can be shown that

$$\varepsilon_f = \varepsilon_i + \frac{\frac{2\rho_f}{a}\sin^{-1}\frac{a}{2\rho_f}}{\frac{2\rho_i}{a}\sin^{-1}\frac{a}{2\rho_i}} - 1 \tag{3}$$

The maximum conductor deflection, Δy, can be found from

$$\Delta y = \rho_f - \rho_i + \sqrt{\rho_i 2 - (a/2)^2} - \sqrt{\rho_f 2 - (a/2)^2} \tag{4}$$

Since the work done on the conductor in going from the initial to final states is equal to the change in internal energy plus the heat generated, the heat generated per unit volume, q, can be calculated from

$$q = Bj\Delta y/2 - 1/2\ E\ (\varepsilon_f{}^2 - \varepsilon_i{}^2) \tag{5}$$

In the limit of large ($\rho f/a$), equations (2) through (4) can be combined and reduced to

$$\varepsilon_f = \frac{Bj\rho_f}{E} = \varepsilon_i + \frac{1}{24}\left(\frac{a}{\rho_f}\right)^2 - \frac{1}{24}\left(\frac{a}{\rho_i}\right)^2 \tag{6}$$

$$\Delta_y = \frac{a^2}{8}\left(\frac{1}{\rho_f} - \frac{1}{\rho_i}\right) \tag{7}$$

It can be seen from equation (5) that an initial prestrain on the conductor reduces the amount of heat generated. Also equation (5) through (7) show that the heat generated can be reduced by decreasing the radius of curvature between the tie points. This latter point is important to the design of dipole windings since improved performance can potentially be achieved by slight modifications in the winding design.

Case II - Final State — Conductor Externally Supported

The mechanical stability model appropriate for a conductor which is externally supported in the final state is illustrated in Figure 2.

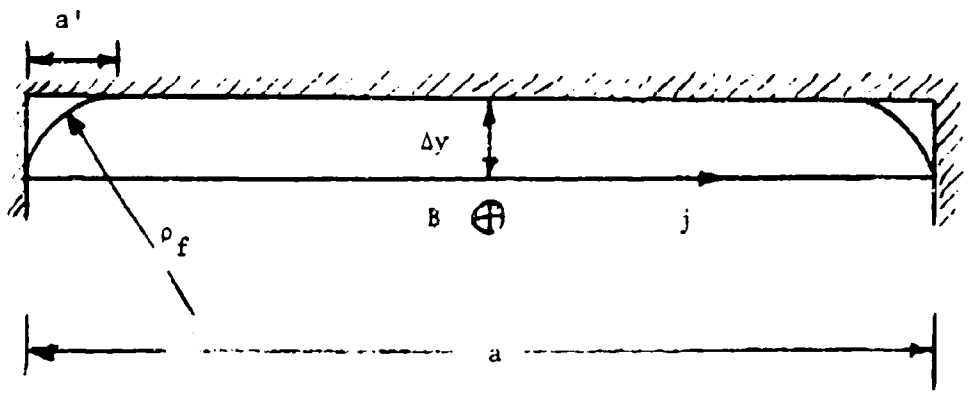

Figure C-2. Mechanical Stability Model for an Externally-supported Conductor in a Dipole Winding.

As in the preceding case, the conductor thickness, t, is assumed to be very small in comparison to the distance between tie points, a. The conductor is subjected to a body force due to the interaction of the conductor current density, j, and the local magnetic field, B, as given by equation (1). The initial strain in the conductor is ε_i and the final strain is ε_f. In the final state, part of the conductor is self-supported and the radius of curvature in this region is found from

$$\varepsilon_f = Bj\rho_f/E \tag{8}$$

Furthermore, the final strain can be found from the geometry of the self-supported regions of the conductor, hence it can be shown that

$$\varepsilon_f = \varepsilon_i + \frac{a'}{a}\ \frac{2\rho_f}{a'}\ \sin^{-1}\ \frac{a'}{2\rho_f}\ -1 \tag{9}$$

To simplify this case, we only consider deflections from an initial condition of a straight conductor. The maximum deflection Δy, is related to the radius of curvature of the unsupported conductor as the following relationship demonstrates:

$$\Delta y = \rho_f - \sqrt{\rho_f^2 - (a'/2)^2} \tag{10}$$

Since the work done on the conductor equals the change in internal energy plus the heat generated, the heat generated per unit volume, q, can be calculated from

$$q = Bj\Delta y\ \ 1 - \frac{1}{2}\ \frac{a'}{a}\ \ - \frac{1}{2}\ E\ \left(\varepsilon_f^2 - \varepsilon_i^2\right) \tag{11}$$

In the limit of large ($\rho f/a'$), equations (8) through (10) can be combined and reduced to

$$\varepsilon_f = \frac{Bj\rho_f}{E} = \varepsilon_i + \frac{1}{24}\ \frac{a'}{\rho_f}^2\ \frac{a'}{a} \tag{12}$$

$$\Delta y = \frac{(a')^2}{8\rho_f} \tag{13}$$

It can be seen from equation (11) that an initial prestrain on the conductor reduces the amount of heat generated.

Adiabatic Temperature Rise

From equations (5) or (11) one can calculate the heating that occurs when the conductor suddenly moves. The maximum temperature rise can be calculated from

$$q = \rho\, c_p\, \delta T \qquad (14)$$

where ρ = the mass density of the conductor

c_p = the specific heat at constant pressure

δT = the maximum temperature rise.

In the preceding memo,[1] the effect of heat input on the conductor temperature has been estimated assuming an adiabatic temperature rise from an initial temperature of 4.2K.

3. EXAMPLE CALCULATIONS

To illustrate the potential magnitude of the temperature rise in superconducting dipoles, let us consider two dipoles. For the case of a typical small superconducting dipole, let us consider a coil for the spin test rotor.(2) Whereas, fo5 the case of a typical large superconducting dipole, let us consider a coil for the 300 MVA generator.(3) For the example calculations let us examine the effects of prestrain, providing an initial curvature to the conductor, and impact with an immovable surface. Tables 1 and 2 summarize these calculations. Table 1 illustrates that the heating can be significantly lowered in a small dipole by either prestraining the conductor or by providing some initial curvature to the winding. The latter having the greatest effect. The second table illustrates that very large prestrains in long superconducting dipoles are required to lower the conductor heating.

The fact that prestrain on the conductor in long dipoles cannot be practically used to reduce the heating during sudden motions leads

TABLE C-1

EXAMPLE CALCULATIONS FOR THE SPIN TEST ROTOR COIL

j, A/m^2	5×10^8	5×10^8	5×10^8	5×10^8	5×10^8
B, T	4	4	4	4	4
E, Pa	1.03×10^{11}	1.03×10^{11}	1.03×10^{11}	1.03×10^{11}	1.03×1011
a, m	0.15	0.15	0.15	0.15	0.15
a', mm	--	--	--	--	9.88
ε_i, %	0	0	0.1	0.3	0
ε_f, %	0.707	0.534	0.738	0.816	0.046
ρ_i, m	∞	0.364	∞	∞	∞
ρ_f, m	0.364	0.275	0.38	0.42	0.024
Δy, inches	0.304	0.098	0.291	0.264	0.020
final state	self	self	self	self	external
q, J/cc	5.24	1.03	4.6S	3.73	0.97
w, J/cc	7.81	2.50	7.40	3.43	0.98
ΔT, K	> 30	27	> 30	> 30	27

TABLE C-2

EXAMPLE CALCULATIONS FOR THE 300 MVA FIELD COIL

j, A/m2	10^4	10^4	10^4
B, T	5	5	5
E, Pa	1.03 x 1011	1.03 x 1011	1.03 x 1011
a, m	2.0	2.0	2.0
a', mm	--	--	6.6
ε_i, %	0	1.0	0
ε_f, %	1.58	1.99	0.005
ρ_i, m	∞	∞	∞
ρ_f, m	3.25	4.1	0.011
Δy, inches	6.06	4.80	0.020
final state	self	self	external
q, J/cc	25.6	15.3	0.254
w, J/cc	38.5	30.5	0.254
ΔT, K	> 30	> 30	18

one to the conclusion that external support structure plays an extremely important role in the mechanical stability of long superconducting dipoles.

4. CONCLUSIONS

The heating in a superconducting dipole can be very large. An interesting comparison of a superconducting solenoid and a superconducting dipole can be made to illustrate the relative difficulty in keeping the heating low in a dipole winding. In a superconducting solenoid with an initial strain of zero which suddenly moves under its Lorentz force, the heating is given by[1]

$$q = Bj\ R\ \varepsilon_f - 1/2\ \varepsilon_f^2 \qquad (15)$$

where R = the radius of the solenoidal windings. Whereas, in a superconducting dipole with an initial strain of zero which suddenly moves under its Lorentz force, the heating is given by equations (5) through (7), which can be reduced to

$$q = Bj\ a\ \sqrt{6\varepsilon_f}/8 - 1/2\ E\ \varepsilon_f^2 \qquad (16)$$

If these two coils are designed to have the same heating per unit volume, same peak magnetic field, same operating current density, same elastic modulus and same final strain, then the radius of the solenoid is related to the distance between tie points and the final strain in the conductor and is given by

$$R = a/8\ \sqrt{6/\varepsilon_f} \qquad (17)$$

This relationship demonstrates the difficulties which can be encountered in the design of a superconducting dipole. For example, if the strain is 0.1%, then an equivalent solenoid has to have a radius which is

approximately ten times the length of the dipole uniform field region. This improves by increasing the strain.

It has been shown that prestrain reduces the amount of heating. However, in the example calculations, we find that this is a practical solution for only the short dipoles. For long dipoles, the practical solution to reducing the heating is to limit conductor motion by external structures. This can take two forms: potting the windings or grouping the conductors in slots of dimensions which significantly reduce the potential motion of any one conductor.

REFERENCES

1. J. H. Murphy, "Examination of Stick-Slip Motion in a Superconducting Solenoid," Westinghouse Memo 78-1F1-SWIND-M2.

2. R. D. Blaugher, "Superconducting Spin-Test Rotor," Westinghouse Report 77-9F1-ROTOR-R1.

3. J. H. Parker, Jr. and R. A. Towne, "Superconducting Generator Design," EPRI RP 429-1, Final Report.

APPENDIX D

Data Acquisition and Telemetry System for the Superconducting Generator Heat Transfer Experiment

G. T. Mallick, Jr. and G. J. Faychak

Some means must be devised to allow the data to be transferred from the rotating machinery into the laboratory for processing. Telemetry is not the only option. Slip rings of very high quality are available to do this task. While it is practical to employ these devices for a number of applications, chiefly involving a limited amount of experimental data transferred at high voltage (volts rather than millivolts) and low current, it was easily decided that this method was less than practical for this experiment, wherein some 17 temperatures must be measured, and where the voltage levels involved for some of the sensors are measured in microvolts. Consequently, it was quite clear that the required data would be delivered to the laby by means of telemetry, rather than slip rings.

This report describes the data acquisition system which has been in use to measure temperatures at 17 positions in a rotating (3600 rpm) cryostat. Details of the design considerations for the telemetry system, which operates to telemeter 100 measure measurements per second with eight bit accuracy, are described.

This subsystem is the most complex in the overall telemetry system. It resides on the rotor, and is subject to a great deal of stress. Reliability is most important in the design considerations for this part of the system.

Two operational models were made for this subsystem. The first model (shown schematically in Figure 1) multiplexes current through each

---

*Westinghouse Report 81-2G6-SUGEN-R1 (Supported by EPRI).

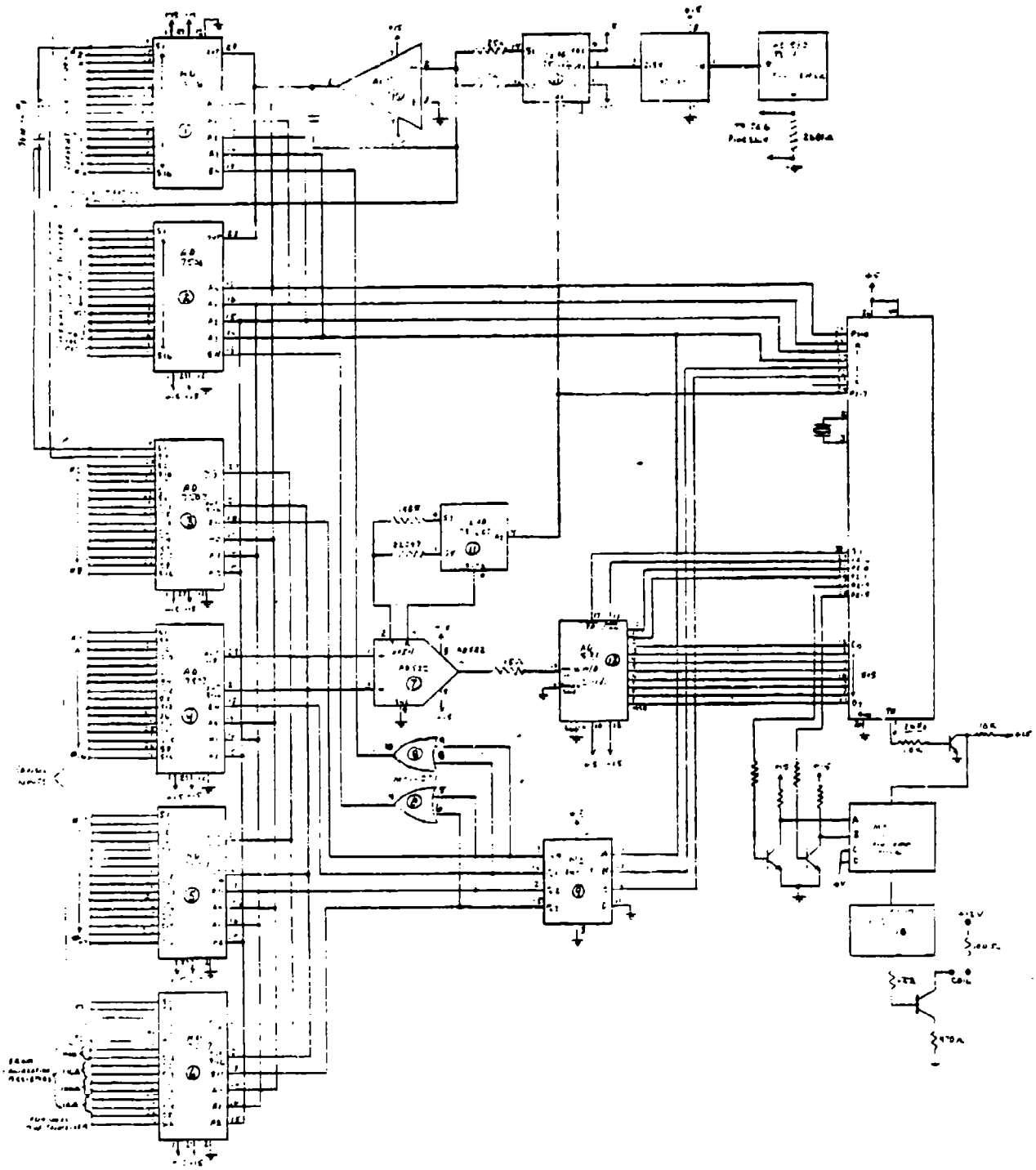

Figure D-1. Acquisition and Telemetry with current multiplexing.

of the sensors, and the second model (Figure 2) provides a regulated constant current through each of the sensors. The two designs were tried because the second permits the application of analog filtering at the output of the sensor, while the former does not. The two circuits have more similarities than differences, and the commonalities will now be discussed.

The basic circuit uses an 8748 microprocessor (Intel) as the control for the board. The processor addresses the multiplexers, steers the analog signal to the A/D converter, operates the A/D converter, and then reads its output. It then formats this binary information along with the multiplexer address information (channel information) and applies it to a binary rate multiplier, which acts as a programmable frequency divider which acts on the system clock output. The output of this circuit is a frequency which depends on the digital input to the device, and by this extremely simple expedient we are able to generator a frequency modulated signal. The output of the modulator is delivered to a frequency divider which simply scales the frequency down to our desired value. This then is provided to a complementary pair of transistors which act as power amplifiers for the data signal. The series capacitor (0.007 microfarad) was experimentally chosen to series tune the inductance of the transmitter coil to the data frequency. The Q of the output circuit is sufficiently low so that the power output is substantially constant for the frequency range which we employ. The digital system just described is so straightforward that no further discussion of that part of the telemetry module is deemed necessary.

The accuracy of the system depends on the accuracy of the analog signal and the accuracy of the A/D converter. Since this is the case, the analog circuits in the "front end" of the system were chosen with substantial deliberation. The silicon diodes are quite insensitive to fluctuations in the measuring current, but this fact notwithstanding, the current in the diodes is regulated by an operational amplifier (AD517) dedicated to this task. Resistors used in the current regulation circuit are precision metal film devices. The ultimate

regulation of this circuit should be traceable to the stability of the ~ 15 volt supply, which is used as the reference. Given the characteristics of the MC1468 in the power supply, it is expected that this source will not contribute an instability in the current greater than a few tenths of a percent, which will hold the effective temperature measurement accurate to within considerably less than a tenth of a degree Kelvin.

Two additional sources of error that must be considered are: (1) The input voltage multiplexer and (2) the instrumentation amplifiers (AD522) used in the system. Of special importance is the effect of mismatch in the different channels of the input multiplexer, since differences in the temperatures in the test cell are of special interest for this experiment. Because of the very high input impedance of the AD522 instrumentation amplifier, this effect is very small. Calculations show that the maximum error expected from the switch unbalance amounts to approximately 3/10 of a microvolt. Since the magnitude of signal voltage expected at $4.2^{o}K$ is on the order of 2.5 volts, clearly this error is completely inconsequential.

Errors in the instrumentation amplifier should be considered separately for the case of the silicon diodes and the carbon-glass thermometers. For the former case, the amplifier is run with a gain of three. The specified offset voltage drift of the AD522A instrumentation amplifier change than we anticipate) is 640 microvolts. This change corresponds to approximately $0.01^{o}K$ for the silicon diodes, making this error also inconsequential for our purposes.

The instrumentation amplifier is operated at a gain of 200 for use in measuring the carbon-glass thermometer. In this case, the offset voltage (referred to the input) is less, being about 240 microvolts for a $40^{o}C$ temperature change. Since the measuring current is ten microamps, a change of input voltage of 240 microvolts corresponds to a resistance change of 24 ohms. Since the resistance of the thermometer is 2000 ohms at $4.2^{o}K$, an uncertainty of 24 ohms represents a worst case error of one percent.

The AD571K A/D converter is specified to be accurate to within ± 3 bits out of 1024 over its entire operating temperature range of 0 to 70°C.

The errors mentioned above assume a temperature excursion far in excess of what we expect in actual operation of the Heat Transfer Experiment, where the temperature of the telemetry module experiences an estimated excursion of 10°C maximum.

The Data Acquisition and Telemetry module was constructed on a single piece of Westinghouse Micarta glass-epoxy material, 1/8" x 7-1/2" x 3-1/2". The electronic circuit was hand wired, and then, after testing, encapsulated in an epoxy resin on the wire side, and over most of the smaller components on the component side. Since the board was to be mounted in such a way that the components would be held on the board under the action of the centrifugal force, it was thought to be unnecessary to cover the integrated circuits with epoxy, since it is much easier to service the board if the circuits are accessible. In order to protect them from the elements, the integrated circuits were covered with RTV Silastic material, which is easily removable. The epoxy used was Hysol ES-4212 flexible casting system, mixed according to a 100-90 ratio by weight, to achieve a modest degree of flexibility. This we considered desirable to allow the module to conform to any irregularities in its supporting structure under the influence of the high g field.

Two models of the module were constructed. The first one, shown schematically in Figure 1, multiplexes the measuring current through the sensors one at a time, as mentioned above. The problem with this method is that it precludes analog filtering of the sensor output voltage, since the introduction of such a time constant would act to cause the current through the sensor to vary with time as the network charges and discharges. It was found experimentally that the data measured without input signal bandwidth limiting, or filtering, was excessively noisy. Very modest filtering, limiting the bandwidth to about 1 kHz, was

incorporated in the model shown in Figure 2, with a significant improvement in the overall noise performance of the unit. The current regulation scheme is quite compact. The improvement in performance is documented in Figure 3, which directly compares the two units.

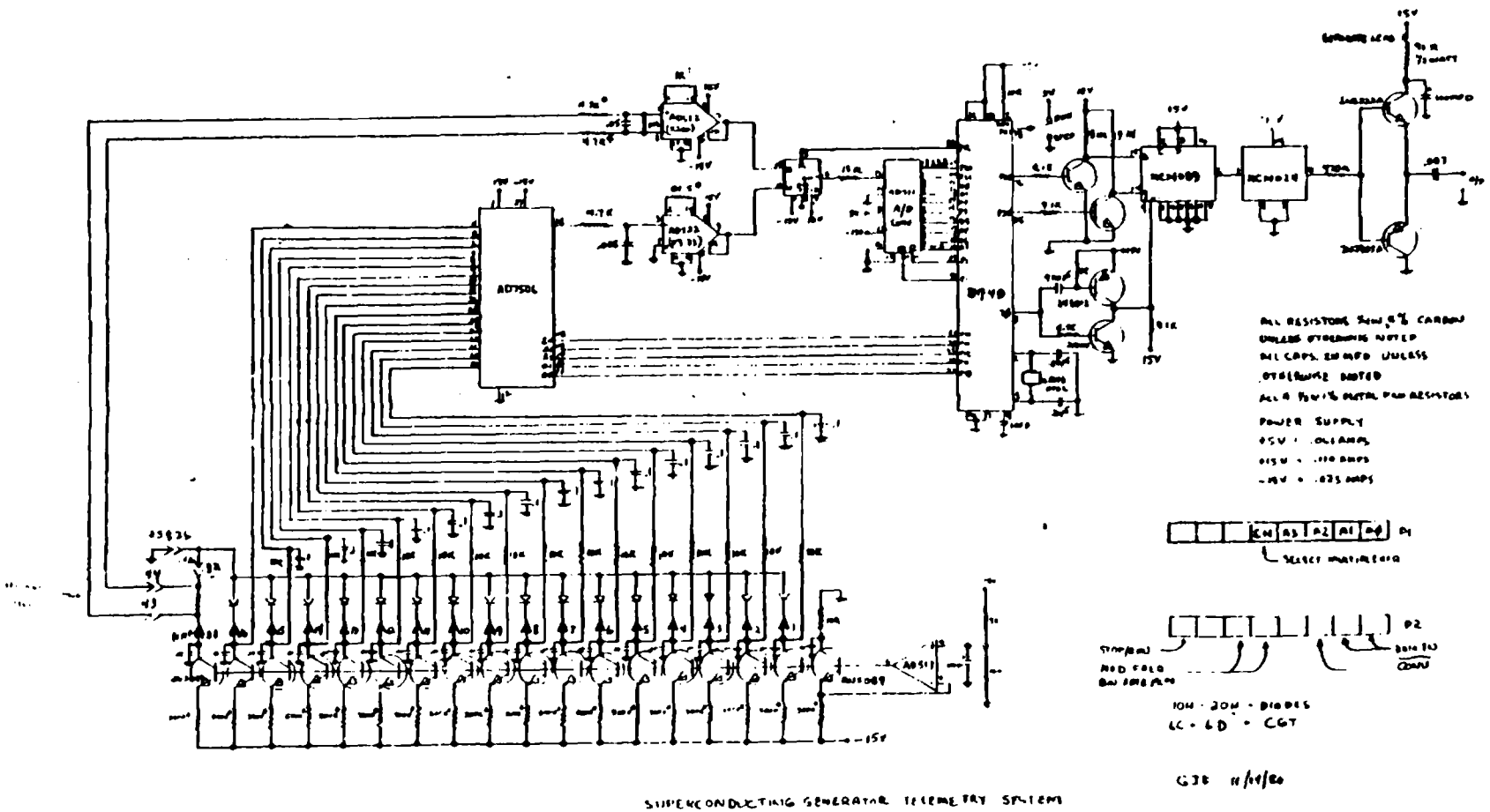

Figure D-2. Data Acquisition and Telemetry -- no current multiplexing.

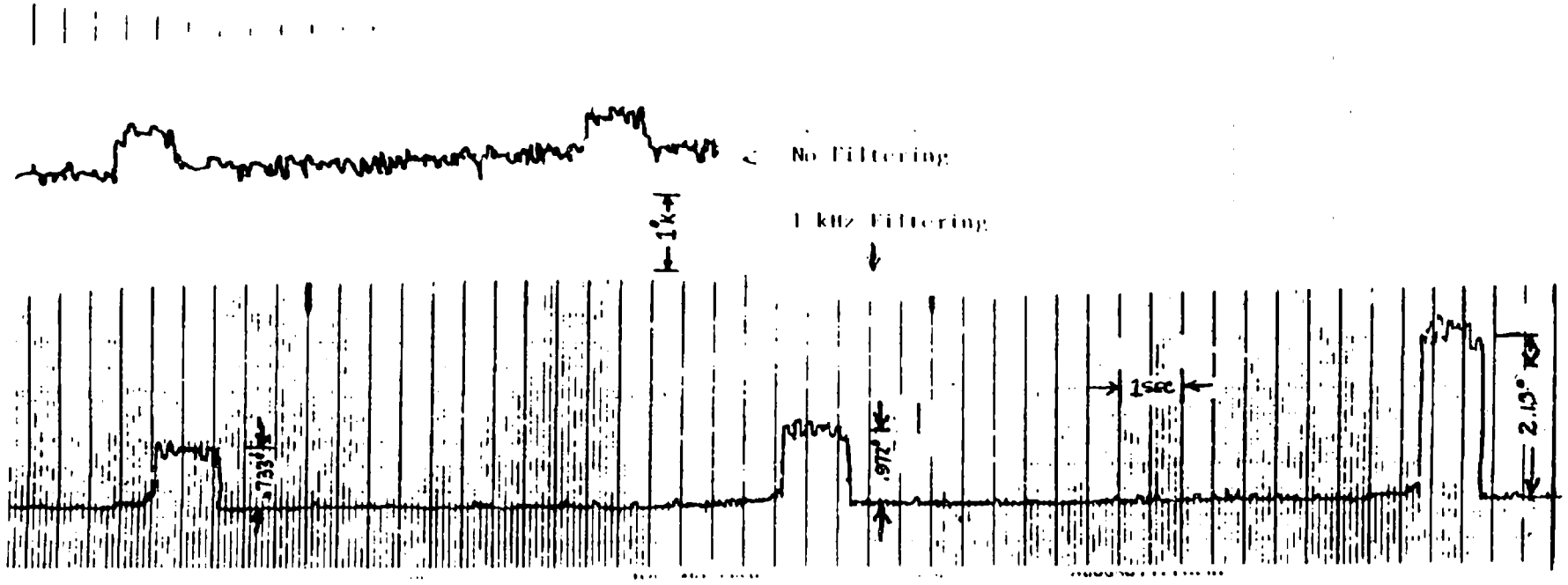

Figure D-3. Comparison between the two modules, one with 1 kHz filter, (lower) and other without filtering.(top)

APPENDIX E

RECENT DEVELOPMENTS ON METHODS FOR SUPERCONDUCTOR JOINING

R. D. Blaugher
Westinghouse Electric Corporation
Research and Development Center
Pittsburgh, Pennsylvania 15235

INTRODUCTION

The subject of superconductor joints and their influence on measured superconducting properties was essentially coincident with the discovery of high-current, high-field (type II) superconductors. It was immediately apparent that a low resistance, almost lossless, connection must be made to the superconductor. Early attempts to solve this problem produced a fairly straightforward approach, which even now provides an excellent method for superconductor joining. A lap joint was implemented between two long lengths of conductor that were soldered with pure indium and then clamped between two copper plates. The recent Westinghouse 5 MVA superconducting generator field winding, the Air Force four-pole superconducting generator, and the 300 kJ pulsed energy coil all utilized soldered and clamped joints.

Every superconducting magnet, almost winding exception, incorporates some form of an electrical joint in its construction. A normal conductor-to-superconductor transition is generally required that completes the external current connection for energizing the magnet. In addition, manufacturing constraints either in winding or in conductor manufacture may necessitate additional joints between lengths of superconductor.

All "superconductor joints" must satisfy specific mechanical, electrical, and thermal constraints that depend on the individual magnet design. The joint resistance should be almost as lossless as the superconductor itself. Otherwise at design current a high heat load presented by the joint may produce excessive cooling requirements or more seriously initiate a conductor normalization and subsequent quench of the magnet. Superconductor joints, in addition, must be as mechanically strong as the actual superconductor since a mechanical failure at the joint would open the winding with possible catastrophic results.

The design and fabrication methods used to implement superconductor joints have shown a number of varied approaches These approaches, for the most part, depend intimately on the desired resistance level and the exact conductor configuration. A laboratory solenoid for nuclear magnetic resonance (NMR) requires an extremely low resistance joint since the magnet is normally operated in the persistent mode. Typical joint resistance for NMR magnets must be less than 10^{-12} Ω for optimum operation. It is thus not surprising that some of the reported joint resistances for NMR magnet applications are among the lowest observed. Leupold and Iwasa[1] produced a joint in a Nb-Ti multifilamentary monolithic conductor that was less than 10^{-14} Ω. This joint was produced by etching away the copper matrix to expose the filaments. The individual filaments were then crimped together in separate copper sleeves. Other variations on this approach have actually welded the individual filaments by microelectron beam welding. The copper stabilizer was then restored through the use of copper foil.[2]

Superconductor joints for large-scale applications, such as generators and fusion magnets, are usually more difficult due to higher current, higher field, and a more complicated conductor configuration. The Lawrence Livermore mirror-fusion test facility (MFTF) conductor for the Ying-Yang coil is an excellent example. A 6.5 mm x 6.5 mm monolith of multifilamentary Nb-Ti is wrapped within a perforated copper stabilizer, which is then soldered by heat treatment to the superconductor core.[3]

Joint development programs at Lawrence Livermore evaluated methods for joining this large multifilamentary superconductor core. Both explosive welding[4] and cold welding[5] demonstrated completely acceptable mechanical and electrical properties. The explosive approach, however, presented serious fabrication problems, which prompted the selection of cold-welding as the preferred method. Recent tests[5] on cold-welded MFTF Nb-Ti superconductors have shown joint resistances at 4.2K of ~ 10^{-8} Ω at ~ 6 kA operating current and 7.5T field.

The preceding examples of superconductor joining demonstrate a wide range in magnet applications from small laboratory magnets to large-scale fusion devices. These different joining approaches also present examples of the two basic methods used for fabricating a superconductor joint, i.e., mechanical or welded. Mechanical joining covers all clamped techniques, which may be soldered in addition to the clamping. As mentioned earlier, the clamped and soldered joining technique has been widely used with nominal joint resistance easily obtained of better than 10^{-8} Ω. A soldered and clamped joint can be readily utilized where there are no space constraints. A large access area is required for assembly, and the resulting joint generally occupies a volume much larger than the adjoining conductor. The DEALS fusion magnet design presents a recent large-scale concept directed at a clamped or pressure joint with a large surface area to minimize the resistance.[6]

The welded joint basically covers all of the other joining approaches that have been investigated: welding of each filament, butt resistance welding, cold welding, ultrasonic and explosive welding. Some joint designs considered for the MFTF-B solenoid coils incorporate both the basic methods, cold welding of the stabilizer followed by a soldered lap joint of the superconductor.

The superconductor joint design for most large-scale applications has traditionally followed the conductor selection, structural

design, and other details of the magnet construction. As a result, the joining problems are often more difficult and usually represent a critical area with respect to magnet stability and performance.[7] The following sections review two recent joint development programs that demonstrate areas of critical joining.

LARGE COIL PROGRAM Nb_3Sn JOINT DEVELOPMENT

The Westinghouse Large Coil Program (LCP) magnet design requires a specific joint resistance and helium flow rate to insure superconducting stability of the conductor. The stability analysis, based on a minimum propagating zone (MPZ) model specifies a joint resistance of less than 1.7×10^{-9} Ω at 2T and 18 kA operating current. Detailed experimental investigation of the joint and header under actual forced-flow conditions verified this analysis. Acceptable stability with even higher joint resistance of $\sim 10^{-8}$ Ω could be obtained by an increased helium flow rate.[8]

The Westinghouse (LCP) conductor is fabricated by cabling 486 strands of multifilamentary Nb_3Sn wire and then compacting and jacketing this cable with a welded steel enclosure. The steel outer jacket is completely sealed over its entire length with respect to helium leakage. A header welded to the end of each conductor provides space for the electrical joint and attachment of helium flow tubes.

This force-cooled, steel-enclosed Nb_3Sn cable thus presented a formidable joining problem. A joint development program to connect the lengths of full-size conductor and individual strands during wire manufacture was pursued by Westinghouse and Airco to evaluate various joining procedures. The development program concentrated on three main approaches: butt-resistance welding, lap joining, and cold welding.

Cold welding, which works quite well for Nb-Ti multifilamentary conductors is not readily adaptable to Nb_3Sn. The unreacted bronze core containing the niobium filaments becomes extremely brittle during cold

welding. In addition, the upset during cold welding almost completely destroys the diffusion barrier and pushes the high-resistivity bronze to the outside of the wire. Annealing, which would be necessary to provide sufficient ductility for the cabling process, would thus contaminate the copper stabilizer. Cold welding, after reaction, would severely degrade the highly fragile A15 Nb_3Sn.

Lap joining of the multistranded cable would require uncabling and placement in a support fixture to minimize bending stresses following reaction. The strands from mating conductors would be overlapped and soldered in a grooved copper cylinder. A copper sleeve would be pressed over the entire structure for mechanical integrity. The resulting lap joint would require a long time for assembly and occupy a fairly large volume. This method was evaluated by constructing a simple 5 cm lap joint as detailed above. Nine strands of 0.7 mm wire were reacted in a special fixture at 700°C for 30h and subsequently soldered with indium between a copper cylinder and sleeve. The observed resistance at 4.2K in zero field was $R = 2.6 \times 10^{-8}$ Ω. Additional joint tests were performed on a termination prepared by swaging a copper tube around the unreacted wire. The ends of two terminations were then prepared with different bias angles and reacted. The two surfaces were then joined by an extremely thin interface of indium solder. The low-temperature resistances were measured in a special fixture fabricated from G10 laminate, which contracted during cooldown, providing slight pressure on the joint. A 45° and 30° bias showed $R45° = 8.6 \times 10^{-8}$ Ω and $R30° = 8.9 \times 10^{-8}$ Ω at zero field and 4.2K for ~ 500A current). These soldered bias tests were directed at a method for reducing the current transfer length through the highly resistive tantalum barrier and bronze matrix.

Previous work by Wilson[9] and more recent work by Ekin[10] established minimum length requirements for lap joints to reduce current transfer resistance. Using the relationship developed by Ekin[10]

$$\frac{X_{min}}{D} = 0.14 \quad \frac{\rho_t}{\rho_{min}}^{1/2}$$

where $\rho_{min} = 10^{-11}$ Ω·cm (the resistivity detection criterion), $\rho_t = 10^{-6}$ Ω·cm (the transverse or matrix resistivity for bronze), X_{min} = current transfer length, D = the conductor effective diameter or 0.762 mm for LCP strands,

$$Xmin = D \times 44.3 = 3.38 \text{ cm.}$$

A Nb_3Sn lap joint would thus require approximately a 4 cm overlap to obtain a low-resistance joint. The lap joint tested above easily met this criterion. The soldered bias joints showed a factor of three higher resistance than the lap joint. This result indicates that a reduced current transfer length was, in fact, obtained. Its fully potential, however, was not realized owing to the difficulty in obtaining good contact between the soldered surfaces. The interface resistance was thus high and contributed added resistance.

Two of the reacted six-strand terminations were prepared with perpendicular surfaces that were then butt-resistance welded. Airco had explored this technique with satisfactory results.[11] This joint showed at zero field and ~ 400A current a resistance of R = ~ 4.5×10^{-9} Ω. This latter test was extremely e encouraging and indicated that the larger full-size 486-strand conductor could be similarly terminated and butt-welded with acceptable properties.

As a result, additional subsize tests were performed coupled with tensile tests, which demonstrated acceptable electrical resistance and mechanical strength. Full-size terminations were then prepared and tested at full-design conditions, forced-flow helium, 2T, and ~ 14 kA current. The observed resistances at 4.2K for the full-size butt-welded joint ranged from 1.5×10^{-9} to 1×10^{-8} Ω at the above field and current.[8] There were no obvious visual differences in the welded joints that might explain the observed range in resistance. Full penetration X-rays of the joint region also showed no obvious difference. A

possible explanation was developed, however, from analysis of the individual strand results explained below.

A parallel effort to joining the full-size cable was directed at the individual strands. The Nb_3Sn (0.69 mm) multifilamentary wire, fabricated by Airco, had 2869 filaments (~ 3.7 μm diam.) with a 63 vol. % copper stabilizing shell.[12] The strand-joining effort concentrated entirely on butt-resistance welding of the unreacted Nb-Sn wire. Sufficient strength, ductility (before reaction), and acceptable electrical properties (after reaction) were observed. Random strand breakage during drawing or cabling could thus be solved by this welding method. The Westinghouse Phase II report for the Large Coil Program contains additional information on the strand and full-size joint development effort.[13]

Additional tests have been performed on butt-resistance welds of Nb_3Sn wire. This wire was supplied by Intermagnetics General Corporation (IGC) for the Air Force Materials Technology Program. The wire we received will be eventually tested under simulated generator cooling conditions in a rotating test facility. Butt-resistance welds of 0.91 mm diameter wire were performed and reacted. The mechanical strength of the welded and unwelded wire was tested before and after reaction, as summarized in Table 1. Welding degraded the strength by as much as 50% of the strength of the unreacted wire, which nevertheless should be strong enough for most cabling operations. The reaction produced no marked difference in strength between the welded and unwelded wire.

Critical current tests using 1 μV/cm as the electric field criterion on welded and unwelded wire are compared in Figure 2. This figure also presents short sample data on the Airco LCP Nb_3Sn strands.[12] The IGC welded strands showed ~ 27% of the current-carrying ability of the unwelded strands.

Table E-1. Average Mechanical Strength for Welded and Unwelded Nb_3Sn Wire in kg/mm^2

Diameter	Before Reaction		After Reaction	
(mm)	Unwelded	Welded	Unwelded	Welded
0.91	54	40	--	--
0.97	69	32	23	26

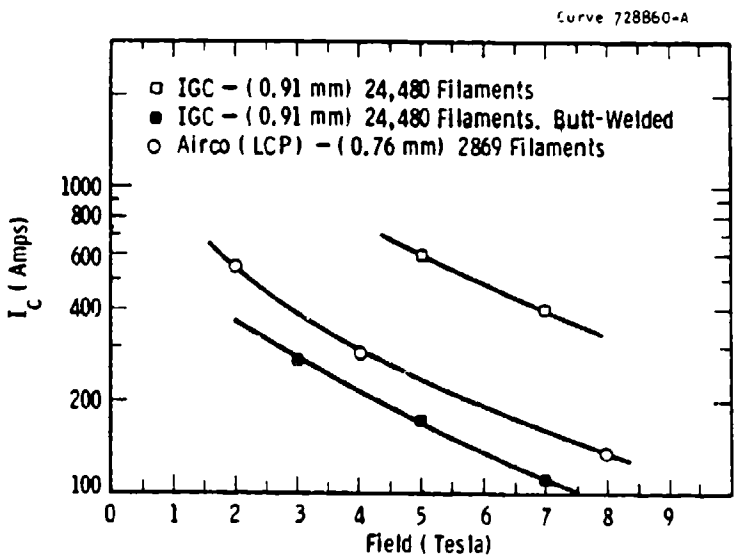

Fig. E-1. Short sample critical current for welded and unwelded Nb_3Sn wire.

This data was considerably better than the data of the Airco welded strands. Typical strand welds of the Airco wire could only carry 7 to 10% of the critical current of the unwelded wire.[11,13] Electron microscopy of the IGC wire was performed to evaluate the weld morphology. A SEM cross section (shown in Figure 2) indicates a number of interesting features. The heat-affected zone extended ~ 1.0 mm with marked overlap of the tantalum stabilizer. No evidence for melting of

the niobium or tantalum components was observed except at the fusion interface. The filaments in the heat-affected zone were observed to buckle or ripple owing to the upset pressure. Subsequent etching with dilute HNO_3 confirmed these features. At the fusion interface shown in Figure 3, a large number of filaments were actually joined end to end over almost the entire cross section. The possibility also exists that some filaments were interspersed from the joining sections. Subsequent reaction actually formed a continuous network of Nb_3Sn across the weld interface. The etched SEM studies also showed no evidence of tantalum or niobium melting except where the filaments were fused.

The observed critical current properties for the welded IGC wire are thus attributed to the high number of filaments actually joined during the welding process. The reduced values for the Airco wire simply follow as a direct result from the decreased number of filaments. If we normalize the two wires for the different cross-sectional areas, percents of copper stabilizer, and filament numbers and diameters, the IGC wire has roughly three times more filaments for an equivalent cross section. Hence the probability of welding filaments for the IGC wire is three times greater, which is almost exactly the difference in critical current between the two welded wires.

These results thus imply that improved critical currents can be obtained by a higher concentration of filaments and good alignment of strands during welding. This conclusion applies directly to the larger 9-strand, 162-strand, and 486-strand butt welds performed for LCP. As we move away from ideal strand-to-strand alignment, the joint properties degrade.[13]

At 2T, the LCP 162-strand subsize cable should carry 90 kA. The observed critical current for the 162-strand butt weld was 400A or less than 0.5%. The full-size 486 LCP strand cable should carry 270 kA, yet at 2T the termination showed a resistance of 10^{-8} to 10^{-9} Ω.

As discussed earlier, no obvious differences for the full-size welded terminations could be detected. The possibility exists that

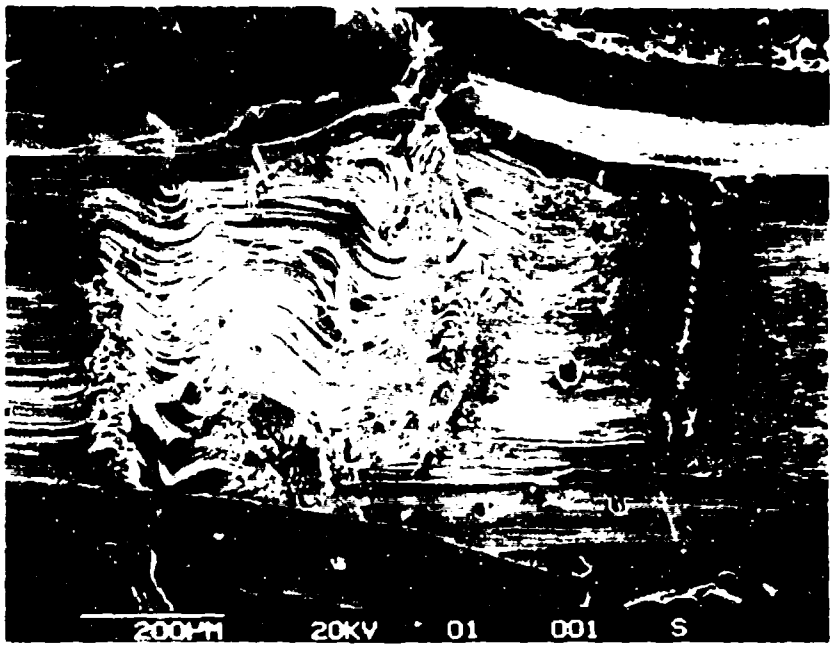

Fig. E-2. Cross section of butt-welded Nb_3Sn wire (SEM).

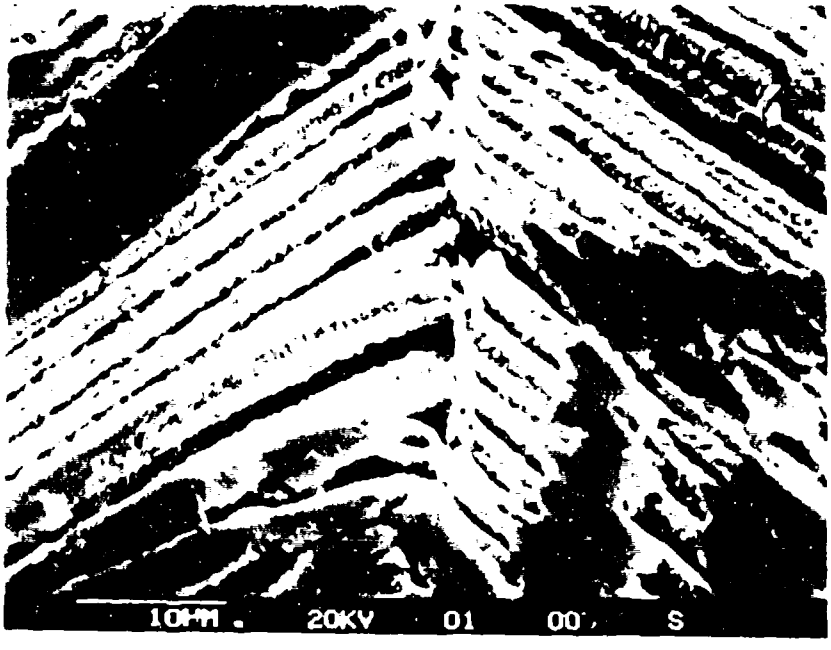

Fig. E-3. Filament joining at butt-welded interface (SEM).

better strand-to-strand alignment was simply obtained for the lower observed resistance. It is interesting to note that the IGC weld data extrapolated to 2T (in Figure 1) would suggest a fully superconducting joint could be obtained for LCP at 2T and 18 kA. This result could only occur for perfect strand alignment and comparable filament count.

SUPERCONDUCTING GENERATOR Nb-Ti JOINT DEVELOPMENT

The superconductor for the Westinghouse/EPRI 300 MVA generator is a copper-stabilized Nb-Ti multifilamentary rectangular superconductor, as specified in Table 2. The design operating current and maximum field as 1800A and 5T, respectively.

Table E-2. 300 MVA Superconductor Specification

Dimension	0.203 cm (0.080 in) x 0.384 cm (0.151 in)
Copper to SC Ratio	2.5:1
Critical Current	3500A at 4.2K and 5T
Resistivity Ratio $\rho(300K)/\rho(20K)$	150
Twist Pitch	4 cm
Filament Size	50 μm

During winding of the field coil, the transitions from adjacent stacks and adjacent slots are facilitated by the ability to splice the conductor. These splices on the ~ 2.0 mm thickness are located in the end turns at the winding outer diameter. This end-turn location presents an extremely confined area for joining the conductors. Approximately 0.60 cm (0.25 in) is available on each side of two overlapped conductors. Since the splice is located at the winding o.d., unlimited space is available above the joint region in the radial direction. In addition, owing to the winding tension and angled slot

configuration, there is no ability to lift the conductor away from the winding surface for improved access. A joint development program was implemented that considered three joining approaches: ultrasonic, butt-resistance welding, and lap/mechanical joining.

Preliminary results on the electrical and mechanical properties of butt-welded joints were encouraging. The limited access for accomplishing the weld, however, essentially ruled out this method.

The lap/mechanical technique was also explored and could be used if absolutely necessary. Such a joint, however, would take up most of the available space and definitely presented an assembly problem.

The ultrasonic welding method, on the other hand, showed considerable potential. This technique offered fast, easy welding with the confined area representing the only major development problem. The ultrasonic joining process was successfully used in the construction of the superconducting MHD (U-25) magnet built by Argonne National Laboratory.[14]

The ultrasonic technique works extremely well with a lap-type configuration. The two conductors are placed between a clamping fixture, pressure is applied, and a cold diffusion bond is effected through a combination of ultrasonic vibration and the applied pressure. The welding time is of the order of 1.0s, and temperatures at the joint rarely exceed 50% of the melting point of the copper matrix. The physical strength is excellent, and when weld parameters are established the joint strength normally exceeds the ultimate strength of the adjoining conductor. This technique, like the lap/mechanical technique, does not affect the cold-worked state of the Nb-Ti superconductor. The process is limited only by the thickness of the joint and accessibility. The present commercial ultrasonic welders have a maximum thickness limitation for copper of ~ 2.0 mm. The 300 MVA conductor thickness of 2.03 mm is, thus, just within the limits of present welders. A bias or scarf configuration, however, would allow these thickness limits to be

extended. Prototype welders are also under development with higher power and thickness capability.

The magnetic field levels at the joint locations in the end-turn region were calculated by different computer programs. These programs indicated that the field intensity for the joints would not exceed 4.5T. Thus, the joint resistance, on the final configuration, will be measured at field levels up to 4.5T and operating current of 1300A.

Using the current transfer relation developed by Ekin[10] with $\rho t = 10^{-8}$ $\Omega \cdot cm$ as the transverse resistivity

$$X_{min} = 1.4 \text{ cm} \quad \text{for } \rho_{min} = 10^{-11} \ \Omega \cdot cm$$

and

$$X_{min} = 4.4 \text{ cm} \quad \text{for } \rho_{min} = 10^{-12} \ \Omega \cdot cm$$

Because a large number of joints were projected, a 4 cm overlap length was selected.

Trial welds at this length were first attempted by two different welder manufacturers. Both units produced satisfactory welds with respect to electrical and mechanical performance.

A Branson unit, however, was eventually selected and purchased for use on the 300 MVA program, since its basic design offered more potential for the confined area application. The Model 3301 Branson unit operates at 20 kHz and generates ~ 3000W output power. A special confined area welding tip was constructed out of a high-strength, high-toughness, lightweight alloy of Ti-6Al-4V. This alloy was selected after a number of other candidates were eliminated for reasons of weight or poor fatigue characteristics.

Weld trials were then conducted on an actual superconductor with specifications nearly identical to those of the 300 MVA conductor. These trials established optimum welding parameters with respect to

power, weld time, and applied pressure. A series of welds were then mechanically tested at room temperature. All of the welds exceeded the physical strength of the parent conductor. Subsequent mechanical tests at 4.2K showed an approximate 40% improvement in mechanical strength over the room temperature value. Failure was again observed in the parent conductor, which approached brittle failure at 4.2K (ductile failure was at room temperature). The point of failure generally occurred adjacent to the overlapped region. Electrical tests at 4.2K at 5.0T and 1000A showed typical resistances of ~ 1.0×10^{-9} Ω. Additional tests at higher currents (~ 2000A) and 5.0T are planned in a special fixture representative of the end turn geometry.

As discussed in the previously published paper by Hofstrom et al.,[14] ultrasonic welded joints offer what may be the only joint configuration for quantitative NDT testing. The present ultrasonically welded joints were NDT testing. The present ultrasonic transducer using immersion and oil contact method. An accurate evaluation of the bond integrity was possible with this procedure. Areas that indicated satisfactory and poor bond integrity were subsequently sectioned and studied metallographically. This latter test completely verified the NDT ultrasonic tests.

In summary, an ultrasonic welding method has been developed for joining the 300 MVA superconductor. This technique offers high mechanical strength with joints actually stronger than the parent material, acceptable electrical properties at low temperature, and the ability to perform quantitative NDT testing.

CONCLUSIONS

These two recent superconductor joint development programs both represent an intensive effort to obtain an acceptable joint. Both programs were highly dependent on a successful joint demonstration. It is not always possible, but it is recommended that more attention be directed to joining problems during the initial magnet design analysis.

Trade-offs in conductor design may be possible that would facilitate the joint fabrication with possibly improved electrical properties. The large fusion magnets of the future will require low overall thermal losses. An optimum superconductor joint design would certainly reduce some of the loss.

ACKNOWLEDGMENTS

I would like to acknowledge the experimental assistance of J. Buttyan and P. D. Vecchio and mechanical tests of W. A. Logsdon.

REFERENCES

1. M. J. Leupold and Y. Iwasa, Superconducting Joint between Multifilamentary Wires, Cryogenics 16:215 (1976).

2. G. Luderer, P. Dullenkopf, and F. Laukien, Cryogenics 14:518 (1974).

3. E. Adam, E. Gregory, and W. Marancik, in: "Proceedings of the 7th Symposium on Engineering Problems of Fusion Research," 77CH1267-4-NPS, IEEE, New York (Oct. 1977), p. 1329.

4. D. Cornish, J. P. Zbasnik, and H. E. Pattee, in: "Proceedings of the 6th Symposium of Engineering Problems of Fusion Research," 75CH1097-5NPS, IEEE, New York (Nov. 1975), p. 106.

5. D. H. Cornish, D. W. Deis, and J. P. Zbasnik, in "Proceedings of the 7th Symposium on Engineering Problems of Fusion Research," 77CH1267-4-NPS, IEEE, New York (Oct. 1977), p. 1267.

6. S. Y. Hsieh, G. Danby, J. R. Powell, P. Bezler, D. Gardner, C. Laverick, M. Finkleman, T. Brown, J. Bundy, T. Bolders, I. Zatz, R. Verzera, and R. Herberman, in: "Advances in Cryogenic Engineering," Vol. 25, Plenum Press, New York (1980), p. 207.

7. H. Fujino, A. Ishihara, K. Veda, Y. Shindo, and S. Nose, "Proceedings of ICEC Eight," IPC Science and Technology Press, Guildford, Surrey, England (1980), p. 600.

8. R. D. Blaugher, M. A. Janocko, P. W. Eckels, A. Patterson, J. Buttyan, and E. J. Shestak, IEEE Trans. Magn. MAG-17:467 (1981).

9. M. Wilson, Internal Report SMR/1, Rutherford Laboratory, Chilton, Didcot, England.

10. J. W. Ekin, J. Appl. Phys. 49:3406 (1978).

11. P. A. Sanger and E. Gregory, 8th Symposium on Fusion Engineering (1979), abstract only.

12. C. R. Spencer, P. A. Sanger, and M. Young, IEEE Trans. Magn. MAG-15:76 (1979).

13. "Superconducting Magnet Coils for the Large Coil Program, Phase 2 Final Report," Westinghouse Electric Corporation, Research and Development Center, Pittsburgh, Pennsylvania (Mar. 1980).

14. J. W. Hofstrom, D. H. Killpatrick, R. C. Nieman, J. R. Purcell, and H. R. Tresch, IEEE Trans. Magn. MAG-13:94 (1977).

REFERENCES

1. "Program for the Development of a Superconducting Generator," Technical Report AFAPL-TR-74-84.

2. "Program for the Development of a Superconducting Generator," Technical Report AFAPL-TR-79-2012.

3. "Superconducting Rotor Research," Phase I Interim Technical Report, Contract No. F33615-76-C-2167.

4. C. E. Oberly and H. L. Southall, "System Considerations for Airborne, High Power Superconducting Generators," IEEE Trans. on Magnetics, Vol. MAG-15, p. 711 (1979).

5. "High Power Study for Superconducting Generators," Technical Report AFAPL-TR-76-37.

6. "Superconducting Spin-Test Rotor," Technical Report AFAPL-TR-77-39.

7. A. Patterson and R. D. Blaugher, "High-Speed Helium Transfer System Evaluation and Testing," Advanced in Cryogenic Engineering, Vol. 23, p. 132 (1978).

8. "A Superconducting Generator Design for Airborne Applications," B. B. Gamble and T. A. Keim, Advances in Cryogenic Eng., Vol. 27, p. 127 (1980).

9. "High Power Density Superconducting Generator," B. B. Gamble and T. A. Keim, ICEC Conf., Vol. I p. 435 (1980).

10. Muller, A. C., "Properties of Plastic Tapes for Cryogenic Power Cable Insulation," 1978 ICMC Meeting, July 10-11, Munich, Germany.

11. Jelinek, F. and Muller, A., "Study of the Dimensional Behavior of Various Thin-Film Polymers in the Temperature Range 4.2°K to 300°K," Advances in Cryogenic Eng. 22, 312 (1977).

12. Benzinger, J. R., "Properties of Cryogenic Grade Laminates," Proceedings 14th Electrical/Electronics Insulation Conference, pp. 145-50, Oct. 8-11, 1979, Boston, MA.

13. G. R. Wagner, S. S. Shen, R. E. Schwall, A. Petrovich, and M. S. Walker, Ibid, p. 228.

14. C. R. Spencer, P. A. Sanger, and M. Young, IEEE Trans. on Magnetics, MAG-15, 76 (1979).